OFFICIAL JOURNAL OF THE SCIENTIFIC SOCIETY OF ANATOMISTS, HISTOLOGISTS, EMBRYOLOGISTS AND TOPOGRAPHIC ANATOMISTS OF UKRAINE

DOI: 10.31393
ISSN 1818-1295
eISSN 2616-6194

ВІСНИК МОРФОЛОГІЇ
REPORTS OF MORPHOLOGY

Vol. 29, №3, 2023

Scientific peer-reviewed journal in the fields of normal and pathological anatomy, histology, cytology and embryology, topographical anatomy and operative surgery, biomedical anthropology, ecology, molecular biology, biology of development

Published since 1993
Periodicity: 4 times a year

Vinnytsya · 2023

ВІСНИК МОРФОЛОГІЇ - REPORTS OF MORPHOLOGY

Founded by the "Scientific Society of Anatomists, Histologists, Embryologists, and Topographic Anatomists of Ukraine" and National Pyrogov Memorial Medical University, Vinnytsya in 1993

Certificate of state registration КВ №9310 from 02.11.2004

Professional scientific publication of Ukraine in the field of medical sciences in specialties 221, 222, 228, 229
According to the list of professional scientific publications of Ukraine, approved by the order of the Ministry of Education and Science of Ukraine No. 1188 of 24.09.2020
Professional scientific publication of Ukraine in the field of biological sciences in specialty 091
According to the list of professional scientific publications of Ukraine, approved by the order of the Ministry of Education and Science of Ukraine No. 1471 of 26.11.2020

Approved by the Academic Council of National Pyrogov Memorial Medical University, Vinnytsya, protocol №1 from 31.08.2023.

Indexation: CrossRef, Index Copernicus, Google Schoolar Metrics, National Library of Ukraine Vernadsky

Address editors and publisher:
Pyrogov Str. 56,
Vinnytsya, Ukraine - 21018
Tel.: +38 (0432) 553959
E-mail: nila@vnmu.edu.ua

Computer page-proofs - Klopotovska L.O.
Translator - Gunas V.I.
Technical support - Levenchuk S.S.
Scientific editing - editorship

The site of the magazine - https://morphology-journal.com

CONTENT

Haddad N. B. Yo., Chaika H. V., Kyrychenko I. M., Shapoval O. M., Dronenko V. G. Correlations of the dermatoscopic index with anthropometric and somatotypological parameters of men with benign nevi **5**

Gontar N. M. Changes in markers of collagen metabolism in the blood serum of white rats during the filling of femur defects with implants based on polylactide and tricalcium phosphate with allogeneous mesenchymal stem cells **12**

Maievskyi O. Ye., Bobr A. M., Gunas I. V. Structural changes in the heart tissue of rats under conditions of acute intoxication with Vipera berus berus venom **20**

Rykalo N. A., Baylo O. V. Investigation of nuclear DNA content and cell cycle phases in rat liver cells under chlorpromazine administration **26**

Khimich S. D., Rautskis V. P. Morphological reasoning of the efficiency of application "Iruksan" in the experiment **32**

Pastukhova V. A., Bakunovsky O. M., Drozdovska S. B., Filippov M. M., Ilyin V. M., Krasnova S. P., Oliinyk T. M. Features of immediate adaptation of the circulatory system to static load in persons with different body mass index **39**

Niyazmetov T. S. Changes in the microscopic organisation of rat adrenal glands under the influence of Vipera berus berus venom **45**

Torchynskyi V. P., Nizalov T. V., Shmelyova L. V., Suprun, A. D. Physical and mathematical modeling of the distribution of load forces on the feminal component of an endoprosthesis of the hip joint under real conditions **52**

Kyrychenko Yu. V., Sarafyniuk L. A., Khapitska O. P., Dus S. V., Yakusheva Yu. I. Peculiarities of correlations between spirometric and anthropometric indicators in practically healthy young women of mesomorphic somatotype **58**

Liulka Ye. M., Bilash S. M. Features of anthropometric indicators and dimensions of the coronary sinus and relationships between these indicators in patients without coronary artery pathology **67**

DOI: 10.31393/morphology-journal-2023-29(3)-01 Reports of Morphology, Vol. 29, №3, Pages 5-11

ISSN 1818-1295 eISSN 2616-6194

REPORTS OF MORPHOLOGY

Official Journal of the Scientific Society of Anatomists, Histologists, Embryologists and Topographic Anatomists of Ukraine

journal homepage: https://morphology-journal.com

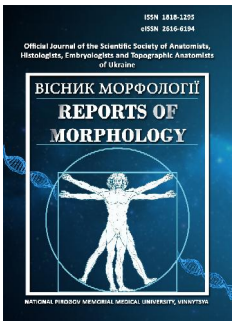

Correlations of the dermatoscopic index with anthropometric and somatotypological parameters of men with benign nevi

Haddad N. B. Yo., Chaika H. V., Kyrychenko I. M., Shapoval O. M., Dronenko V. G.
National Pirogov Memorial Medical University, Vinnytsya, Ukraine

ARTICLE INFO
Received: 05 April 2023
Accepted: 08 May 2023

UDC: 616.53-008.811.1-037-084-036.1:616-071.2

CORRESPONDING AUTHOR
e-mail: dr_ahmad_khasawneh@yahoo.com
Haddad N. B. Yo.

CONFLICT OF INTEREST
The authors have no conflicts of interest to declare.

FUNDING
Not applicable.

Malignant transformation of benign nevi is one of the factors that leads to increased scientific interest in the study of the pathogenesis of their occurrence, the influence of external factors on them, etc. One of the still unsolved issues is the study of the relationship between the features of nevi indicators and the anthropometric parameters of the human body. The purpose of the work is to investigate the peculiarities of correlations of the dermatoscopic index with anthropometric and somatotypological indicators of Ukrainian men with benign nevi. A clinical, laboratory and pathogistological examination of 34 Ukrainian men of first adulthood with melanocytic benign simple nevi, 27 with melanocytic benign dysplastic nevi, 14 with melanocytic benign congenital nevi, and 17 with non-melanocytic benign nevi was carried out. The dermatoscopic index was calculated according to the "ABCD rule of dermatoscopy". Anthropometric examination was carried out according to Bunak's scheme. The Heath-Carter mathematical scheme was used to assess the somatotype. Matiegka formulas were used to calculate fat, bone and muscle components of body mass. In addition, the muscle component of body weight was estimated according to the method of the American Institute of Nutrition. The assessment of correlations between the dermatoscopic index and body parameters was carried out in the license package "Statistica 6.0" using the non-parametric method of Spearman. An analysis of multiple reliable and average strength of unreliable correlations between the value of the dermatoscopic index and anthropo-somatotypological indicators in men with benign nevi was performed. In men with simple melanocytic nevi, only moderately strong direct (r = from 0.30 to 0.34), mostly unreliable, correlations with all sizes of the pelvis were established. In men with melanocytic dysplastic nevi, inverse correlations of medium strength, mostly reliable (r = from -0.38 to -0.52) were established with all dimensions of the pelvis and almost all transverse dimensions of the trunk, as well as with almost half of the indicators of the skinfold thickness. In men with melanocytic congenital nevi, direct, mostly unreliable (r = from 0.30 to 0.47) correlations were established with all dimensions of the pelvis, with almost all transverse dimensions of the trunk, with almost half of the girth of the body and indicators of the skinfold thickness and almost all indicators of the component composition of body weight. In men with non-melanocytic nevi, direct, mostly unreliable (r = from 0.30 to 0.47) correlations were established with all transverse dimensions of the trunk and pelvis, most of the total and girth dimensions of the body. Quantitative analysis of reliable and average strength of unreliable correlations between the value of the dermatoscopic index and anthropo-somatotypological indicators was also carried out. The established features of the correlations expand modern ideas about the risk of benign nevi.

Keywords: *skin diseases, benign nevi, dermatoscopic index, anthropometric and somatotypological body parameters, correlations, men.*

Introduction

Nevi are benign melanocytic tumors that can be both congenital and acquired [24]. According to scientists, the key element in the occurrence of mutations leading to the emergence or transformation of nevi is the genetic factor. Among the genetic factors associated with the occurrence of nevi, there are four single-nucleotide polymorphisms that

reliably show a connection with an increase or decrease in the number of nevi, namely IRF4 (increase in number) and PARP1, CDK6, and PLA2G6 (decrease in number) [17].

The exact source of nevi still remains unknown. However, the classic model, which is still considered the main one, states that the epidermal melanocyte is the source of both nevi and melanoma, which in the process of loss of differentiation can either develop into a benign tumor, which is a nevus, or a malignant tumor, which is melanoma [10]. The results of histological studies showed that in 30 % of cases melanoma is formed against the background of an already existing nevus. This condition is known as nevus-associated melanoma. In other 70 % of cases, melanoma is formed without previous damage to the skin [6].

During dermatoscopy, congenital nevi have a different type of pattern. It can be either globular (most common) or reticular-globular, homogeneous, reticular-homogeneous, globular-homogeneous (least common), reticular-spotted or cobblestone pattern. Also, they may include the presence of dots, focal or perifollicular hypopigmentation and such rare signs as a bluish-whitish veil [5].

According to a review of 1164 people with nevi, in the first 20 years of life the distribution of the frequency of observation of melanocytic nevi is as follows: the largest number is complex nevi (62 %), followed by the less common dermal nevus (20 %), Spitz nevus (9 %), connective nevus (4 %), blue nevus (2 %) and the least common - spindle cell nevus (1 %), Halo nevus (1 %), atypical spitzoid tumor (1 %) and deep penetrating nevus (<1 %) [23].

One of the non-invasive methods that facilitates the differential diagnosis of benign and malignant melanocytic formations is the ABCD rule of dermoscopy, which calculates a special dermatoscopic index. This method has a sensitivity of 83 % and a specificity of 45 % [1].

Malignant transformation of nevi into melanoma is probably the most important problem facing patients, doctors and scientists. Long-term follow-up of 2355 patients with choroidal nevi showed that malignant transformation into melanoma occurred in 1.2 % of cases after 1 year, 5.8 % after 5 years, and 13.9 % after 10 years [21].

Thus, melanoma is the most common skin cancer among children. Spitzoid melanoma is the most common type and affects children under the age of 11. It is also worth considering the high risk of malignant transformation of congenital nevi, which are also one of the common types of nevi in childhood [16]. In Finland, the incidence of melanoma among children and adolescents has increased from 1.4 per 1 million people in 1990-1994 to 5.8 per 1 million people in 2010-2014. The most noticeable increase in the number of melanoma cases occurred due to the increase in the number of Spitzoid type [19].

Thus, there is a need to conduct research that would involve the study of the interrelationships of light from a technical and financial point of view for the study of indicators. In this context, it was most appropriate to study the relationship between dermatoscopic indicators and anthropometric and somatotypological indicators.

The purpose of the work is to investigate the peculiarities of correlations of the dermatoscopic index with anthropometric and somatotypological indicators of Ukrainian men with benign nevi.

Materials and methods

On the basis of the Military Medical Clinical Center of the Central Region and the Department of Skin and Venereal Diseases with a postgraduate course at the National Pirogov Memorial Medical University, Vinnytsya, a clinical-laboratory and pathogistological examination of Ukrainian men aged 22 to 35 years with benign nevi (34 with melanocytic benign simple nevi, 27 with melanocytic benign dysplastic nevi, 14 with melanocytic benign congenital nevi and 17 with non-melanocytic benign nevi) have been done.

Committee on Bioethics of National Pirogov Memorial Medical University, Vinnytsya (protocol № 10 From 26.11.2020) found that the studies do not contradict the basic bioethical standards of the Declaration of Helsinki, the Council of Europe Convention on Human Rights and Biomedicine (1977), the relevant WHO regulations and laws of Ukraine.

The diagnosis of nevi is established according to the two-stage algorithm for the classification of pigment neoplasms, which was adopted at the First World Congress on Dermatology (Rome, 2001) [18].

The dermatoscopic index was calculated according to the so-called "ABCD rule of dermatoscopy". "A" - Asymmetry. To determine this indicator, the studied neoplasm was visually divided along two asymmetrically favorable lines; in the presence of asymmetry along two axes, index 2 was assigned. "B" - Border sharpness. To evaluate this feature, the neoplasm was visually divided into eight equal parts, each part with a clear border was assigned an index of 1. "C" - Color. There are 6 dermatoscopic colors: light brown, dark brown, black, gray-blue, white, red. Each color present in the neoplasm was assigned an index of 1. "D" - Dermoscopic structures. The following structural elements were distinguished in the dermatoscopic picture: "pigment network", "stripes" ("radial radiance", "pseudopods"), "points", "granules", "structureless areas", "blue-white veil", "structures of regression", "vascular structures" (areas of a milky-red color, microvessels are visualized). Each element, if present in the neoplasm, was assigned an index of 1. The general dermatoscopic index (Iderm) is calculated according to the formula "A"+"B"+"C"+"D", where the constant coefficients A = 1.3; B = 0.1; C = 0.5; D = 0.5. With a total dermatoscopic index of 4.75 to 5.45, the neoplasm is considered a dysplastic nevus, and with values above 5.45, a preliminary diagnosis of skin melanoma is made.

Anthropometric examination was carried out according to the scheme of V. V. Bunak [3]. J. Carter and B. Heath mathematical scheme was used to assess somatotype [4]. The formulas of J. Matiegka [13] were used to calculate

the fat, bone, and muscle components of body weight. In addition, the muscle component of body weight was estimated according to the method of the American Institute of Nutrition [20].

Correlation analysis was carried out in the license package "Statistica 6.0" using the non-parametric method of Spearman.

Results

In Ukrainian men with a diagnosis of nevus, the following values of the dermatoscopic index were established: melanocytic simple nevus - 2.806±1.154; melanocytic dysplastic nevus - 4.522±0.884; melanocytic congenital nevus - 2.943±1.917; non-melanocytic nevus - 0.382±0.626. In all cases, with a melanocytic dysplastic nevus, the value of the dermatoscopic index is significantly ($p<0.05$-0.001) higher, and with a non-melanocytic nevus, it is significantly ($p<0.001$) lower than with other nevi. No reliable or tentative differences were established between melanocytic simple and melanocytic congenital nevi.

The results of correlations of the dermatoscopic index value with total (body weight - W; body length - H; body surface area - S), longitudinal (height of the upper thoracic point - ATND; height of the pubic point - ATL; height of the acromial point - ATPL; height of the digital point - ATP; height of the acetabular point - ATV), transverse (width of the distal epiphysis of the shoulder - EPPL; width of the distal epiphysis of the forearm - EPPR; width of the distal epiphysis of the thigh - EPB; width of the distal epiphysis of the tibia - EPG; transverse mid-thoracic size - PSG; transverse lower-thoracic size - PNG; anterior-posterior size of the chest - SGK; shoulder width - ACR; interspinous distance - SPIN; intercristal distance - CRIS; intertrochanteric distance - TROCH), girth (shoulder girth in a tense state - OBPL1; shoulder girth in a relaxed state - OBPL2; Upper Forearm girth - OBPR1 Lower Forearm girth - OBPR2, Hip girth - OBB, Upper Calf girth - OBG1, Lower Calf girth - OBG2, neck girth - OBSH; waist circumference - OBT; hip girth - OBBB; hand girth - OBK; foot girth - OBS; girth of the chest on inspiration - OBGK1; chest girth on exhalation - OBGK2; chest girth during calm breathing - OBGK3) body dimensions, skinfold thickness (on the back surface of the shoulder - GZPL; on the front surface of the shoulder - GPPL; on the forearm - GPR; under the lower angle of the scapula - GL; on the chest - GGR; on the stomach - GG; on the side - GB; on the thigh - GBD; on the lower leg - GGL), the size of the components of the somatotype (endomorphic component of the somatotype - FX; mesomorphic the somatotype component - MX; the ectomorphic component of the somatotype - LX), the type of somatotype (SOMAT) and the value of indicators of the component composition of body weight (muscle component of body weight according to Matiegka - MM; bone component of body weight according to Matiegka - OM; fat component of body weight according to Matiegka - DM; muscle component of body weight according to the method of the American Institute of Nutrition - MA) in Ukrainian men with benign nevi are listed in Table 1.

Table 1. Correlations of the dermatoscopic index with body size and structure indicators of Ukrainian men with benign nevi.

Anthropo-somatotypo-logical indicators	Nevi			
	melanocytic simple (n=34)	melanocytic dysplastic (n=27)	melanocytic congenital (n=14)	non-melanocytic (n=17)
W	0.22	***-0.32***	0.27	***0.38***
H	0.21	0.13	0.09	0.01
S	0.20	-0.25	***0.36***	***0.40***
ATND	0.22	0.12	0.03	0.02
ATL	0.16	***0.37***	***-0.38***	***0.42***
ATPL	0.25	0.21	-0.02	-0.14
ATP	**0.34**	-0.13	***0.37***	-0.20
ATV	0.26	***0.33***	***-0.43***	***0.30***
EPPL	-0.01	-0.12	0.02	0.03
EPPR	0.14	0.08	***-0.33***	***0.38***
EPB	0.22	-0.06	0.16	0.05
EPG	0.04	0.10	0.20	-0.11
PSG	0.13	***-0.33***	***0.42***	***0.34***
PNG	0.15	***-0.35***	***0.41***	***0.41***
SGK	0.19	***-0.41***	***0.33***	**0.57**
ACR	-0.22	0.17	-0.03	***0.40***
SPIN	***0.30***	**-0.52**	**0.60**	***0.43***
CRIS	***0.33***	**-0.38**	**0.65**	***0.32***
TROCH	**0.34**	**-0.39**	***0.38***	***0.31***
OBPL1	0.13	-0.18	***0.41***	0.25
OBPL2	0.09	-0.26	***0.47***	***0.34***
OBPR1	0.02	-0.20	***0.39***	***0.39***
OBPR2	0.02	-0.20	0.10	**0.72**
OBK	0.14	0.06	-0.02	***0.31***
OBB	0.22	-0.22	***0.42***	-0.07
OBBB	0.14	-0.28	0.27	***0.35***
OBG1	***0.31***	-0.13	0.20	***0.33***
OBG2	0.01	-0.10	***0.44***	0.20
OBS	0.00	0.04	0.16	0.10
OBSH	0.11	***-0.38***	0.04	***0.37***
OBT	0.12	***-0.36***	***0.34***	**0.52**
OBGK1	0.23	-0.26	0.23	***0.47***
OBGK2	0.21	-0.28	0.31	***0.44***
OBGK3	0.21	-0.25	0.24	***0.41***
GZPL	0.06	-0.06	0.17	0.10
GPPL	-0.06	0.27	***0.36***	0.02
GPR	0.01	0.07	***0.47***	0.26
GL	0.28	***-0.36***	0.24	***0.43***
GGR	-0.14	0.08	0.30	0.04
GG	0.16	***-0.32***	0.15	**0.56**
GB	0.29	**-0.48**	0.14	0.12

Continuation of table 1.

Anthropo-somatotypo-logical indicators	Nevi			
	melanocytic simple (n=34)	melanocytic dysplastic (n=27)	melanocytic congenital (n=14)	non-melanocytic (n=17)
GBD	0.28	-0.24	-0.01	0.12
GGL	0.06	**-0.44**	***0.38***	-0.03
FX	***0.30***	**-0.44**	0.27	0.28
MX	0.13	-0.22	0.29	0.20
LX	-0.13	***0.34***	-0.24	***-0.33***
SOMAT	0.15	0.08	-0.17	-0.25
MM	0.11	-0.17	***0.47***	***0.33***
MA	0.04	-0.18	***0.38***	0.26
OM	0.12	-0.03	0.17	0.08
DM	0.21	-0.29	***0.39***	***0.37***

Notes: reliable strong direct correlations are highlighted in red; reliable medium-strength direct correlations are highlighted in orange; unreliable direct correlations of average strength are highlighted in yellow; reliable feedback correlations of medium strength are highlighted in blue; unreliable average strength correlations are highlighted in green.

Discussion

When analyzing the correlations of the *dermatoscopic index with the anthropo-somatotypological* indicators of Ukrainian men with benign nevi, the following multiple reliable and medium-strength unreliable correlations were established:

in men with melanocytic simple nevi, there are only medium-strength direct (r = from 0.30 to 0.34), mostly unreliable, correlations with all dimensions of the pelvis;

in men with melanocytic dysplastic nevi, the inverse of average strength is reliable (r = from -0.38 to -0.52) and unreliable (r = -0.33 and -0.35) correlations with almost all transverse dimensions of the trunk and pelvis, as well as the inverse of average strength is reliable (r = from -0.44 to -0.48) and unreliable (r = -0.32 and -0.36) correlations with almost half the skinfold thickness and the endomorphic component of the somatotype;

in men with melanocytic congenital nevi, there are moderate-strength, unreliable (r = from 0.33 to 0.42) and strong reliable (r = 0.60 and 0.65) correlations with almost all transverse dimensions of the trunk and pelvis, as well as moderate-strength, imprecise (r = from 0.30 to 0.47) correlations with almost half of body girths, skinfold thickness, and almost all and indicators of the component composition of body mass (except bone). The average strength of the unreliable inverse (r = -0.38 and -0.43) correlations with the height of the acromial and trochanteric anthropometric points against the background of the average strength of the unreliable direct (r = 0.37) correlations with the height of the finger anthropometric point attracts attention;

in men with non-melanocytic nevi, straight of medium strength, mostly unreliable (r = from 0.31 to 0.47) correlations with all transverse dimensions of the trunk and pelvis, most girth dimensions of the body, weight, body surface area, muscle component of body weight according to the methods of Matiegka and the American Institute of Nutrition.

When conducting a quantitative analysis of reliable and average strength of unreliable correlations in Ukrainian men with benign nevi between the dermatoscopic index and anthropo-somatotypological indicators, it was established:

in men with melanocytic simple nevi - 6 correlations out of 51 possible (11.76 %), among which 3.92 % of the average strength of direct reliable and 7.84 % of the average strength of direct unreliable ones. The relative majority of correlations is established with the size of the pelvis (75.0 % of the average strength of direct unreliable and 25.0 % of the average strength of direct reliable);

in men with melanocytic dysplastic nevi, there were 17 correlations out of 51 possible (33.33 %), including 5.88 % of the average strength of direct unreliable, 13.73 % of the average strength of inverse reliable and 13.73 % of the average strength of inverse unreliable. The relative majority of connections are established with the transverse dimensions of the pelvis (100 % of the average power of the inverse reliable) and trunk (50.0 % of the average power of the inverse reliable and 25.0 % of the average power of the inverse reliable), skinfold thickness (22.22 % each of the average power of the inverse reliable and unreliable), somatotype components (33.33 % of the average power of the direct unreliable and with portal reliable), longitudinal dimensions of the body (40.0 % of the average strength of direct unreliable);

in men with melanocytic congenital nevi, there are 25 correlations out of 51 possible (49.02 %), among which 39.22 % of the average strength of direct unreliable, 3.92 % of strong direct reliable and 5.88 % of the average strength of reverse unreliable. The relative majority of correlations is established with the transverse dimensions of the pelvis (75.0 % strong direct reliable and 25.0 % average strong direct unreliable) and trunk (75.0 % average strong direct unreliable), somatotype components (75.0 % average strong direct unreliable), girth body dimensions (46.67 % average strong direct unreliable), skinfold thickness (44.44 % average strong direct unreliable), longitudinal dimensions of the body (20.0 % of the average strength of direct unreliable and 40.0 % of the average strength of reverse unreliable);

in men with non-melanocytic nevi, there were 28 correlations out of 51 possible (54.90 %), among which 45.10% of the average strength of direct non-reliable, 5.88 % of the average strength of direct reliable, 1.96 % of strong direct reliable and 1.96 % of the average strength of inverse non-reliable. The relative majority of correlations are established with the transverse dimensions of the pelvis (100 % of the average strength of direct imprecises) and trunk (75.0 % of the average strength of direct imprecises and 25.0 % of the average strength of direct imprecises), girth dimensions of the body (60.0 % of the average strength of direct imprecises, 6.67 % of the average strength of direct imprecises and 6.67% of strong direct reliables), total

dimensions of the body (75.0 % of the average strength of direct unreliable), indicators of the component composition of body mass (50.0 % of the average strength of direct unreliable), longitudinal dimensions of the body (40.0 % of the average strength of direct unreliable).

The connections of such a numerous nature revealed by us in the study are consistent with the generally accepted theory regarding the nature of the occurrence of melanocytic formations, which states that the key mechanism in the initiation and further triggering of the development of this pathology is an excessive amount of adipose tissue, which affects various links of processes in the human body. These are inflammatory processes and processes of vitamin D metabolism, occurrence of tissue hypoxia, etc. Equally important is the proven role of leptin in the pathogenetic chain of melanoma [11].

When examining French women, it was found that there was a positive correlation (RR = 1.27, 95 % CI = 1.05-1.55 for $\geq$164 cm vs.<160 cm; p for trend = 0.02) between height and the risk of melanoma (when models were adjusted for age). At the same time, the relationship with such indicators as body mass index, leg length, waist circumference, and others was not revealed [12].

Growth in childhood can be a prognostic factor for the occurrence of various forms of melanoma. In a study that included more than 2,200 cases of melanoma, data analysis revealed a positive significant relationship between growth in childhood and the occurrence of such forms of melanoma as superficial, nodular, and unspecified [15].

In general, the analysis of literary sources indicates that such an anthropometric indicator as height has a sufficiently strong and proven connection with the risk of melanoma [22]. For example, a meta-analysis that included more than 12,000 cases of melanoma and 23,000 healthy individuals of the control group revealed the existence of a positive relationship between genetically predicted human height and the risk of melanoma (OR 1.08, 95 % CI: 1.02-1.13, per 1 SD (9.27 cm) increase in height) [7]. Another review of the literature, which included almost 5 million controls and 20.000 people with melanoma, found a positive correlation between a 10-cm increase in height and an increased risk of melanoma (RR = 1.46, 95 % CI 1.24 to 1.73; p<0.001) [25].

A review of 44 literature sources revealed that 85 correlations of nevi risk factors with non-genetic factors have been identified so far. Thirteen of them had a sufficiently high level of reliability. Among them, the following deserve special attention: hair color in old age, vitamin D level, presence of actinic keratosis, sunburn, density of freckles, hair color, eye color, skin type, presence of precancerous skin lesions, history of melanoma [2].

C. Fortes [8] and co-authors created a multivariate logistic model to identify differences in external and individual factors affecting the occurrence of melanoma and Spitz nevus. Patients with Spitz tumor compared to melanoma patients were found to have fewer freckles (p = 0.020), fewer common nevi (p = 0.002), lower body mass index (p = 0.001) and fewer episodes of sunburn (p = 0.008).

A team of researchers led by T. C. Grazziotin [9] established a relationship between histological and clinical phenotypes of various types of melanocytic tumors. Thus, the dendritic cell form was more associated with an older age of manifestation and phototype 2, 3, while round cell melanoma was more often observed in individuals with phototype 1.

Analysis of anthropometric data and the number of melanocytic nevi in 573 people established that there is a weak relationship between the body surface area index and the number of melanocytic nevi. No relationships were found for other indicators [14].

Thus, the correlations between the value of the dermatoscopic index and the anthropo-somatotypological indicators established by us in patients with benign nevi of Ukrainian men expand the modern ideas regarding the risk of the occurrence of this disease.

Conclusion

1. During the analysis of multiple reliable and medium-strength unreliable correlations of the dermatoscopic index with anthropo-somatotypological indicators of Ukrainian men with benign nevi, it was established: in patients with melanocytic simple nevi, only with all dimensions of the pelvis (straight of medium strength); in patients with melanocytic dysplastic nevi - reverse of medium strength with almost all the transverse dimensions of the trunk and pelvis and with almost half of the indicators of the skinfold thickness; in patients with melanocytic congenital nevi - straight, mostly of medium strength, with almost all transverse dimensions of the trunk and pelvis and indicators of the component composition of body weight, with almost half of the girth dimensions of the body and indicators of the skinfold thickness; in patients with non-melanocytic nevi - straight, mostly of medium strength, with all transverse dimensions of the trunk and pelvis, most of the total, girth dimensions of the body and the muscle component of body weight according to the methods of Matiegka and the American Institute of Nutrition.

2. As a result of the quantitative analysis of reliable and average strength of unreliable correlations in Ukrainian men with benign nevi, it was established: in patients with melanocytic simple nevi - 11.76 % of correlations (3.92 % of the average strength of direct reliable and 7.84 % of the average strength of direct unreliable); in patients with melanocytic dysplastic nevi - 33.33 % of correlations (5.88 % average strength of direct unreliable, 13.73 % average strength of inverse reliable and 13.73 % average strength of inverse unreliable); in patients with melanocytic congenital nevi - 49.02 % of correlations (39.22 % average strength of direct unreliable, 3.92 % strong direct reliable and 5.88 % average strength of reverse unreliable); in patients with non-melanocytic nevi - 54.90 % of correlations (45.10 % average strength of direct unreliable, 5.88 % average strength of direct reliable, 1.96 % strong direct reliable and 1.96 % average strength of reverse unreliable).

References

[1] Ahnlide, I., Bjellerup, M., Nilsson, F., & Nielsen, K. (2016). Validity of ABCD rule of dermoscopy in clinical practice. *Acta Dermato-venereologica,* 96(3), 367-372. doi: 10.2340/00015555-2239

[2] Belbasis, L., Stefanaki, I., Stratigos, A. J., & Evangelou, E. (2016). Non-genetic risk factors for cutaneous melanoma and keratinocyte skin cancers: an umbrella review of meta-analyses. *Journal of Dermatological Science,* 84(3), 330-339. doi: 10.1016/j.jdermsci.2016.09.003

[3] Bunak, V. V. (1941). *Антропометрия [Anthropometry].* M.: Наркомпрос РСФСР - M.: People's Commissariat of the RSFSR.

[4] Carter, J. L., & Heath, B. H. (1990). *Somatotyping - development and applications*. Cambridge University Press.

[5] Cengiz, F. P., Emiroglu, N., Ozkaya, D. B., Su, O., & Onsun, N. (2017). Dermoscopic features of small, medium, and large-sized congenital melanocytic nevi. *Annals of dermatology,* 29(1), 26-32. doi: 10.5021/ad.2017.29.1.26

[6] Dessinioti, C., Geller, A. C., & Stratigos, A. J. (2022). A review of nevus-associated melanoma: What is the evidence? *Journal of the European Academy of Dermatology and Venereology,* 36(11), 1927-1936. doi: 10.1111/jdv.18453

[7] Dusingize, J. C., Olsen, C. M., An, J., Pandeya, N., Law, M. H., Thompson, B. S., ... & Whiteman, D. C. (2020). Body mass index and height and risk of cutaneous melanoma: Mendelian randomization analyses. International Journal of Epidemiology, 49(4), 1236-1245. doi: 10.1093/ije/dyaa009

[8] Fortes, C., Mastroeni, S., Capuano, M., Ricozzi, I., Bono, R., Ricci, F., ... & Nudo, M. (2022). Differences in individual and environmental factors between cutaneous melanoma and atypical Spitz tumour in children and adolescents. *European Journal of Pediatrics,* 181, 263-269. doi: 10.1007/s00431-021-04204-x

[9] Grazziotin, T. C., Alarcon, I., Bonamigo, R. R., Carrera, C., Potrony, M., Aguilera, P., ... & Puig, S. (2016). Association between confocal morphologic classification and clinical phenotypes of multiple primary and familial melanomas. *JAMA Dermatology,* 152(10), 1099-1105. doi: 10.1001/jamadermatol.2016.1189

[10] Grichnik, J. M., Ross, A. L., Schneider, S. L., Sanchez, M. I., Eller, M. S., & Hatzistergos, K. E. (2014). How, and from which cell sources, do nevi really develop? *Experimental Dermatology,* 23(5), 310-313. doi: 10.1111/exd.12363

[11] Karimi, K., Lindgren, T. H., Koch, C. A., & Brodell, R. T. (2016). Obesity as a risk factor for malignant melanoma and non-melanoma skin cancer. *Reviews in Endocrine and Metabolic Disorders,* 17, 389-403. doi: 10.1007/s11154-016-9393-9

[12] Kvaskoff, M., Bijon, A., Mesrine, S., Vilier, A., Clavel-Chapelon, F., & Boutron-Ruault, M. C. (2014). Anthropometric features and cutaneous melanoma risk: a prospective cohort study in French women. *Cancer Epidemiology*, 38(4), 357-363. doi: 10.1016/j.canep.2014.05.008

[13] Matiegka, J. (1921). The testing of physical efficiency. *Am. J. Phys. Antropol.*, 2(3), 25-38. doi: 10.1002/ajpa.1330040302

[14] McClenahan, P., Jagirdar, K., Lee, K., McEniery, E., Beh, S., Burke, B., ... & Sturm, R. A. (2015). Nevus count and dermoscopic pattern associated with MC1R RHC-variant alleles in a case-control study of melanoma. *Cancer Research,* 75(15_Supplement), 5588. . doi: 10.1158/1538-7445.AM2015-5588

[15] Meyle, K. D., Gamborg, M., Holmich, L. R., & Baker, J. L. (2016). Associations between childhood height and morphologically different variants of melanoma in adulthood. *European Journal of Cancer,* 67, 99-105. doi: 10.1016/j.ejca.2016.08.002

[16] Neves, J. M., Duarte, B., & Lopes, M. P. (2020). Pediatric Melanoma: Epidemiology, Pathogenesis, Diagnosis and Management. *Journal of the Portuguese Society of Dermatology and Venereology,* 78(2), 107-114. doi: 10.29021/spdv.78.2.1197

[17] Orlow, I., Satagopan, J. M., Berwick, M., Enriquez, H. L., White, K. A. M., Cheung, K., ... & Halpern, A. C. (2015). Genetic factors associated with naevus count and dermoscopic patterns: preliminary results from the Study of Nevi in Children (SONIC). *British Journal of Dermatology,* 172(4), 1081-1089. doi: 10.1111/bjd.13467

[18] Potekayev, N. N., Shuginina, Y. K., Kuzmina, T. S., & Arutyunyan, L. S. (2011). *Дерматоскопия в клинической практике. Руководство для врачей [Dermatoscopy in clinical practice. A guide for doctors].* M: МДВ, 144 - M: MDV, 144.

[19] Rousi, E. K., Kallionpää, R. A., Kallionpää, R. E., Juteau, S. M., Talve, L. A., Hernberg, M. M., ... & Koskivuo, I. O. (2022). Increased incidence of melanoma in children and adolescents in Finland in 1990-2014: nationwide re-evaluation of histopathological characteristics. *Annals of Medicine*, 54(1), 244-252. doi: 10.1080/07853890.2022.2026001

[20] Shephard, R. J. (2005). *Body composition in biological anthropology.* Cambridge University Press, Cambridge, UK; New York. https://www.nhbs.com/body-composition-in-biological-anthropology-book

[21] Shields, C. L., Dalvin, L. A., Ancona-Lezama, D., Michael, D. Y., Di Nicola, M., Williams Jr, B. K., ... & Shields, J. A. (2019). Choroidal nevus imaging features in 3,806 cases and risk factors for transformation into melanoma in 2,355 cases: the 2020 Taylor R. Smith and Victor T. Curtin Lecture. *Retina,* 39(10), 1840-1851. doi: 10.1097/IAE.0000000000002440

[22] Vena, G. A., Cassano, N., Caccavale, S., & Argenziano, G. (2019). Association between melanoma risk and height: a narrative review. *Dermatology Practical & Conceptual,* 9(2), 82-89. doi: 10.5826/dpc.0902a02

[23] Yang, C., Gru, A. A., & Dehner, L. P. (2018). Common and not so common melanocytic lesions in children and adolescents. *Pediatric and Developmental Pathology,* 21(2), 252-270. doi: 10.1177/1093526617751720

[24] Yeh, I. (2020). New and evolving concepts of melanocytic nevi and melanocytomas. *Modern Pathology,* 33, 1-14. doi: 10.1038/s41379-019-0390-x

[25] Yu, D. J., Li, X. J., Morice, A., Wu, L. J., Sun, W., & Zhao, T. L. (2018). Height and risk of melanoma: a systematic review and meta-analysis. *Int. J. Clin. Exp. Med.,* 11(5), 4426-4435.

КОРЕЛЯЦІЇ ДЕРМАТОСКОПІЧНОГО ІНДЕКСУ З АНТРОПОМЕТРИЧНИМИ ТА СОМАТОТИПОЛОГІЧНИМИ ПАРАМЕТРАМИ ЧОЛОВІКІВ ІЗ ДОБРОЯКІСНИМИ НЕВУСАМИ

Хаддад Н. Б. Ю., Чайка Г. В., Кириченко І. М., Шаповал О. М., Дроненко В. Г.

Злоякісна трансформація доброякісних невусів є одним із тих факторів, що зумовлює підвищений науковий інтерес до вивчення патогенезу їх виникнення, впливу на них зовнішніх факторів тощо. Одним з нерозкритих досі питань, є питання вивчення зв'язку між особливостями показників невусів та антропометричними параметрами тіла людини. Мета роботи - дослідити особливості кореляцій дерматоскопічного індексу з антропетричними та соматотипологічними показниками українських чоловіків, хворих на доброякісні невуси. Проведено клініко-лабораторне та патогістологічне обстеження 34

українських чоловіків першого зрілого віку з меланоцитарними доброякісними простими невусами, 27 - з меланоцитарними доброякісними диспластичними невусами, 14 - з меланоцитарними доброякісними вродженими невусами, 17 - з немеланоцитарними доброякісними невусами. Дерматоскопічний індекс розраховували згідно "ABCD правилу дерматоскопії". Антропометричне обстеження проведено відповідно до схеми Бунака. Для оцінки соматотипа використовували математичну схему Heath-Carter. Для обрахування жирового, кісткового та м'язового компонентів маси тіла використовували формули Matiegka. М'язовий компонент маси тіла оцінювали за методом Американського інституту харчування. Оцінку кореляцій між дерматоскопічним індеском і параметрами тіла проведено в ліцензійному пакеті "Statistica 6.0" з використанням непараметричного методу Спірмена. Проведений аналіз множинних достовірних та середньої сили недостовірних кореляцій між величиною дерматоскопічного індексу та антропо-соматотипологічними показниками у чоловіків, хворих на доброякісні невуси. У чоловіків з меланоцитарними простими невусами встановлені лише середньої сили прямі (r = від 0,30 до 0,34), переважно недостовірні, зв'язки з усіма розмірами таза. У чоловіків з меланоцитарними диспластичними невусами встановлені зворотні середньої сили, переважно достовірні (r = від -0,38 до -0,52) зв'язки з усіма розмірами таза та практично усіма поперечними розмірами тулуба, а також майже з половиною показників товщини шкірно-жирових складок. У чоловіків з меланоцитарними вродженими невусами встановлені прямі, переважно середньої сили недостовірні (r = від 0,30 до 0,47) зв'язки з усіма розмірами таза, практично усіма поперечними розмірами тулуба, майже з половиною обхватних розмірів тіла та показників товщини шкірно-жирових складок і практично з усіма показниками компонентного складу маси тіла. У чоловіків з немеланоцитарними невусами встановлені прямі, переважно середньої сили недостовірні (r = від 0,30 до 0,47) зв'язки з усіма поперечними розмірами тулуба й таза, більшістю тотальних й обхватних розмірів тіла. Також проведений кількісний аналіз достовірних та середньої сили недостовірних кореляцій між величиною дерматоскопічного індексу та антропо-соматотипологічними показниками. Встановлені особливості кореляцій розширюють сучасні уявлення щодо ризику виникнення доброякісних невусів.

Ключові слова: *захворювання шкіри, доброякісні невуси, дерматоскопічний індекс, антропометричні та соматотипологічні параметри тіла, кореляції, чоловіки.*

DOI: 10.31393/morphology-journal-2023-29(3)-02 Reports of Morphology, Vol. 29, №3, Pages 12-19

ISSN 1818-1295 eISSN 2616-6194

REPORTS OF MORPHOLOGY

Official Journal of the Scientific Society of Anatomists, Histologists, Embryologists and Topographic Anatomists of Ukraine

journal homepage: https://morphology-journal.com

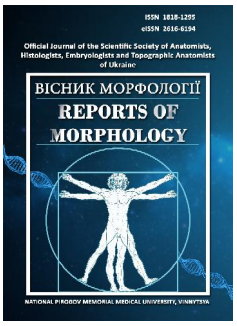

Changes in markers of collagen metabolism in the blood serum of white rats during the filling of femur defects with implants based on polylactide and tricalcium phosphate with allogeneous mesenchymal stem cells

Gontar N. M.

Educational and Scientific Institute of Postgraduate Education of the Kharkiv National Medical Institute, Kharkiv, Ukraine

ARTICLE INFO

Received:11 April 2023

Accepted: 15 May 2023

UDC: 616.71-003.93-089.843:611.018.54:611.018-08

CORRESPONDING AUTHOR

e-mail: gontarnazar@ukr.net

Gontar N. M.

CONFLICT OF INTEREST

The authors have no conflicts of interest to declare.

FUNDING

The work was carried out using the funds of the state budget of Ukraine.

The use of synthetic materials in combination with osteogenesis stimulators is one of the advanced directions of the development of traumatology. The purpose of the study: based on the analysis of biochemical markers of collagen metabolism in the blood serum of laboratory rats with a femur defect, to evaluate the course of bone remodeling after filling the defect with implants based on polylactide and tricalcium phosphate with simultaneous and delayed administration of allogeneic mesenchymal stem cells (MSCs). On the model of a defect in the metaphysis of the femur in white rats, the indicators of collagen exchange in blood serum were studied: the content of protein-bound, free fractions, the amount of hydroxyproline (HOP), the ratio of the content of protein-bound HOP to free PB/F was calculated. Comparison of the results of different groups was performed using the Student-Fisher method. The difference was considered statistically significant if p<0.05. Filling the defect with implants led to a decrease in the content of protein-bound HOP by 16.69 % and 14.34 % on the 15th and 90th days (p<0.05), an increase in the content of free HOP by 74.96 %; 67.31 % and 56.74 % (p<0.001), the content of the amount of HOP by 25.37 %; 23.66 % and 18.28 % (p<0.05), and reduction of PB/F by 52.20 %; 49.90 % and 45.30 % (p<0.001) relative to intact on the 15th; 30th and 90th days. Addition of MSCs to the implants at the same time as the installation caused a decrease in the content of free HOP by 63.90 %; 54.63 % and 42.76 % on the 15th; on the 30th and 90th days (p<0.001), the total metabolite by 21.87 % and 18.58 % on the 15th and 30th days (p<0.05) and a decrease in PB/F by 47, 50 %; 43.20 %; 37.60 % on the 15th; on the 30th and 90th days (p<0.001) relative to the intact. Postponing the introduction of MSCs increased the content of free HOP by 40.48 % (p<0.001); 20.49 % and 16.58 % (p<0.05) with a lower PB/F by 38.20 %; 25.80 % and 23.40 % (p<0.05) on the 15th; 30th and 90th days relatively intact. When the defect was filled with implants without MSCs, a moderate inhibition of anabolism and rapid activation of collagen destruction was observed. With the simultaneous use of implants and MSCs, the rate of formation and intense destruction of collagen was observed. When the introduction of MSCs was delayed, a moderate rate of destruction was recorded, which most contributed to collagen metabolism.

Key words: *defect, implant, mesenchymal stem cell, regeneration, hydroxyproline.*

Introduction

Half of all orthopedic operations require bone grafting for the successful treatment of bone defects resulting from trauma, tumor, infection or congenital deformity [2]. Large diaphyseal defects of long bones of critical size are by definition considered incapable of spontaneous healing and, therefore, require surgical intervention [7]. Violation of consolidation is often associated with an imbalance of the opposite action of osteoblasts and osteoclasts [1].

Although autografts are still considered the gold standard in the treatment of fusion disorders, their limited volume and disruption of the donor site necessitated the development of alternative methods, such as tissue engineering based on scaffolds. In particular, scaffolds made of polycaprolactone and tricalcium phosphate (PCL-

TCP) demonstrated decent biocompatibility and osteoconductivity with biomechanical strength in animal experiments [11].

Advances in the field of bone tissue engineering have led to a constant increase in the use of artificial frameworks [10, 15, 20]. However, the properties of the new products are far from optimal, in particular, the low rate of bone growth in them and side effects were reported [10]. To overcome these limitations, biohybrid bone grafts are used, which combine the mechanical properties of synthetic polymers and biologically active elements of natural polymers or minerals. It should be noted that there were attempts to use calcium phosphate/poly-?-caprolactone particles [16] and poly(N-acryloyl-2-glycine)/methacrylate-gelatin hydrogel [9].

Over the last decade, the main efforts have been focused on the development of innovative bone substitutes that not only provide immediate mechanical support, but also proper fixation of the graft, for example, promoting the formation of new bone tissue [19]. A successful example of clinical use is a bovine bone mineral matrix reinforced with a resorbable poly(lactate-co-caprolactone) block copolymer that incorporates collagen fragments into its surface (SmartBone ®, IBI) [8].

A new stage in the development of a bioengineering approach for bone healing is the use of mesenchymal stem cells (MSCs) in combination with biomaterials. At the same time, an additional stage of multiplication, concentration and activation of cells in vitro is possible, which entails numerous risks and costs. It should be noted that this stage can significantly increase positive therapeutic results when properly planned [19].

The use of 3D printing in bone grafts is becoming more and more important, which allows treating bone defects thanks to the creation of porous frameworks with sufficient mechanical strength and a favorable macro- and microstructure [3].

The purpose of the study is to evaluate the course of bone remodeling after filling the defects with printed implants based on polylactide and tricalcium phosphate with simultaneous and delayed introduction of allogeneic mesenchymal stem cells, based on the analysis of biochemical markers of collagen metabolism in the blood serum of laboratory rats with femur transcortical defects of critical size.

Materials and methods

Work with animals. The article was carried out with the funds of the state budget of Ukraine, the research was carried out as part of the Scientific Research Work of the State Institution "Sytenko Institute of Spine and Joint Pathology National Academy of Medical Sciences of Ukraine" "To study the mechanisms of optimization of bone regeneration depending on the age of the recipient in the case of using allogeneic bone implants in combination with mesenchymal stromal cells and biologically active factors of blood plasma" (2020-2022) Subject code CF.2020.2.NAMNU (fundamental), № state registration 0119U102341.

When conducting research, the requirements of humane treatment of experimental animals established in the Law of Ukraine "On the Protection of Animals from Cruelty Treatment" (№ 3447-IV dated 21.02.2006) and the European Convention "On the Protection of Vertebrate Animals Used for Research and other scientific goals" (Strasbourg, March 18, 1986) [5, 6, 17]. The plan of experimental research was approved by the Bioethics Committee of the State Institution "Sytenko Institute of Spine and Joint Pathology National Academy of Medical Sciences of Ukraine" (protocol № 217 of 14.06.2021).

In study used 53 non-linear white rats from the population of the experimental biological clinic of the institute, aged 5-6 months and with a body weight of 200-260 g at the beginning of the experiment, males (groups intact, control and Experiment I), females (group Experiment II). The animals were randomly divided into groups: intact - 5 animals, control - 15 animals, Experiment I - 15 animals and Experiment II - 15 animals. 3 rats were used to obtain allogeneic MSCs.

In the rats of the control group, Experiment I and Experiment II groups, under general anesthesia (ketamine, 50 mg/kg of body weight, intramuscularly), a transcortical defect of the femur of a critical size (diameter 2.6 mm, depth 3 mm) was created. A critical size defect is considered to be a size defect that does not heal on its own throughout the life of the animal or the duration of the experiment [18]. The minimum size of a critical defect for the zone of the distal metaphysis of the femur of laboratory rats is considered to be 2.5 mm in diameter and depth [21]. The defect in these groups of animals was filled with a 1.75 mm polylactide (PL) tricalcium phosphate (TCP) composite suture made by mixing 60 % PL granules and 40 % mineral compound (20 % PL + 80 % TCP), heating and extrusions on the 3D printer "Easy3DPrint" with an extruder (printing technology using composite filament welding) on the basis of the limited liability company "Easy 3D Print 3D Printing Studio", Kharkiv, Ukraine. PL granules (L-polylactide, manufactured in China) and compound granules (TCP medical, diameter 10 μm, manufactured in China) were used in the manufacture of the composite thread. Structure: implants: internal - a frame made of interweaves of composite thread forming vertical and horizontal channels (pore size is 300 μm, porosity 45 %); external - cylinders with a diameter of 2.5 mm and a length of 30 mm. For this experiment, the cylinders were mechanically divided into 3 mm long fragments.

Before the introduction of groups Experiment I and Experiment II, the implants were impregnated with 0.5 ml of culture medium with approximately 10^6 MSCs. Additionally, using a syringe, approximately 10^6 MSCs in 0.5 ml of medium were injected into the area of the defect: to the animals of the Experiment I group simultaneously

with the introduction of implants, and to the animals of the Experiment II group - with a delay of 7 days. After the intervention, the wound was sutured in layers and treated with *Betadin*® antiseptic (EGIS Pharmaceutical Plant, Hungary). Animals were taken out of the experiment on the 15th, 30th, and 90th days of the experiment, 5 animals from the group for each term by decapitation in conditions of an overdose of ether anesthesia. During the experiment, blood was taken for biochemical studies.

Allogeneic MSCs were obtained by culturing active cells from the omentum of 3 white rats on the basis of the Department of Transplantology of the Sytenko Institute of Spine and Joint Pathology of the National Academy of Medical Sciences of Ukraine.

Biochemical research. The research was carried out in the department of laboratory diagnostics and immunology and the laboratory of clinical diagnostics of SI "Sytenko Institute of Spine and Joint Pathology National Academy of Medical Sciences of Ukraine" (Certificate of compliance of the measurement system with the requirements of DSTU ISO 10012:2005 № 01-0019/2019 dated February 8, 2019, valid until February 8, 2021). Serum was separated from the obtained blood by centrifugation at 1500 rpm for 30 minutes and fractional analysis of hydroxyproline (HOP) was performed in it. The content of fractions of protein-bound free HOP, as well as the total content of the metabolite, was determined by the reaction of oxidative polycondensation with paradimethylbenzaldehyde in the presence of the oxidizing agent chloramine followed by photoelectrocolorimetry (Krel-Furtseva method) [14]. A KFK-3 photoelectrocolorimeter was used to record optical density indicators.

In addition, the ratio of the content of protein-bound and free fractions of HOP in blood serum was calculated.

Statistical methods. The obtained results were processed statistically using the programs "IBM SPSS Statistics 20" and "Microsoft Office Excel 2007". Measurement results are presented as mean value ± standard error. The results of different groups were compared using the Student-Fisher method. The difference was considered statistically significant under the condition of $p<0.05$ [12].

Results

Control group, *15 day*

On the 15th day of the study, in animals of the control group, in which the transcortical defect of a critical size was filled only with a printed allograft, a decrease in the content of the protein-bound fraction of HOP in the blood serum of the control group of rats was established by 16.69 % with a parallel increase by 74.96 % content of free HOP fraction in blood serum and total HOP content by 25.37 % (Table 1, Fig. 1). This is characteristic of the state of excess activity of catabolic processes over anabolic ones and may indicate the breakdown of a part of collagen in the loci of connective tissue bordering the defect zone with slow, low-activity restoration of collagen structures, provided new bone is built.

30 day

When analyzing the changes in the biochemical parameters of the laboratory rats of the control group on the 30th day of the experiment, a change in the parameters of collagen metabolism similar to the previous period of the study was established. Thus, on the 30th day, a 67.31 % increase in the content of the free HOP fraction was recorded in the blood serum of control animals with a parallel increase in total HOP by 23.66 % and a corresponding decrease in the ratio of protein-bound and free HOP fractions by 49.90 % (Table 1, Fig. 2). Accordingly, this term was also probably

Table 1. Indicators of collagen metabolism in blood serum of laboratory rats with transcortical femur defect of critical size with different types of defect filling in dynamics (M±m).

Group	Indicators			
	protein-bound HOP (g/l)	free HOP (g/l)	total HOP (g/l)	HOP PB/F
Intact group	7.250±0.140	6.150±0.150	13.40±0.25	1.180±0.028
Control group, 15 days (n=5)	6.043 0.122 -16.69 %[1)6)]	10.76±0.24 +74.96 %[1)8)]	16.80±0.14 +25.37 %[1)8)]	0.564±0.022 -52.20 %[1)8)]
Control group, 30 days (n=5)	6.282±0.151 -13.38 %[1)5)] +3.98 %[4)5)]	10.29±0.17 +67.31 %[1)8)] -4.37 %[4)5)]	16.57±0.27 +23.66 %[1)7)] -1.40 %[4)5)]	0.591±0.018 -49.90 %[1)8)] +4.79 %[4)5)]
Control group, 90 days (n=5)	6.213±0.131 -14.34 %[1)6)] -1.12 %[4)5)]	9.64±0.16 +56.74 %[1)8)] -6.32 %[4)5)]	15.85±0.16 +18.28 %[1)6)] -4.30 %[4)5)]	0.645±0.020 -45.30 %[1)8)] +9.14 %[4)5)]
experiment I, 15 days (n=5)	6.252±0.144 -13.79 %[1)5)] +3.48 %[2)5)]	10.08±0.15 +63.90 %[1)8)] -6.32 %[2)5)]	16.33±0.28 +21.87 %[1)7)] -2.80 %[2)5)]	0.620±0.007 -47.50 %[1)8)] +9.90 %[2)5)]
experiment I, 30 days (n=6)	6.381±0.163 -12.00 %[1)5)] +1.59 %[2)5)] +2.00 %[4)5)]	9.512±0.164 +54.63 %[1)8)] -7.58 %[2)5)] -5.70 %[4)5)]	15.89±0.33 +18.58 %[1)6)] -4.10 %[2)5)] -2.69 %[4)5)]	0.670±0.006 -43.20 %[1)8)] +3.88 %[2)5)]) +8.07 %[4)5)]
experiment I, 90 days (n=6)	6.452±0.154 -11.03 %[1)5)] +3.86 %[2)5)] +1.98 %[4)5)]	8.783±0.152 +42.76 %[1)8)] -8.92 %[2)5)] -7.68 %[4)5)]	15.23±0.18 +13.66 %[1)5)] -3.91 %[2)5)] -4.15 %[4)5)]	0.736±0.023 -37.60 %[1)8)] +14.11 %[2)6)] +9.86 %[4)5)]
experiment II, 15 days (n=5)	6.302±0.131 -13.10 %[1)5)] +4.30 %[2)5)] +0.80 %[3)5)]	8.643±0.182 +40.48 %[1)8)] -19.71 %[2)7)] -14.29 %[3)6)]	14.94±0.30 +11.49 %[1)5)] -11.07 %[2)5)] -8.51 %[3)5)]	0.729±0.010 -38.20 %[1)8)] +29.30 %[2)7)] +17.60 %[3)6)]
experiment II, 30 days (n=5)	6.482±0.171 -10.62 %[1)5)] +3.18 %[2)5)] +1.57 %[3)5)] +2.86 %[4)5)]	7.412±0.154 +20.49 %[1)7)] -27.99 %[2)7)] -22.08 %[3)7)] -14.24 %[4)6)]	13.89±0.20 +3.66 %[1)5)] -16.17 %[2)6)] -12.59 %[3)5)] -7.03 %[4)5)]	0.876±0.031 -25.80 %[1)7)] +48.22 %[2)8)] +30.70 %[3)8)] +20.17 %[4)6)]
experiment II, 90 days (n=6)	6.482±0.151 -10.62 %[1)5)] +4.35 %[2)5)] +0.47 %[3)5)] 0.00 %[4)5)]	7.173±0.142 +16.58 %[1)6)] -25.62 %[2)7)] -18.34 %[3)6)] -3.24 %[4)5)]	13.65±0.29 +0.07 %[1)5)] -13.88 %[2)5)] -10.37 %[3)5)] -1.73 %[4)5)]	0.904±0.007 -23.40 %[1)6)] +60.28 %[2)8)] +22.83 %[3)7)] +3.20 %[4)5)]

Notes: [1)] - in relation to the parameters of the intact group of rats; [2)] - in relation to the parameters of the control group of rats of the same term; [3)] - in relation to the group of rats Experiment I of the same term; [4)] - in relation to the parameters of the same group of the previous term of the experiment; [5)] - $p>0.05$; [6)] - $p<0.05$; [7)] - $p<0.01$; [8)] - $p<0.001$.

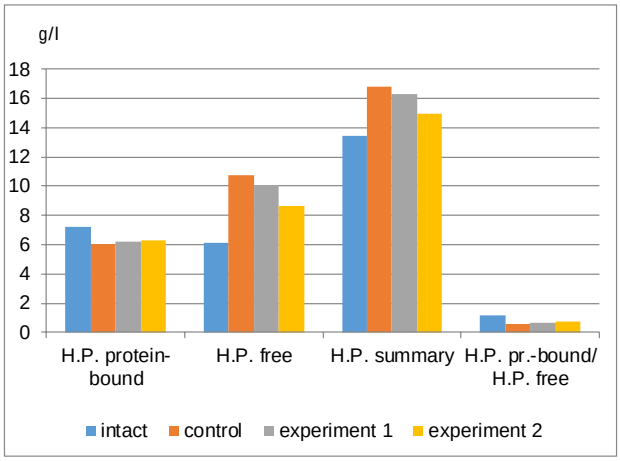

Fig. 1. The content of HOP in the blood serum of experimental animals on the 15th day of the experiment.

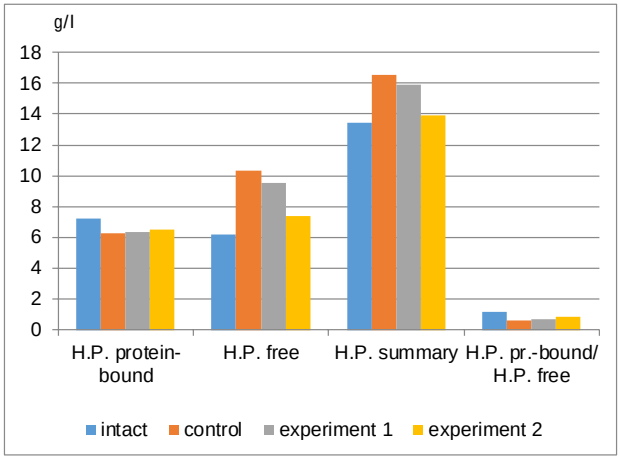

Fig. 2. The content of HOP in the blood serum of experimental animals on the 30th day of the experiment.

characterized by the predominance of the processes of destruction of the damaged collagen network over the formation of a newly constructed collagen structure. Such a situation is possible, in particular, under the condition of the destruction of the affected areas of the bone adjacent to the defect zone, under conditions of insignificant activity of the formation of new bone tissue.

90 day

On the 90th day of the experiment, rats of the control group showed not only an increase in the content of the free HOP fraction in blood serum by 56.74 % and total HOP by 18.28 %, with a simultaneous decrease in the ratio of the protein-bound and free fractions of this metabolite by 45.30 %, but also a significant decrease by 14.34 % in the content of the protein-bound fraction of HOP in blood serum (Table 1, Fig. 3). This confirms the assumption that structural transformations (maturation) of collagen fibers subside against the background of rather high activity of collagen destructive processes.

Experiment group I, *15 day*

When analyzing the results of the biochemical examination of laboratory rats of Experiment I group, in which the defect was filled with printed implants based on polylactide and tricalcium phosphate with the simultaneous introduction of mesenchymal stem cells, a significant distortion attracted attention, namely, an increase in the content of free HOP in the blood serum by 63.90 % and due to this - the total metabolite - by 21.87 % (Table 1, Fig. 1). The ratio of the content of protein-bound and free fractions of HOP in blood serum decreased by 43.20 % relative to the data of the intact group of animals. This indicated a significant activation of the destruction of the collagen network against the background of relative suppression of the formation of new collagen structures, which serves as the organic basis of bone tissue and is necessary for the beginning of mineralization of bone tissue during its formation at the site of the lesion. There was no significant difference between the indicators of collagen metabolism of this experimental group and similar indicators of the control group of animals of the same period of the experiment.

30 day

In experimental rats with printed implants based on PL and TCP with simultaneous administration of MSCs on the 30th day, an increase in the content of the free HOP fraction in the blood serum of laboratory animals by 54.63 % and due to this, total HOP by 18.58 % was observed (Table 1, Fig. 2), which indicates the active destruction of collagen structures, probably in the area of bone tissue damage, and inhibition of the formation of a new collagen network, which was accelerated under the conditions of the use of mesenchymal stem cells in the early stages of the regeneration process, compatible with printed implants based on PL and TCP.

90 day

When analyzing the results of the biochemical examination of laboratory animals of the group with printed implants based on PL and TCP with the simultaneous addition of MSCs on the 90th day, an excess of the content of the free fraction of HOP in blood serum was determined by 42.76 % when compared with a similar indicator of the group of intact animals in the absence of reliable of discrepancies with the data of the comparison group according to the content of the protein-bound fraction of the metabolite. As a result, the ratio of the content of protein-bound and free fractions of HOP in the blood serum was also reduced by 37.60 %, which indicates a significant activation of the destruction of the existing collagen network with slow and non-scale formation of new collagen formations (Table 1, Fig. 3).

It should also be noted a 14.11 % increase in the ratio of the content of protein-bound and free fractions of HOP in the blood serum of laboratory rats with printed implants based on PL and TCP and the simultaneous administration of MSCs compared to the data of the control group, which indicates an even small, but still the predominance of anabolic processes in the collagen system over catabolic ones (Table 1, Fig. 3).

There were no significant differences between the

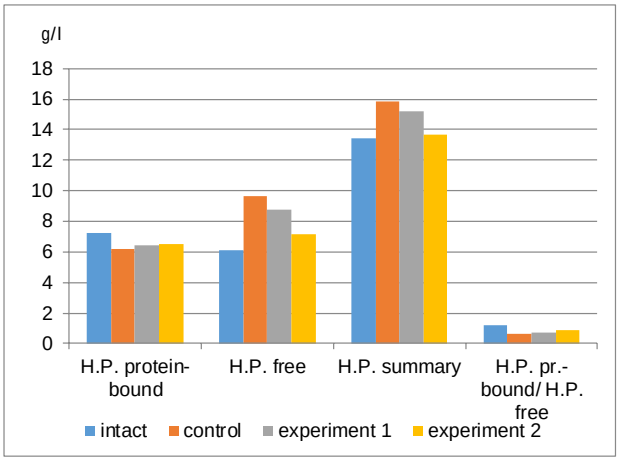

Fig. 3. The content of HOP in the blood serum of experimental animals on the 90th day of the experiment.

collagen metabolism indicators of this experimental group (90 days) and the previous period of the experiment (30 days).

Experiment group II, *15 day*

During the analysis of biochemical indicators in a group of laboratory rats in which the defect was filled with printed implants based on PL and TCP with a delayed introduction of MSCs (which distinguishes this group from the group of Experiment I), on the 15th day of the experiment, an excess in the content of the free HOP fraction in the serum was determined blood by 40.48 % relative to the similar indicator of intact animals. This level, however, was 19.71 % lower than the corresponding indicators in animals of the control group, in which the defect was filled with similar implants without MSCs. It was also 14.21 % inferior to rats in the group with the simultaneous use of printed implants of a similar composition and MSCs also on the 15th day of the experiment.

Similar changes, but with the opposite sign, were recorded in relation to the ratio of the content of protein-bound and free fractions of HOP in blood serum. Thus, when compared with the data of intact animals, the PB/F index was inferior by 38.20 %, relative to the indicators of the control group on the 15th day of the experiment - it exceeded by 29.30 %, and relative to the indicators of the group of rats in which the defect was simultaneously filled with printed implants and MSCs in the same period of the experiment, was also higher by 17.60% (Table 1, Fig. 1). This indicates that the use of mesenchymal stem cells with a delay had a significantly more favorable effect on bone tissue remodeling than the treatment of a similar defect without MSCs at all, or in the conditions of using mesenchymal stem cells simultaneously with the introduction of implants.

30 day

When considering the indicators of collagen metabolism in the conditions of using printed implants based on PL and TCP with delayed introduction of MSCs on the 30th day, it was found that the content of the protein-bound fraction of HOP in the blood serum of this experimental group of animals remained at an unchanged level (Table 1). The content of the free fraction of HOP in the blood serum of laboratory animals showed greater lability and exceeded that of intact animals by 20.49 %, and was inferior to control animals and laboratory rats treated with printed implants with simultaneous administration of MSCs for the same period by 27.99 % and 22.08 %, respectively. On the 30th day of the experiment, the content of the free HOP fraction decreased by 14.24 % (Table 1, Fig. 2). The total content of HOP in the blood serum of experimental animals changed slightly and was only significantly lower (by 16.17 %) compared to the indicators of control animals during the same period of observation. As a result, the ratio of the content of protein-bound and free fractions of HOP in the blood serum of the considered group of animals was 25.80 % lower than that of intact rats, but exceeded the indicators of control animals and laboratory rats with printed implants and simultaneous administration of MSCs on similar term of the experiment: by 48.22 % and 30.70 %, respectively. An increase in the PB/F index was established (by 20.17 %) compared to the group of rats of the previous period of the study (Table 1, Fig. 2).

90 day

When studying the results of biochemical parameters of blood serum in laboratory rats with printed implants based on PL and TCP and the delayed introduction of MSCs on the 90th day, an excess of the free HOP fraction in the blood serum of the level in intact animals was recorded by 16.58 %. At the same time, according to this parameter, the considered group of animals was significantly inferior to the control animals from the group treated with printed implants with the simultaneous use of MSCs, by 25.62 % and 18.34 %, respectively (Table 1, Fig. 3). Against this background, the ratio of protein-bound and free fractions of HOP in blood serum was 23.40 % lower than that in intact animals (Table 1, Fig. 3). The animals of the control group and the group with printed implants with the simultaneous use of MSCs exceeded this indicator by 60.28 % and 22.83 %, respectively (Table 1, Fig. 3). Based on these results, it can be assumed that the delayed use of MSCs, compatible with the filling of the defect with implants based on PL and TCP, led to more favorable results for the biosynthesis and accumulation of collagen, which constitutes the organic basis for the formation of new bone tissue, particularly in the defect area.

Discussion

In general, printed implants based on PL and TCP showed good biocompatibility, which corresponds to the data of P. Kobbe et al. (2020), who tested bioscaffolds based on TCP in combination with PCL [11].

One of the common features in all studied groups of animals was an increase in markers of catabolic processes in the collagen system, the role of which in this study was performed by the content of the fraction of free HOP in the blood serum of laboratory rats. This property is a

consequence of the activation of collagen destruction near the bone defect zone as a result of disruption of metabolic processes, destruction of blood vessels, swelling, inflammation and other pathological processes. The degree of destruction of the collagen network in general gradually decreased and differed in each individual group. The greatest manifestation of the marker of collagen destruction was recorded in the group of animals whose defect was filled with a printed implant based on PL and TCP with simultaneous administration of MSCs. In this group, the most acute reaction to implantation was observed, especially in the first control period, the 15th day after surgery. Administration of MSCs delayed for 7 days led to a significantly lower manifestation of the biochemical marker of collagen destruction, which especially distinguished the indicated groups on the 15th and 30th days. It should also be noted: with this treatment regimen, the content of free HOP was lower in comparison with the control group, which indicates favorable conditions for faster restoration of the appropriate environment in the bone around the defect zone. In a similar way, the content and amount of the metabolite changed due to the content of fractions of free HOP. This coincides with the data of I. Sallent and co-authors (2020), which indicate the use of stem cells in combination with biomaterials. In most clinical studies, this combination has been shown to be similar to or superior to the clinical results of using autografts [19].

The dynamics of the ratio between the content of the protein-bound fraction of HOP, which characterizes anabolic processes in the collagen system, and the free metabolite, which characterizes catabolic processes, is interesting. In all groups with pathology, a sharp decrease in this ratio was observed, indicating the predominance of collagen catabolism and a gradual improvement as the study period extended. The worst results were recorded in rats in which the bone defect was filled without MSCs and confirms the data of H. J. Haugen and co-authors (2019) about the insufficient active ingrowth of bone tissue to bioscaffolds without cell therapy [10].

Rats that were treated with the studied implant simultaneously with allogeneic MSCs to fill the defect differed little in the studied parameters of collagen metabolism from the animals of the control group, which means that the use of MSCs simultaneously with the introduction of the implant did not lead to positive consequences in the restoration of collagen structures. At the same time, a delay of 7 days led to a shift in the balance of metabolic processes in the collagen system towards anabolism, as evidenced by the values of this indicator close to those of intact animals, which, in general, confirms the positive effect of cell therapy based on MSCs in the treatment fractures when certain physiological conditions of natural processes are met [19]. This indicates that in order to create optimal conditions for the development of regenerative processes in the damaged bone, it is advisable to use MSCs as stimulators of new bone formation, possibly due to the reduction of inflammation of immune genesis in the first days and days after the damage. This is confirmed by the relation to this problem of Y. Chen et al. (2020) [4], who believe that disruption of local healing conditions can cause delayed regeneration, non-union or form a persistent bone defect. At the same time, according to H. Lin and co-authors (2019), the mechanism of action of MSCs can be direct differentiation into bone cells, attraction and recruitment of other cells, or creation of a regenerative environment due to the production of trophic growth factors [13].

The use of the method proposed by the author will significantly expand the prospects and increase the effectiveness of bone plastic surgery in case of significant bone defects, which is definitely important in the conditions of both combat trauma and planned orthopedics.

Conclusions

1. When filling a transcortical defect of a critical size in the femur of white rats with printed implants based on PL and TCP, a moderate inhibition of anabolic processes in the collagen system and a rapid activation of the destruction of the collagen network with a decrease in the content of the protein-bound HOP fraction in the blood serum of laboratory animals were observed in the early stages of the experiment with a significant increase in the content of the fraction of free HOP, which decreased during the experiment with a parallel increase in the ratio of the content of protein-bound HOP to the free metabolite.

2. In the conditions of filling the defect with printed implants based on PL and TCP with the simultaneous introduction of allogeneic MSCs, the rate of formation of collagen structures was established unchanged in the case of rather intensive processes of collagen destruction, as evidenced by high values of the fraction of free HOP in the blood serum of rats, which corresponded to those of the control group , as well as low indicators of the content ratio of protein-bound and free HOP fractions.

3. Postponing the introduction of allogeneic MSCs for 7 days when filling a defect in the femur with printed implants based on PL and TCP led to unchanged markers of collagen formation with a moderate acceleration of the destruction of collagen structures, as evidenced by only a slight increase in the content of the free HOP fraction in the blood serum. which was significantly inferior to that in the previously considered groups and the value of the ratio of the content of protein-bound to free HOP, which at the end of the experiment approached the indicator of intact animals.

4. Of the investigated options for filling a transcortical defect of a critical size of the femur, the most favorable effect on collagen metabolism was established when using printed implants based on PL and TCP with a 7-day delay in the introduction of MSCs.

Acknowledgments. The author expresses his gratitude to the senior researcher of the laboratory of experimental modeling of the State Institution "Sytenko Institute of Spine

and Joint Pathology National Academy of Medical Sciences of Ukraine" candidate of biological sciences O. A. Nikolchenko for participating in the performance of experimental operations, T. I. Gulida - junior researcher an employee of the department of laboratory diagnostics and immunology of the institute for carrying out biochemical research, K. M. Samoilova - junior researcher of the laboratory of experimental modeling of the institute and O. V. Maiboroda - junior researcher of the department of transplantology of the institute, who provided technical support in the preparation of allografts.

References

[1] Ambrosi, T. H., Marecic, O., McArdle, A., Sinha, R., Gulati, G. S., Tong, X. … & Chan, C. K. F. (2021). Aged skeletal stem cells generate an inflammatory degenerative niche. *Nature,* 597, (7875), 256-262. doi: 10.1038/s41586-021-03795-7

[2] Bracey, D. N., Cignetti, N. E., Jinnah, A. H., Stone, A. V., Gyr, B. M., Whitlock, P. W. & Scott, A. T. (2020). Bone xenotransplantation: A review of the history, orthopedic clinical literature, and a single-center case series. *Xenotransplantation,* 27 (5), e12600. doi: 10.1111/xen.12600

[3] Brachet, A., Belzek, A., Furtak, D., Geworgjan, Z., Tulej, D., Kulczycka, K. … & Baj, J. (2023). Application of 3D Printing in Bone Grafts. *Cells,* 12(6), 859. doi: 10.3390/cells12060859

[4] Chen, Y., Lin, J., Yu, Y. & Du X. (Eds.) (2020). Role of mesenchymal stem cells in bone fracture repair and regeneration. Chapter 7 / Mesenchymal Stem Cells in Human Health and Diseases /*Eds. Ahmed H. K. El-Hashash.* Academic Press. doi: 10.1016/B978-0-12-819713-4.00007-4

[5] Directive 2010/63/eu of the EUROPEAN Parliament and of the council of 22 September (2010) on the protection of animals used for scientific purposes (Text with EEA relevance) Official Journal of the European Union, 20.10., 276/33 - 276/79. https://eur-lex.europa. eu/LexUriServ/ LexUriServ.do?uri =OJ:L:2010:276:0033:0079:en:PDF

[6] European Convention for the Protection of Vertebrate Animals used for Experimental and Other Scientific Purposes Strasbourg, 18.III.1986. - 11 p. https://rm.coe.int/168007a67b

[7] Feltri, P., Solaro, L., Di Martino, A., Candrian, C., Errani, C. & Filardo, G. (2022). Union, complication, reintervention and failure rates of surgical techniques for large diaphyseal defects: a systematic review and meta-analysis. *Sci. Rep.,* 12, 9098. https://doi.org/10.1038/s41598-022-12140-5

[8] Ferracini, R., Bistolfi, A., Garibaldi, R., Furfaro, V., Battista, A. & Perale, G. (2019). Composite xenohybrid bovine bone-derived scaffold as bone substitute for the treatment of tibial plateau fractures. *Appl. Sci.*, 9(13), 2675. doi: 10.3390/app9132675

[9] Gao, F., Xu, Z., Liang, Q., Li, H., Peng, L., Wu, M. ... & Liu, W. (2019). Osteochondral regeneration with 3D-Printed biodegradable high-strength supramolecular polymer reinforced-gelatin hydrogel scaffolds. *Adv. Sci.,* 6, 1900867. doi: 10.1002/advs.201900867

[10] Haugen, H. J., Lyngstadaas, S. P., Rossi, F. & Perale, G. (2019). Bone grafts: which is the ideal biomaterial? *J. Clin. Periodontol.,* 46, 92-102. doi: 10.1111/jcpe.13058

[11] Kobbe, P., Laubach, M., Hutmacher, D. W., Alabdulrahman, H. & Hildebrand F. (2020). Convergence of scafold-guided bone regeneration and RIA bone grafting for the treatment of a critical-sized bone defect of the femoral shaft. *Eur. J. Med. Res.,* 25, 70. doi: 10.1186/s40001-020-00471-w

[12] Lang, T. A. & Sesik, M. M. (Eds.) (2011). *Как описывать статистику в медицине. Аннотированное руководство для авторов, редакторов и рецензентов [How to describe statistics in medicine. An annotated guide for authors, editors, and reviewers].* M: Практическая медицина - M: Practical medicine. ISBN: 978-5-98811-173-3

[13] Lin, H., Sohn, J., Shen, H., Langhans, M. T. & Tuan, R. S. (2019). Bone marrow mesenchymal stem cells: Aging and tissue engineering applications to enhance bone healing. *Biomaterials,* 203, 96-110. doi: 10.1016/j.biomaterials.2018.06.026

[14] Morozenko, D. V. & Leontjeva, F. S. (2016). Methods of researching markers of connective tissue metabolism in clinical and experimental medicine. *Молодий вчений - A Young Scientist,* 29(2),168-172. http://www.irbis-nbuv.gov.ua/cgi-bin/irbis_nbuv/cgiirbis_64.exe?I21DBN=LINK&P21DBN=UJRN&Z21ID=&S21REF=10&S21CNR=20&S21STN=1&S21FMT=ASP_meta&C21COM=S&2_S21P03=FILA=&2_S21STR=molv_2016_2_43

[15] Morris, M. T., Tarpada, S. P. & Cho, W. (2018). Bone graft materials for posterolateral fusion made simple: a systematic review. *Eur. Spine J.,* 27, 1856-1867. doi: 10.1007/s00586-018-5511-6

[16] Neufurth, M., Wang, X., Wang, S., Steffen, R., Ackermann, M., Haep, N. D. … & Muller, W. E. G. (2017). 3D printing of hybrid biomaterials for bone tissue engineering: calcium-polyphosphate microparticles encapsulated by polycaprolactone. *Acta Biomater,* 64, 377-388. doi: 10.1016/j.actbio.2017.09.031

[17] On the protection of animals from brutal treatment. Verkhovna Rada of Ukraine [online], revision: February 13, 2020, accessed: January 20, 2021 (in Ukrainian). https://zakon.rada. gov.ua/laws/show/en/3447-15/ed20200213#Text

[18] Poser, L., Matthys, R., Schawalder, P., Pearce, S., Alini, M. & Zeiter, S. (2014). A standardized critical size defect model in normal and osteoporotic rats to evaluate bone tissue engineered constructs. *Biomed. Res. Int.,* e348635. doi: 10.1155/2014/348635

[19] Sallent, I., Capella-Monsonis, H., Procter, P., Bozo, I. Y., Deev, R. V., Zubov, D. … & Zeugolis, D. I. (2020). The few who made it: commercially and clinically successful innovative bone grafts. *Front Bioeng Biotechnol.,* 8, 952. doi: 10.3389/fbioe.2020.00952

[20] Stark, J. R., Hsieh, J. & Waller, D. (2019). Bone graft substitutes in single- or double-level anterior cervical discectomy and fusion: a systematic review. *Spine,*44, E618-E628. doi: 10.1097/BRS.0000000000002925

[21] Tao, Z. S., Wu, X. J., Zhou, W. S., Liao, W., Wu, X. J., Yang M. … & Yang, L. (2019). Local administration of aspirin with β-tricalcium phosphate/poly-lactic-co-glycolic acid (β-TCP/PLGA) could enhance osteoporotic bone regeneration. J. Bone Miner. Metab., 37, 1026-1035. doi: 10.1007/s00774-019-01008-w

ЗМІНИ МАРКЕРІВ МЕТАБОЛІЗМУ КОЛАГЕНУ У СИРОВАТЦІ КРОВІ БІЛИХ ЩУРІВ ПРИ ЗАПОВНЕННІ ДЕФЕКТІВ СТЕГНОВОЇ КІСТКИ ІМПЛАНТАТАМИ НА ОСНОВІ ПОЛІЛАКТИДУ ТА ТРИКАЛЬЦІЙФОСФАТУ ІЗ АЛОГЕННИМИ МЕЗЕНХІМАЛЬНИМИ СТОВБУРОВИМИ КЛІТИНАМИ

Гонтар Н. М.

Використання синтетичних матеріалів сумісно зі стимуляторами остеогенезу є одним із передових напрямків розвитку травматології. Мета дослідження: на основі аналізу біохімічних маркерів метаболізму колагену в сироватці крові

лабораторних щурів із дефектом стегнової кістки оцінити перебіг ремоделювання кістки після заповнення дефекту імплантатами на основі полілактиду та трикальційфосфату з одночасним та відтермінованим введенням алогенних мезенхімальних стовбурових клітин (МСК). На моделі дефекту у метафізі стегнової кістки у білих щурів досліджено показники обміну колагену у сироватці крові: вміст білково-зв'язаної, вільної фракцій, суми гідроксипроліну (ГОП), розраховано відношення вмісту ГОП білково-зв'язаного до вільного (БЗ/В). Порівняння результатів різних груп виконували за методом Стьюдента-Фішера. Різницю вважали статистично значущою за умови p<0,05. Заповнення дефекту імплантатами призводило до зменшення вмісту білково-зв'язаного ГОП на 16,69 % та 14,34 % на 15-у та 90-у добу (p<0,05), збільшення вмісту вільного ГОП на 74,96 %; 67,31 % та 56,74 % (p<0,001), вмісту суми ГОП на 25,37 %; 23,66 % та 18,28 % (p<0,05), і зниженні БЗ/В на 52,20 %; 49,90 % та 45,30 % (p<0,001) відносно інтакту на 15-у; 30-у та 90-у доби. Додавання до імплантатів МСК водночас зі встановленням викликало зменшення вмісту вільного ГОП на 63,90 %; 54,63 % та 42,76 % відповідно на 15-у; 30-у та 90-у доби (p<0,001), сумарного метаболіту на 21,87 % та 18,58 % на 15-у та 30-у доби (p<0,05) та зменшення БЗ/В на 47,50 %; 43,20 %;37,60 % на 15-у; 30-у та 90-у доби (p<0,001) відносно інтакту. При відтермінуванні введення МСК вміст вільного ГОП збільшувався на 40,48 % (p<0,001); 20,49 % та 16,58 % (p<0,05) при меншому БЗ/В на 38,20 %; 25,80 % та 23,40 % (p<0,05) на 15-у; 30-у та 90-у доби відносно інтакту. При заповненні дефекту імплантатами без МСК спостерігалося помірне пригнічення анаболізму, бурна активація руйнування колагену. При одночасному використанні імплантатів і МСК спостерігалася незмінність темпу формування та інтенсивне руйнування колагену. При відтермінуванні введення МСК зафіксовано помірний темп руйнування, що найбільш сприяло метаболізму колагену.

Ключові слова: *дефект, імплантат, мезенхімальна стовбурова клітина, регенерація, гідроксипролін.*

DOI: 10.31393/morphology-journal-2023-29(3)-03 Reports of Morphology, Vol. 29, №3, Pages 20-25

ISSN 1818-1295 eISSN 2616-6194

REPORTS OF MORPHOLOGY

Official Journal of the Scientific Society of Anatomists, Histologists, Embryologists and Topographic Anatomists of Ukraine

journal homepage: https://morphology-journal.com

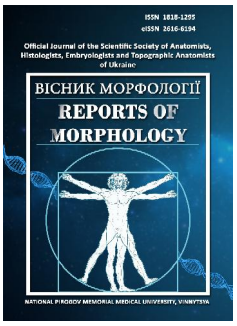

Structural changes in the heart tissue of rats under conditions of acute intoxication with Vipera berus berus venom

Maievskyi O. Ye.[1], Bobr A. M.[2], Gunas I. V.[2]

[1]Educational and Scientific Center "Institute of Biology and Medicine", Taras Shevchenko National University of Kyiv, Kyiv, Ukraine
[2]National Pirogov Memorial Medical University, Vinnytsia, Ukraine

ARTICLE INFO
Received: 19 April 2023
Accepted: 23 May 2023

UDC: 61:612.1:615.9.616.1:616-099

CORRESPONDING AUTHOR
e-mail: maevsklyalex8@gmail.com
Maievskyi O. Ye.

CONFLICT OF INTEREST
The authors have no conflicts of interest to declare.

FUNDING
Not applicable.

Among all poisonous animals, snakes attract the special attention of mankind. Cases of poisoning by their toxins are extremely common and are an unsolved public health problem worldwide. It has been established that among a number of complications due to snakebites, an important role is played by disturbances in the normal functioning of the organs of the cardiovascular system. The aim of the research is to study the features of histological changes in the heart tissue of rats under conditions of acute intoxication with Vipera berus berus venom. Experimental studies were carried out on white non-linear male rats. The animals were conditionally divided into two groups - a control and an experimental group of 10 individuals each. Experimental rats were injected intraperitoneally with a semi-lethal dose (LD50) (1.576 mg/g^{-1}) of Vipera berus berus venom in saline solution. Animals of the control group were injected intraperitoneally with only saline solution. Rats were removed from the experiment 24 hours after exposure to the venom, anesthetized by cervical dislocation. Heart samples were taken for microscopic examination. Fixation of the material and preparation of paraffin blocks were carried out according to generally accepted methods. Histological heart preparations were stained with Picro Sirius Red/Fast Green. Histological preparations were studied using a SEO SCAN light microscope. Thus, under the conditions of acute intoxication with Vipera berus berus venom in experimental rats, microscopic examination of the heart tissue revealed pathological shifts in the structural organization of all layers of the organ. In the epicardium, an increase in the volume of collagen fibers and thickening of vessel walls were characteristic. The most pronounced histological changes were observed in the myocardium. Swelling, disorganization of muscle fibers, their fragmentation, lysis, destruction, loss of characteristic transverse striations, necrosis were detected in it. In addition, an increase in the number of fibroblasts, their activation and, as a result, the growth of connective tissue components, including collagen fibers, in the myocardial tissue were revealed. The endocardium of experimental rats was distinguished by desquamation of the endothelial lining and an increase in the number of active fibroblasts in the outer connective tissue layer.

Keywords: *vipera, venom, heart, fibroblasts, destruction, rats.*

Introduction

Among all poisonous animals, snakes attract the special attention of mankind. On the one hand, this interest is due to the fact that cases of poisoning by their toxins are extremely common and belong to unsolved health problems worldwide, as they cause numerous fatal consequences. According to WHO estimates, 81,000 to 138,000 people die from snake bites every year, and another 400,000 victims have severe complications or even disability [8, 9, 10]. However, despite this, snake toxins are also considered valuable sources for the production of various medicines [2, 12]. Snakes use their venom to neutralize prey and to scare or weaken predators. The realization of these goals is possible due to the fact that toxins cause the development of muscle paralysis (by blocking the transmission of nerve impulses), cause changes in the functioning of the cardiovascular system, or cause pronounced local lesions at the sites of bites.

Snake venom is a mixture of enzymes and proteins without catalytic properties. The main enzymes include metalloproteinases (SVMPs), phospholipases A2 (PLA2), serine proteases (SVSPs), acetylcholinesterase, L-amino

acid oxidases (LAAOs), hyaluronidase, and nucleotidase [7, 20]. Proteins with non-enzymatic properties include three-finger toxins (3FTXs), C-type lectin-like peptides, natriuretic factor, proteinase inhibitors, and bradykinin-potentiating peptides (BPP) [3, 4, 19]. According to the literature, the composition of snake venom is not stable and may vary depending on sex, features of ontogenesis, geographic distribution, and environmental conditions [27]. Therefore, the compounds of their toxins are able to cause a number of biological effects both at the local and systemic levels [5]. It is known that severe pain, swelling and tissue necrosis usually occur at the site of venom inoculation [11]. At the level of organs and systems, the venom causes neuro-, myo-, cardio-, nephrotoxic effects, coagulopathy [1]. Such life-threatening complications force scientists to investigate in more detail the components of snake toxins in order to develop effective treatment methods.

The aim of the research is to study the features of histological changes in the tissue of the heart of rats under the conditions of acute intoxication with the venom of Vipera berus berus.

Materials and methods

Experimental studies were carried out on white non-linear male rats. For preliminary acclimatization, the animals were kept for 7 days in the animal facility of Taras Shevchenko National University of Kyiv, and then kept in laboratory conditions at constant temperature (22±3°C), humidity (60± 5 %) and light (12 h light/12 h dark cycle), being fed standard rodent food and water ad libitum. All experiments were conducted in accordance with the National Institutes of Health Guidelines for the care and use of laboratory animals and the European Council Directive of 24 November 1986 for the Care and Use of Laboratory Animals (86/609/EEC). The research was approved and confirmed by the Bioethics Commission of the NSC "Institute of Biology and Medicine" of the Taras Shevchenko National University of Kyiv (protocol No. 2 dated August 19, 2021).

Vipera berus berus venom was obtained from the V. N. Karazin Kharkiv National University. The lyophilized crude venom was stored at -20°C and then dissolved in saline solution immediately before the experiment.

The animals were conditionally divided into two groups - a control and an experimental group of 10 individuals each. Experimental rats were injected intraperitoneally with a semi-lethal dose (LD50) (1.576 mg/g^{-1}) of Vipera berus berus venom in saline solution. Animals of the control group were injected intraperitoneally with only saline solution. Rats were removed from the experiment 24 hours after exposure to the venom, anesthetized by cervical dislocation.

Heart samples were taken from pre-weighed animals of all groups for microscopic examination. The pieces were fixed in a 10 % formalin solution, while the duration of exposure did not exceed 1-2 days. The applied fixing solution prevents the process of autolysis and stabilizes cells and tissues for their further processing and use in staining procedures. Next, the pieces were dehydrated in alcohols of increasing concentration and embedded in paraffin blocks. Staining of histological preparations of hearts was performed according to the Picro Sirius Red/Fast Green method [21]. Histological preparations were studied using a SEO SCAN light microscope and photo-documented using a Vision CCD Camera with a system of image output from histological preparations.

Results

Under the conditions of acute intoxication with Vipera berus berus venom in the heart of experimental rats significant changes in the normal histostructure of all layers of the organ were observed. The composition of the epicardium was dominated by connective tissue elements, mainly collagen fibers, which, growing, formed a so-called mesh and later interwoven into the adjacent myocardial tissue. These fibers were subject to intensive dyeing. It should be noted that during microscopic examination, in addition to collagen fibers, which typically form the framework of this heart layer, an increase in the content of young fibers was noted. Against their background, the mesothelium layer was almost not visualized. The blood vessels of the epicardium had wide lumens. Deformation of the walls was observed in the arteries. The endothelial layer of their intima was thinned, subject to local detachment from the basement membrane into the vessel lumen, while in other areas, erythrocytes tightly adhered to the epithelial lining. Tunica media in the vast majority of arterial blood vessels of the epicardium consisted of a significant number of fibers and single smooth myocytes. The adventitia was thickened, collagenized. The arteries were characterized by signs of pronounced full blood, numerous erythrocytes and leukocytes were noted in their lumens (Fig. 1).

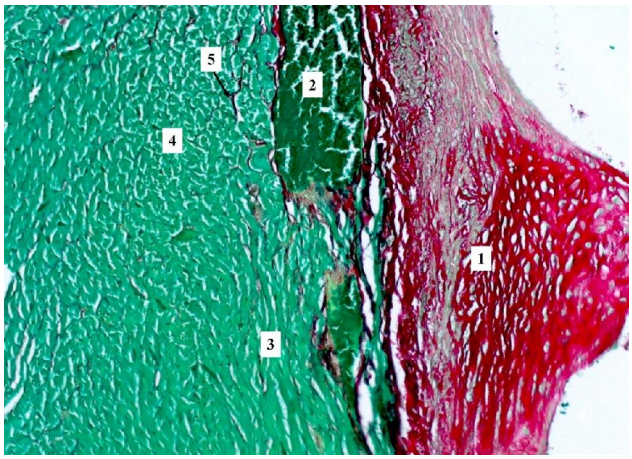

Fig. 1. Histological changes in the heart of rats under the conditions of exposure to Vipera berus berus venom. The growth of collagen fibers in the epicardium (1), the lumen of a blood vessel with formal elements (2), muscle fibers of the myocardium (3), cells of the conducting system of the heart (4), collagen fibers in the intermyofibrillar spaces (5). Picro Sirius Red/Fast Green. x200 magnification.

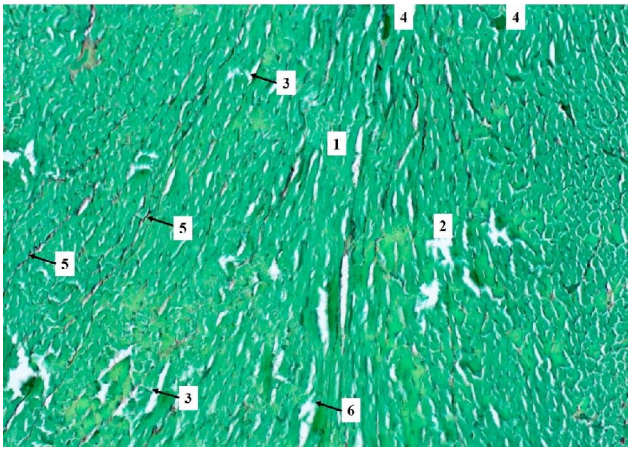

Fig. 2. Microscopic changes in the heart of rats exposed to Vipera berus berus venom. Thickening and swelling of muscle fibers (1), areas of myocardial tissue destruction (2), fragmentation of myocardial muscle fibers (3), areas of hemorrhage (4), collagen fibers (5), dissection of myocardial muscle fibers (6). Picro Sirius Red/Fast Green. x200 magification.

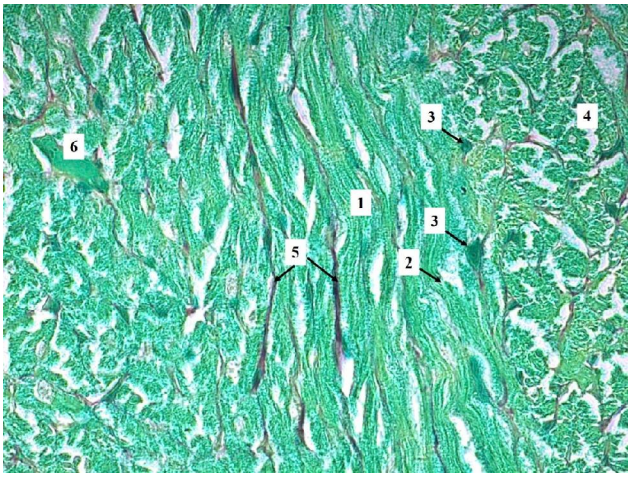

Fig. 3. Histological organization of the heart of rats under the influence of Vipera berus berus venom. Wave-like orientation of myocardial muscle fibers (1), sarcolemma destruction zone (2), fibroblasts (3), hydropic dystrophy of Purkinje cells (4), collagen fibers (5), blood vessel lumen (6). Picro Sirius Red/Fast Green. x1000 magnification.

In the myocardium of experimental animals, muscle fibers were swollen, lost their characteristic longitudinal orientation and acquired a winding shape. In most fields of view, zones of destruction of the sarcolemma were noted, and the transverse striation of the myocardial fibers was not clearly expressed. Zones of destruction of contractile elements and fragmentation of fibers were also determined in cardiac muscle tissue (Fig. 2). Between the latter, the volume of loose connective tissue increased significantly, the gaps between them widened. Contractile cardiomyocytes under these conditions lost their usual rectangular shape. Their nuclei could not be clearly visualized and identified in almost all fields of view due to severe swelling of the myocardial fibers. Some of them, which were able to be differentiated, were hypochromic, had an elongated shape. Also, due to the destruction of muscle fibers, some nuclei were outside the contractile cardiomyocytes. Intercalated discs had barely noticeable outlines on micropreparations. Zones of smoothing and lysis of muscle fibers were characteristic findings, as well as foci of necrosis. Cells of the leukocyte line were rarely recorded under the specified conditions, and therefore, myocardial infiltration during acute intoxication with Vipera berus berus venom is moderately pronounced.

The venom of Vipera berus berus in experimental rats caused a significant growth of collagen fibers in the tissue of the myocardium. Thus, the activation of fibroblasts, which were the main producers of components of loose connective tissue, including collagen fibers, was observed. Their number increased in the spaces between contractile and conducting cardiomyocytes. Fibroblasts had an elongated spindle-like or stellate shape. Against the background of cardiomyocytes, they were stained more intensively. Their nuclear-cytoplasmic index was high, which indicates the activity of synthetic processes in the cells. Fibroblast nuclei were located centrocentrically, were normochromic, chromatin had a diffuse distribution with a predominance of euchromatin. Under these conditions, the blood vessels of the myocardium of experimental animals were also subject to structural changes. The walls of the arteries thickened considerably. Endotheliocytes of the inner layer of the vessel wall had the appearance of palisades, protruding into the lumen of the arteries. Desquamation of the endothelial lining of the vascular wall from the components of the basement membrane was observed. In some histopreparations, loosening and swelling of the intima of the arteries were noted. The tunica media of arterial vessels was characterized by a pronounced increase in the number of collagen fibers, while the number of smooth muscle cells decreased. Most of the arteries had a thickened tunica adventitia. Myocardial vessels were full of blood, their lumens were filled with formal blood elements, namely erythrocytes. The latter formed sludge, columns, adhesion of erythrocytes to the epithelial lining of the intima and transversely arranged fibrin threads were often noted. The venous blood vessels of the myocardium had uneven lumens. Their endotheliocytes were swollen, and in some places they underwent desquamation in the lumen of the veins. The tunica media and tunica adventitia of veins are represented mainly by collagen fibers, the number of smooth myocytes is low. In the lumens of these vessels, the presence of hemorrhagic, serous content, single formal elements of blood were observed. As a whole, the venous system of the myocardium during acute intoxication with Vipera berus berus venom was characterized by signs of stasis. The defining features of the structural organization of the myocardium were zones of massive hemorrhages, in some places the hemorrhages were of a diffuse character with impregnation of the heart muscle tissue. Erythrocytes often

went beyond blood vessels and were located in interfibrillar spaces (Fig. 3).

Conductive cardiomyocytes (Purkinje fiber cells) were localized between the components of the contractile system of the heart. They stained less intensively than contractile cardiomyocytes, were wider, shorter, sometimes had the appearance of light cords or disordered structures with a small number of myofibrils. The majority of Purkinje cells were characterized by lightening of the cytoplasm due to their pronounced hydropic dystrophy. The latter fact explained the difficult recognition of their nuclei. The nuclei of conducting cardiomyocytes were located in the center of the cells, had signs of heterochromia, and the nuclear-cytoplasmic index was low. In individual cells, the nuclei shifted to the periphery (see Fig. 3).

In the endocardium of animals of the experimental group, swelling of endotheliocytes was detected. The nuclei of these cells were hyperchromic. Areas of detachment of the endothelial lining from the subendothelial layer were observed. In the subendothelial layer, the connective tissue elements increased in volume. In the outer connective tissue layer of the endocardium, the activity of fibroblasts increased and the growth of collagen fibers took place, just as in the previously mentioned layers of the heart.

Discussion

Cardiotoxicity and pronounced electrocardiographic changes are frequent complications of snake bites [16, 18, 24]. The most common are sinus arrhythmia, atrioventricular block and sinus bradycardia. Cases of bites by snakes of the Viperidae family are often associated with such pathologies as myocardial infarction and ischemic stroke, resulting from activation blood coagulation cascade and direct cardiotoxicity of venom proteolytic enzymes, in particular SVMPs. Also, the components of their toxins cause the development of hypofibrinogenemia, damage of the endothelium of vessels and impaired platelet aggregation [17, 25, 26].

According to the literature, the basis of the pathogenesis of myocardial infarction due to bites of snakes of the Viperidae family is also a violation of oxygen supply to cardiomyocytes due to excessive hemolysis of erythrocytes, vasoconstriction of coronary vessels due to significant production of endothelin and the influence of venom safatoxins. Scientists note that the development of myocarditis with pronounced necrosis of contractile myocytes, hemorrhages and accumulation of blood clots in the vessels of the microcirculatory channel of the heart muscle is possible [6, 15, 23].

L. O. Simoes and co-authors [22] studied the effect of Crotalus durissus cascavella venom on the cardiovascular system of rats. In the course of the experiment, it was found that the introduction of the venom of these snakes to animals leads to the development of morphological changes in the heart tissue. Light microscopy established the presence of inflammation and hemorrhages and a decrease in the volume of cells, eosinophilic infiltration, loss of transverse striation of myofibrils, changes in the nuclei of cardiomyocytes, accumulation of granules in the sarcoplasmic reticulum, violation of the integrity of muscle fibers. The venom has also been shown to exert a pronounced inotropic effect by activating NO/cGMP/protein kinase G, leading to hypotension and bradycardia in vivo. NO reduces the flow of Ca2+ ions through L-type channels in rat myocardium. In addition, it increases the activity of cGMP / protein kinase G-dependent phosphorylation of cardiac troponin I and the binding of myosin to protein C, causing muscle relaxation and a negative inotropic effect.

S. Karabuva and co-authors [13, 14] established that the venom of Vipera ammodytes, as well as related European vipers, can have a cardiotoxic effect. The main component that determines the pattern of heart damage is an analogue of secretory PLA2 - amodytilin L. In the isolated perfused heart of rats, it induced pronounced and irreversible conduction disturbances, namely severe atrioventricular blocks. The process was accompanied by an increase in CPK, LDH, AST, troponin I in the blood of the animals, which indicated damage of the heart tissue.

Conclusions

1. Under the conditions of acute intoxication with Vipera berus berus venom in experimental rats, microscopic examination of heart tissue revealed pathological shifts in the structural organization of all layers of the organ. In the epicardium, an increase in the volume of collagen fibers and thickening of vessel walls were characteristic.

2. The most pronounced histological changes were observed in the myocardium. Swelling, disorganization of muscle fibers, their fragmentation, lysis, destruction, loss of characteristic transverse striations, necrosis were detected in it. In addition, an increase in the number of fibroblasts, their activation and, as a result, the growth of connective tissue components, including collagen fibers, in the myocardial tissue were revealed.

3. The endocardium of experimental rats was distinguished by desquamation of the endothelial lining and an increase in the number of active fibroblasts in the outer connective tissue layer.

References

[1] Al-Sadoon, M. K., Diab, M. S., Bauomy, A. A., & Abdel Moneim, A. E. (2014). Cerastes cerastes gasperetti venom induced hematological alterations and oxidative stress in male mice. *Journal of Pure & Applied Microbiology,* 8, 693-702.

[2] Alangode, A., Rajan, K., & Nair, B. G. (2020). Snake antivenom: Challenges and alternate approaches. *Biochem Pharmacol,* 81, 114135. doi: 10.1016/j.bcp.2020.114135

[3] Almeida, J. R., Resende, L. M., Watanabe, R. K., Carregari, V. C., Huancahuire-Vega, S., da S Caldeira, C. A. … & Da Silva, S. L. (2017). Snake venom peptides and low mass proteins: Molecular tools and therapeutic agents. *Curr. Med. Chem.,* 4(30), 3254-3282. doi: 10.2174/0929867323666161028155611

[4] Balija, T., Leonardi, A., Brgles, M., Sviben, D., Kurtovic, T., Halassy, B., … & Krizaj, I. (2020). Biological activities and proteomic profile of the venom of Vipera ursinii ssp., a very rare Karst Viper from Croatia. *Toxins* (Basel), 12(3), 187. doi: 10.3390/toxins12030187

[5] Bhattacharya, S., Krishnamurthy, A., Gopalakrishnan, M., Kalra, S., Kantroo, V., Aggarwal, S. … & Surana, V. (2020). Endocrine and metabolic manifestations of snakebite envenoming. *Am. J. Trop. Med. Hyg.,* 103(4), 1388-1396. doi: 10.4269/ajtmh.20-0161

[6] Binu, A. J., Mishra, A. K., Gunasekaran, K., & Iyadurai, R. (2019). Cardiovascular manifestations and patient outcomes following snake envenomation: a pilot study. *Trop. Doct.,* 49(1), 10-13. doi: 10.1177/0049475518814019

[7] Bocian, A., Urbanik, M., Hus, K., Łyskowski, A., Petrilla, V., Andrejcakova, Z. … & Legath, J. (2016). Proteome and peptidome of vipera berus berus venom. *Molecules*, 21(10), 1398. doi: 10.3390/molecules21101398

[8] Bolon, I., Durso, A. M., Mesa, S. B., Ray, N., Alcoba, G., Chappuis, F. … & Ruiz de Castaneda, R. (2020). Identifying the snake: first scoping review on practices of communities and healthcare providers confronted with snakebite across the world. *PLoS One,* 15(3), e0229989. doi: 10.1371/journal.pone.0229989

[9] Di Nicola, M. R., Pontara, A., Kass, G. E. N., Kramer, N. I., Avella, I., Pampena, R. … & Paolino, G. (2021). Vipers of major clinical relevance in Europe: Taxonomy, venom composition, toxicology and clinical management of human bites. *Toxicology,* 453, 152724. doi: 10.1016/j.tox.2021.152724

[10] Gutierrez, J. M., Calvete, J. J., Habib, A. G., Harrison, R. A., Williams, D. J., & Warrell, D. A. (2017). Snakebite envenoming. *Nat. Rev. Dis. Primers,* 3, 17063. doi: 10.1038/nrdp.2017.63

[11] Gutierrez, J. M., Rucavado, A., Escalante, T., Herrera, C., Fernandez, J., Lomonte, B. … & Fox, J. W. (2018). Unresolved issues in the understanding of the pathogenesis of local tissue damage induced by snake venoms. *Toxicon,* 148, 123-131. doi: 10.1016/j.toxicon.2018.04.016

[12] Herzig, V., Cristofori-Armstrong, B., Israel, M. R., Nixon, S. A., Vetter, I., & King, G. F. (2020). Animal toxins - nature's evolutionary-refined toolkit for basic research and drug discovery. *Biochem. Pharmacol.,* 181, 114096. doi: 10.1016/j.bcp.2020.114096

[13] Karabuva, S., Brizic, I., Latinovic, Z., Leonardi, A., Krizaj, I., & Luksic, B. (2016). Cardiotoxic effects of the Vipera ammodytes ammodytes venom fractions in the isolated perfused rat heart. *Toxicon*, 121, 98-104. doi: 10.1016/j.toxicon.2016.09.001

[14] Karabuva, S., Luksic, B., Brizic, I., Latinovic, Z., Leonardi, A., & Krizaj, I. (2017). Ammodytin L is the main cardiotoxic component of the Vipera ammodytes ammodytes venom. *Toxicon,* 139, 94-100. doi: 10.1016/j.toxicon.2017.10.003

[15] Kariyanna, P. T., Jayarangaiah, A., Kamran, H., Schechter, J., Soroka, S., Amarnani, A. … & McFarlane, S. I. (2018). Myocardial infarction after snakebite envenomation: a scoping study. *Scifed. J. Cardiol.,* 2(3), 21.

[16] Li, F., Shrivastava, I. H., Hanlong, P., Dagda, R. K., & Gasanoff, E. S. (2020). Molecular mechanism by which cobra venom cardiotoxins interact with the outer mitochondrial membrane. *Toxins* (Basel), 12(7), 425. doi: 10.3390/toxins12070425

[17] Lopez-Davila, A. J., Weber, N., Kraft, T., Matinmehr, F., Arias-Hidalgo, M., Fernandez, J. … & Gutierrez J. M. (2021). Cytotoxicity of snake venom Lys49 PLA2-like myotoxin on rat cardiomyocytes ex vivo does not involve a direct action on the contractile apparatus. *Sci. Rep.,* 11(1), 19452. doi: 10.1038/s41598-021-98594-5

[18] Razok, A., Shams, A., & Yousaf, Z. (2020). Cerastes cerastes snakebite complicated by coagulopathy and cardiotoxicity with electrocardiographic changes. *Toxicon,* 188, 1-4. doi: 10.1016/j.toxicon.2020.10.003

[19] Sanhajariya, S., Duffull, S. B., & Isbister, G. K. (2018). Pharmacokinetics of snake venom. *Toxins* (Basel), 10(2), 73. doi: 10.3390/toxins10020073

[20] Santos-Filho, N. A., & Santos, C. T. (2017). Alpha-type phospholipase A2 inhibitors from snake blood. *J. Venom. Anim. Toxins Incl. Trop. Dis.*, 23, 19. doi: 10.1186/s40409-017-0110-2

[21] Segnani, C., Ippolito, C., Antonioli, L., Pellegrini, C., Blandizzi, C., Dolfi, A. … & Bernardini, N. (2015). Histochemical Detection of Collagen Fibers by Sirius Red/Fast Green Is More Sensitive than van Gieson or Sirius Red Alone in Normal and Inflamed Rat Colon. *PLoS One,* 10(12), e0144630. doi: 10.1371/journal.pone.0144630

[22] Simoes, L. O., Alves, Q. L., Camargo, S. B., Araujo, F. A., Hora, V. R. S., Jesus, R. L. C., … & Silva, D. F. (2021). Cardiac effect induced by Crotalus durissus cascavella venom: morphofunctional evidence and mechanism of action. *Toxicol. Lett.*, 337, 121-133. doi: 10.1016/j.toxlet.2020.11.019

[23] Simpson, C. H., Richardson, W. H., Swartzentruber, G. S., & Lloyd, V. J. (2018). ST segment elevation myocardial infarction following a Crotalus horridus envenomation. *Wilderness Environ. Med.,* 29(3), 383-387. doi: 10.1016/j.wem.2018.02.010

[24] Sunil, K. K., Joseph, J. K., Joseph, S., Varghese, A. M., & Jose, M. P. (2020). Cardiac involvement in vasculotoxic and neurotoxic snakebite - a not so uncommon complication. J. Assoc. *Physicians India,* 68(11), 39-41. PMID: 33187035

[25] Variawa, S., Buitendag, J., Marais, R., Wood, D., & Oosthuizen, G. (2021). Prospective review of cytotoxic snakebite envenomation in a paediatric population. *Toxicon,* 190, 73-78. doi: 10.1016/j.toxicon.2020.12.009

[26] Virmani, S., Bhat, R., Rao, R., Kapur, R., & Dsouza, S. (2017). Paroxysmal atrial fibrillation due to venomous snake bite. *J. Clin. Diagn. Res.,* 11(6), OD01-OD02. doi: 10.7860/JCDR/2017/27553.9971

[27] Zanetti, G., Duregotti, E., Locatelli, C. A., Giampreti, A., Lonati, D., Rossetto, O. … & Pirazzini, M. (2018). Variability in venom composition of European viper subspecies limits the cross-effectiveness of antivenoms. *Sci. Rep.,* 8(1), 9818. doi: 10.1038/s41598-018-28135-0

СТРУКТУРНІ ЗМІНИ В ТКАНИНІ СЕРЦЯ ЩУРІВ ЗА УМОВ ГОСТРОЇ ІНТОКСИКАЦІЇ ОТРУТОЮ ГАДЮК VIPERA BERUS BERUS

Маєвський О. Є., Бобр А. М., Гунас І. В.

Серед усіх отруйних тварин змії привертають особливу увагу людства. Випадки отруєнь їх токсинами є надзвичайно поширеними та належать до невирішених проблем охорони здоров'я в усьому світі. Встановлено, що серед цілого ряду ускладнень внаслідок зміїних укусів важливу роль відіграють порушення нормального функціонування органів серцево-судинної системи. Метою дослідження є вивчення особливостей гістологічних змін тканини серця щурів за умов гострої інтоксикації отрутою гадюк Vipera berus berus. Експериментальні дослідження проводили на білих нелінійних щурах самцях. Тварин умовно розподіляли на дві групи - контрольну і дослідну по 10 особин в кожній. Дослідним щурам внутрішньоочеревинно вводили напівлетальну дозу (LD50) (1,576 мг/г$^{-1}$) отрути Vipera berus berus на фізіологічному розчині. Тваринам контрольної

групи внутрішньоочеревинно вводили лише фізіологічний розчин. Виводили щурів з експерименту через 24 години після впливу отрути, знеживлюючи шляхом цервікальної дислокації. Для мікроскопічного дослідження забирали зразки серця. Фіксація матеріалу та приготування парафінових блоків проводили за загальноприйнятими методиками. Забарвлення гістологічних препаратів серця здійснювали Picro Sirius Red/Fast Green. Гістологічні препарати вивчали за допомогою світлового мікроскопа SEO SCAN. Таким чином, за умов гострої інтоксикації отрутою гадюк Vipera berus berus в експериментальних щурів при мікроскопічному дослідженні тканини серця виявлено патологічні зрушення структурної організації всіх шарів органу. В епікарді характерним було збільшення об'єму колагенових волокон, потовщення стінок судин. Найбільш виражені гістологічні зміни спостерігали в міокарді. В ньому відмічали набряк, дезорганізації м'язових волокон, їх фрагментацію, лізис, деструкцію, втрату характерної поперечної посмугованості, некроз. Крім того, виявлено зростання чисельності фібробластів, їх активацію та, як результат, розростання в тканині міокарда компонентів сполучної тканини, в тому числі колагенових волокон. Ендокард дослідних щурів відрізнявся десквамацією ендотеліального вистилення та збільшенням кількості активних фібробластів в зовнішньому сполучнотканинному шарі.

Ключові слова: *гадюки, отрута, серце, фібробласти, деструкція, щури.*

DOI: 10.31393/morphology-journal-2023-29(3)-04 Reports of Morphology, Vol. 29, №3, Pages 26-31

ISSN 1818-1295 eISSN 2616-6194

REPORTS OF MORPHOLOGY

Official Journal of the Scientific Society of Anatomists, Histologists, Embryologists and Topographic Anatomists of Ukraine

journal homepage: https://morphology-journal.com

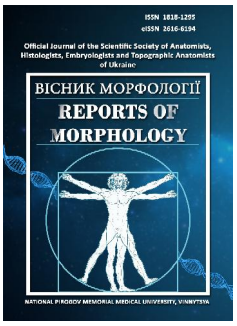

Investigation of nuclear DNA content and cell cycle phases in rat liver cells under chlorpromazine administration

Rykalo N. A.[1], Baylo O. V.[2]

[1]Medical University of Innsbruck, Innsbruck, Austria
[2]Pirogov Vinnytsia National Medical University, Vinnytsia, Ukraine

ARTICLE INFO
Received: 25 April 2023
Accepted: 31 May 2023

UDC: 577.213.3:616.36-03.93:615.214

CORRESPONDING AUTHOR
e-mail: bayloov@gmail.com
Baylo O. V.

CONFLICT OF INTEREST
The authors have no conflicts of interest to declare.

FUNDING
Not applicable.

Hepatotoxicity of antipsychotic drugs remains an urgent problem of modern medicine. Therefore, the purpose of the study was to investigate the nuclear DNA content and cell cycle phases of rat liver cells under Chlorpromazine administration at doses ranging from 3.5 mg/kg to 28 mg/kg for 30 and 60 days. The study was conducted on 60 sexually mature female rats. Chlorpromazine was administered once daily for 30 and 60 days at doses of 3.5 mg/kg, 7 mg/kg, 14 mg/kg, 21 mg/kg and 28 mg/kg. The DNA content in the nuclei of rat liver cells was determined by flow cytometry. Cytological analysis of cells was performed using FloMax software (Partec, Germany), where the percentage of nuclei in the G0G1 interval of the cell cycle, in the S phase, G2M interval, and the apoptosis index - SUB-G0G1 area on DNA histograms were determined. Statistical processing of the results was performed using the Mann-Whitney U test. The results of the study showed that Chlorpromazine has a dose-dependent hepatotoxic effect: with an increase in the dose of this drug in rats from 7 to 28 mg/kg, the percentage of fragmented nuclei in liver tissue significantly increased, which is a sign of hepatocyte death by apoptosis. It was found that Chlorpromazine at a dose of 3.5 mg/kg did not increase hepatocyte apoptosis, while at a dose of 21 and 28 mg/kg the drug showed the highest hepatotoxicity, increasing the level of apoptosis by 1.9 and 2.1 ($p<0.05$) times, respectively. The hepatotoxic effect is enhanced by the use of Chlorpromazine for 60 days, which is manifested in a significant increase in hepatocyte nuclear DNA fragmentation, which, in our opinion, should be taken into account when conducting long-term therapy in patients.

Key words: *chlorpromazine, apoptosis, cell cycle phases, liver.*

Introduction

The liver is a unique unpaired organ that performs more than a dozen vital functions around the clock, one of which is the metabolism of xenobiotics. The vast majority of drugs are metabolized by liver cells, so it is difficult to overestimate the importance of this organ. Hepatotoxicity of antipsychotic drugs remains an urgent problem of modern medicine, and concerns many branches of medicine, including psychiatry, not only pharmacology and hepatology [1, 16, 21]. This is due to the fact that most of the syndromes and diseases encountered by psychiatrists in their daily practice, such as bipolar disorders or schizophrenia, require long-term, sometimes life-long medication correction and support [3, 11]. Most of the drugs used in psychiatric practice are hepatotoxic [8, 12]. Chlorpromazine as an antipsychotic, neuroleptic, sedative, muscle relaxant, and antiemetic continues to be used both in Ukraine [10, 11] and around the world, despite its side effects [4, 22]. However, the mechanisms of the toxic effect on the liver and other organs and tissues have not been fully elucidated and are still being investigated [4].

It is an interesting scientific fact that patients with schizophrenia who receive treatment with antipsychotic drugs with an antitumor effect, such as Chlorpromazine, have a lower incidence of cancer [9]. That is, on the one hand, hepatotoxicity is a significant side effect of the drug, which can limit the spectrum of its use and cohort of patients for treatment, on the other hand, it can be a promising drug for use in oncology practice [13, 20].

The purpose of the work is to investigate the content of nuclear DNA and the cell cycle phase of rat liver cells under the conditions of administration of Chlorpromazine in doses from 3.5 mg/kg to 28 mg/kg for 30 and 60 days.

Materials and methods

The study was conducted on 60 sexually mature female rats. All experiments were conducted in accordance with the "General Ethical Principles for Animal Experiments" approved by the First National Congress on Bioethics (Kyiv, 2001) and harmonized with the provisions of the "European Convention for the Protection of Vertebrate Animals Used for Experimental and Other Purposes" (Strasbourg, 1986). The bioethics committee of the National Pirogov Memorial Medical University, Vinnytsia approved that the work was performed in compliance with ethical principles (protocol No. 8 dated 22.10.2020). Before the start of the experiment, the animals were kept for 14 days in a vivarium under quarantine conditions. The drug Chlorpromazine (trade name - "Aminazine", dose - 25 mg/ml) produced by PrJSC "Halychpharm" ("Arterium") was used for the study.

The experimental animals were divided evenly into 12 groups (group 1 was the control group, groups from 2 to 12 were experimental). The hepatotoxicity of Chlorpromazine was studied for 30 and 60 days, depending on the dose of the drug.

Chlorpromazine was administered intragastrically with a metal probe with oil once a day at a dose of 3.5 mg/kg, 7 mg/kg, 14 mg/kg, 21 mg/kg, and 28 mg/kg. The calculation of doses of chlorpromazine was carried out according to the constant of biological activity according to the recommendations of Yu. R. Rybolovlev and R. S. Rybolovlev [18]. The control group (group 1) included intact animals. Animals from groups 2 to 6 (average initial body weight was 128.2±17.4 g) received Chlorpromazine for 30 days in a dose: animals of group 2 - 3.5 mg/kg, group 3 - 7 mg/kg, group 4 - 14 mg/kg, 5 group - 21 mg/kg, 6 group - 28 mg/kg. Experimental animals from groups 6 to 11 (average initial body weight was 125.0±18.7 g) for 60 days received Chlorpromazine in a dose: animals of group 7 - 3.5 mg/kg, group 8 - 7 mg/kg, group 9 - 14 mg/kg, 10 group - 21 mg/kg, 11 group - 28 mg/kg). It should be noted that during the experiment all animals of 11 groups died.

After completion of the 30- and 60-day experiment, all rats were subjected to euthanasia by intraperitoneal injection of Thiopental solution at the rate of 0.1 mg/g followed by decapitation. At the end of each part of the experiment, blood was collected from all rats for further biochemical research.

Materials and methods used to determine the DNA content (cell cycle, DNA fragmentation) in the nuclei of liver cells in rats. DNA content in the nuclei of rat liver cells was determined by DNA flow cytometry.

Nucleus suspensions from rat liver cells were obtained using a ready-made solution for the study of nuclear DNA CyStain DNA Step 1 from Partec, Germany, according to the manufacturer's protocol-instructions. This solution allows extraction of nuclei and labeling of nuclear DNA with diamidinophenylindole (DAPI). In the process of manufacturing nuclear suspensions, disposable CellTrics 50 μm filters (Partec, Germany) were used.

Flow analysis was performed on a multifunctional research flow cytometer "Partec PAS" by Partec, Germany. UV radiation was used to excite DAPI fluorescence. From each sample of nuclear suspension, 20,000 events were registered. Events (cell nuclei) with a DNA content of $\leq$4c were subject to analysis.

Cyclic analysis of cells was performed using FloMax software (Partec, Germany) in full digital correspondence according to a mathematical model, where:

G0G1 - percentage ratio of G0G1 phase cells to all cells of the cell cycle (DNA content = 2c);

S is the percentage ratio of cells in the phase of DNA synthesis to all cells of the cell cycle (DNA content>2c and <4c);

G2+M - percentage ratio of the G2+M phase to all cells of the cell cycle (DNA = 4 c, or polyploid);

Determination of DNA fragmentation (apoptosis) is performed by highlighting the SUB-G0G1 area on DNA histograms - RN2 before the G0G1 peak, which indicates cell nuclei with DNA content<2c.

Statistical processing of the obtained results was carried out in the license package "Statistica 6.0" using non-parametric estimation methods. The nature of the distributions for each of the variation series was evaluated, the average values for each characteristic and the standard square deviation were determined. The reliability of the difference in values between independent quantitative indicators was determined using the Mann-Whitney U-test.

Results

When analyzing the G0G1 indicator - percentage ratio of cells in the G0G1 phase (with diploid DNA content) to all cells of the cell cycle of rat liver tissue (Fig. 1), a dose-dependent effect of Chlorpromazine on this indicator is observed both in animals that were administered the drug for 30 and 60 days. Thus, in the liver cells of rats, when Chlorpromazine was administered for 60 days at a dose of 21 mg/kg, the G0G1 interval increased by 21.5 % ($p<0.05$ compared to the control), 14 mg/kg - by 14.8 % ($p<0.05$), 7 mg/kg - by 12.0 % ($p<0.05$) and 3.5 mg/kg - by 13 % ($p<0.05$). When animals were administered Chlorpromazine at the same dose (14 mg/kg), but for different durations, the G0G1 interval increased by 11.1 % during the 60-day experiment, compared to the 30-day experiment ($p<0.05$). In animals administered the drug for 30 days, a significant increase in the percentage of diploid nuclei was registered in the 5 (by 15.3 %, $p<0.05$) and 6 group (by 20.4 %, $p<0.05$).

S phase research - percentage ratio of cells in the phase of DNA synthesis to all cells of the cell cycle (DNA content >2c and <4c) showed an increase in this indicator in all animals under the condition of drug administration (Fig. 2), which, in our opinion, indicates the activation of the cell cycle in response for alteration. Significant changes, compared to the control, were registered in animals of all groups that received Chlorpromazine for 60 days (in group 7 - by 48.2 %, 8 - 89.9 %, 9 - 74.0 %, 10 - 92.9 %, $p<0.05$). When the drug was administered for 30 days, there was a significant

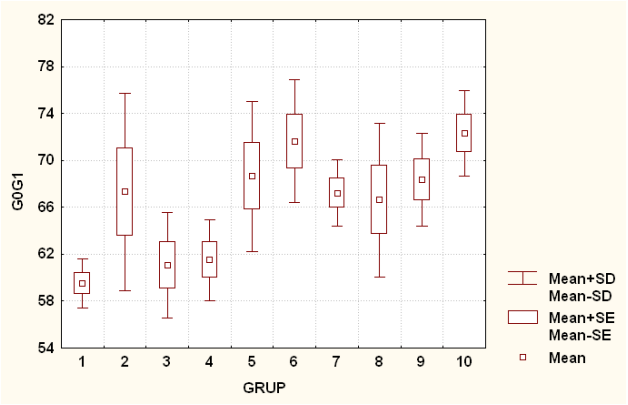

Fig. 1. G0G1 interval (%) in animals of 1-10 experimental groups when Chlopromazine was administered in different doses for 30 and 60 days. On this and the following graphs of the section: Mean - the average value; Mean±SE - mean value ± error of the mean; Mean±SD - average value ± standard deviation; GRUP - study groups (1 - control (intact animals), 2 - Chlorpromazine at a dose of 3.5 mg/kg for 30 days, 3 - Chlorpromazine at a dose of 7 mg/kg for 30 days, 4 - Chlorpromazine at a dose of 14 mg/kg for 30 days, 5 - Chlorpromazine at a dose of 21 mg/kg for 30 days, 6 - Chlorpromazine at a dose of 28 mg/kg for 30 days, 7 - Chlorpromazine at a dose of 3.5 mg/kg for 60 days, 8 - Chlorpromazine at a dose of 7 mg/kg for 60 days, 9 - Chlorpromazine at a dose of 14 mg/kg for 60 days, 10 - Chlorpromazine at a dose of 21 mg/kg for 60 days).

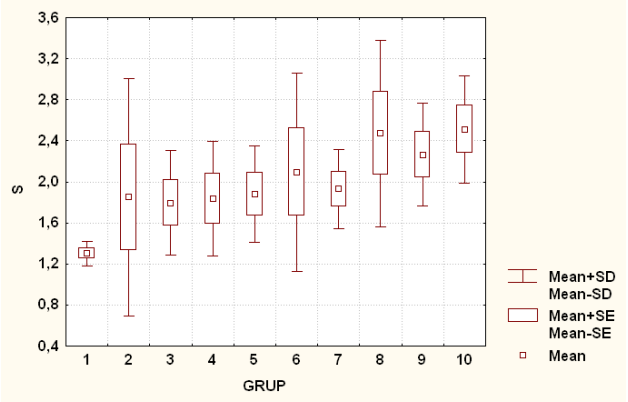

Fig. 2. S phase (%) in animals of 1-10 experimental groups when Chlopromazine was administered in different doses for 30 and 60 days.

difference in animals of 5 (increase by 44.4 %, p<0.05) and 6 group (increase by 60.9 %, p=0.06) compared to intact animals.

When analyzing the G2+M interval - the percentage ratio of the G2+M phase to all cells of the cell cycle showed a decrease in the percentage of polyploid nuclei (Fig. 3), which may indicate a violation of mitotic processes, and, therefore, the regeneration of the liver tissue as a whole in response to the influence of Chlorpromazine. According to the results of the statistical analysis, there was a significant difference in animals of all groups that received Chlorpromazine for 60 days (in group 7, a decrease of 21.3 %, 8 - 21.2 %, 9 - 25.0 %, 10 - 35.8 %, p<0.05 vs. intact animals). When using Chlorpromazine for 30 days, the parameters of animals 5 (decrease by 24.8 %, p<0.05) and 6 group (by 33.0 %, p<0.05) differed significantly from the control compared to animals of the 1 group.

Determination *of DNA fragmentation (apoptosis)* showed, that in animals of all groups, with the exception of the 2nd group (which received Chlorpromazine at a dose of 3.5 mg/kg daily for 30 days), the SUB-G0G1 interval was statistically different from the intact animals of the control group (Fig. 4). In particular, when Chlorpromazine was administered at a dose of 7 to 28 mg/kg for 30 days, nuclear DNA fragmentation significantly increased, compared to both intact animals and a group of animals that received Chlorpromazine at a dose of 3.5 mg/kg, which suggests apoptosis of hepatocytes. When Clopromazine was administered at a dose of 7 mg/kg, SUB-G0G1 significantly increased by 68.2 % (p<0.05 compared with intact rats and p<0.05 compared with animals that received Chlorpromazine at a dose of 3.5 mg/kg), at 14 mg/kg - at 72.7 % (p<0.05 and p<0.05, respectively), 21 mg/kg - significantly more than 1.9 times (p<0.05 and p<0.05, respectively). The highest level of apoptosis was in animals of the 6th group that received Chlorpromazine at a dose of 28 mg/kg, as the fragmentation index increased by 2.1

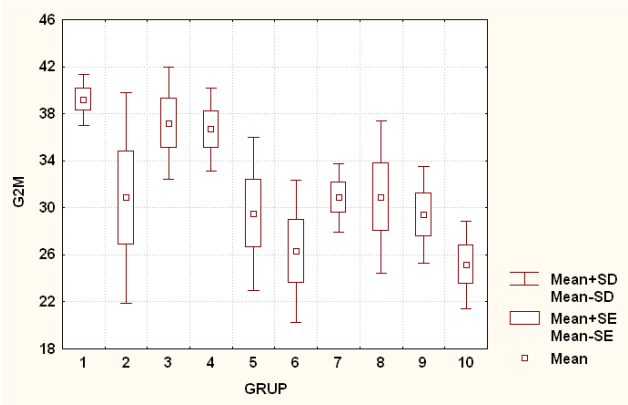

Fig. 3. G2M interval (%) in animals of 1-10 experimental groups when Chlopromazine was administered in different doses for 30 and 60 days.

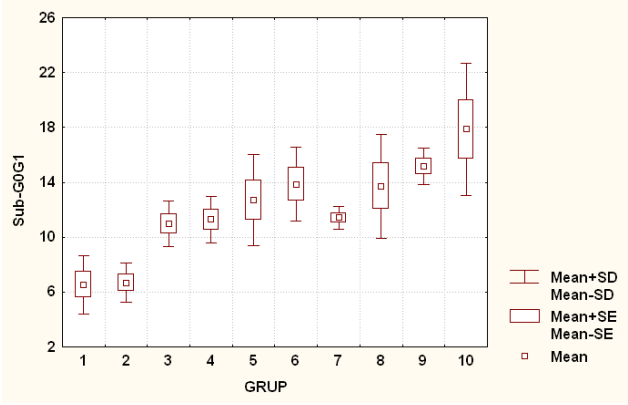

Fig. 4. Interval of Sub-G0G1 (%) in animals of 1-10 sub-experimental groups when Chlopromazine was administered in different doses for 30 and 60 days.

times (p<0.05 and p<0.05, respectively, compared to intact animals and a dose of 3.5 mg/kg), and also by 22.9 % in comparison with animals that received Chlorpromazine at a dose of 14 mg/kg. When Chlorpromazine was administered for 60 days, apoptosis increased by 74.8 % in animals of group 7, 2.1 times in group 8, 2.3 times in group 9, and 2.7 times in animals in group 10. In our opinion, it should be noted that when the same doses of Chlorpromazine were administered for 30 and 60 days, nuclear DNA fragmentation was higher when the drug was administered for a longer period of time. Thus, in animals of group 7, the percentage of fragmented nuclei was higher by 70.9 % (p<0.05) compared to animals of group 2, between groups 8 and 3 the difference was 25.0 % (p<0.05), 9 and 4 - 34.6 % (p< 0.05), 5 and 10 - 40.7 % (p<0.05).

Discussion

The data of the statistical analysis of the results obtained by us indicate a direct dependence of the effect of Chlopromazine on the nuclear DNA of rat liver tissue cells on the dose and duration of administration. The higher the dose and, especially, the duration of drug administration, the more intensive changes in the phases of the cell cycle are registered in animals. Thus, in animals 5 (Chlopromazine was administered at the rate of 21 mg/kg for 30 days) and 6 groups (28 mg/kg for 30 days), all the studied indicators (G0G1, S, G2M and SUB-G0G1) had a statistically significant difference with animals control group. When the drug was administered for 60 days to animals of all groups (7-10), from the minimum to the maximum dose (3.5 to 21 mg/kg), all the studied parameters were statistically significantly different from the inactive animals of the control group. It should be added that all animals that received Chlorpromazine at a dose of 28 mg/kg for 60 days died during the experiment.

According to the results of the data we obtained, using the flow cytometry method, namely measuring the percentage of hepatocyte DNA with a diploid, tetra-, polyploid and subdiploid DNA set (which is a sign of the death of liver cells by apoptosis [6, 19]), a clear dose-dependent effect of Chlorpromazine was established, as well as an increase in the hepatotoxicity of the studied drug during long-term administration. The data we obtained do not contradict the literature, according to which no toxic effect was detected when chlorpromazine was administered to mice at a dose of 3 mg/kg [5].

Our previously published data [2] regarding the morphological changes in liver tissue upon administration of Chlorpromazine in different doses and durations are significantly supplemented and logically explained by this study of nuclear DNA content and cell cycle phases of rat liver cells under the conditions of Chlorpromazine administration.

In our opinion, the index of nuclear DNA fragmentation, which induces apoptosis [6], which is determined by isolating SUB-G0G1, i.e. cell nuclei with DNA content <2c, deserves special attention.

According to the results of our research, apoptosis of hepatocytes significantly increased when Clopromazine was administered for 30 days at a dose of 7, 14, 21, and 28 mg/kg, and when the drug was used for 60 days at a dose of 3.5-21 mg/kg. The obtained data correspond to the data of the literature [7, 8, 15], according to which Chlopromazine, together with tyrosine kinase inhibitors, increases the apoptosis of tumor cells. Chlorpromazine also acts as a destabilizer of lysosomal membranes, which also promotes apoptosis [17]. On the other hand, [22] indicate that Chlorpromazine inhibits the mitochondrial pathway of apoptosis due to increased expression of tissue factor. Also, mechanisms of increased apoptosis during chlorpromazine therapy include increased autophagy by inhibiting the phosphatidylinositol 3-kinase Akt/mTOR pathway in human U-87MG glioma cells [20].

According to the authors, this proapoptotic therapeutic potential of Chlorpromazine can be used in complex therapy of various types of neoplasms [5, 7, 14, 23].

According to A. J. Jhou and co-authors [8] Chlorpromazine enhances the proliferation block precisely in the G2/M phase due to the regulation of the PI3K/AKT/mTOR-mediated autophagy mechanism in cancer.

Prospects for further development, in our opinion, can be a scientifically based review of the indications and contraindications for the appointment of Chlorpromazine, based on the results of experimental studies, namely the antitumor properties of this drug.

Conclusions

1. Chlorpromazine has a dose-dependent hepatotoxic effect: increasing its dose to experimental animals from 7 to 28 mg/kg significantly increases the percentage of nuclear DNA fragmentation in liver tissue, which is a sign of hepatocyte death by apoptosis. Chlorpromazine at a dose of 3.5 mg/kg did not increase the process of apoptosis of hepatocytes, while at a dose of 21 mg/kg and 28 mg/kg it showed the maximum effect of hepatotoxicity, increasing the level of apoptosis by 1.9 and 2.1 times, respectively.

2. With long-term use of Chlorpromazine, the hepatotoxic effect manifested in increased fragmentation of hepatocyte nuclear DNA increases, which, in our opinion, should be taken into account when treating patients.

References

[1] Arustamyan, O. M., Tkachyshyn, V. S., Kondratyuk, V. E., & Aleksiychuk, O. Yu. (2019). Застосування в медичній практиці нейролептиків й отруєння ними [Use of neuroleptics in medical practice and poisoning by them]. *Медицина невідкладних станів - Emergency medicine*, 100(5), 7-12. doi: 10.22141/2224-0586.5.100.2019.177012

[2] Bailo, O. V., & Rykalo, N. A. (2023). Morphological changes in the liver of rats after administration of chlorpromazine, depending on the dose and duration of administration. *Reports of Morphology,* 29(1), 67-76. doi: 10.31393/morphology-

journal-2023-29(1)-10
[3] Chaban, O. S. (2015). Порівняльний аналіз атипових нейролептиків [Comparative analysis of atypical antipsychotics]. *Нейроnews (психоневрологія та нейропсихіатрія) - Neuronews (Psychoneurology and Neuropsychiatry),*74(10), 13-17. https://neuronews.com.ua/uploads/issues/2015/10(74)/9294171202.pdf
[4] Chu, C. S., Lin, Yu.-Sh., & Liang, Wei-Zhe. (2022). The Impact of the Antipsychotic Medication Chlorpromazine on Cytotoxicity through Ca2+ Signaling Pathway in Glial Cell Models. *Neurotox. Res.,* 40(3), 791-802. doi: 10.1007/s12640-022-00507-5
[5] Cui, Y., Wu, H., Yang, L., Huang, T., Li, J., Gong, X. ... & Wang, Y. (2021). Chlorpromazine Sensitizes Progestin-Resistant Endometrial Cancer Cells to MPA by Upregulating PRB. *Front. Oncol.,* 11, 665-832. doi: 10.3389/fonc.2021.665832
[6] Dey, P., Biswas, S., Das, R., Chatterjee, S., & Ghosh, U. (2023). p38 MAPK inhibitor SB203580 enhances anticancer activity of PARP inhibitor olaparib in a synergistic way on non-small cell lung carcinoma A549 cells. *Biochem. Biophys. Res. Commun.,* 670, 55-62. doi: 10.1016/j.bbrc.2023.05.116
[7] Fujiwara, R., Taniguchi, Ya., Rai, Sh., Iwata, Yo., Fujii, A., Fujimoto, K. … & Matsumura, I. (2022). Chlorpromazine cooperatively induces apoptosis with tyrosine kinase inhibitors in EGFR-mutated lung cancer cell lines and restores the sensitivity to gefitinib in T790M-harboring resistant cells. *Biochem. Biophys. Res. Commun.,* 626, 156-166. doi: 10.1016/j.bbrc.2022.08.010
[8] Jhou, A. J., Chang, H. C., Hung, C. C., Lin, H. C., Lee, Y. C., Liu, W. T. … & Lee, C. H. (2021). Chlorpromazine, an antipsychotic agent, induces G2/M phase arrest and apoptosis via regulation of the PI3K/AKT/mTOR-mediated autophagy pathways in human oral cancer. *Biochem. Pharmacol.,* 184, 114403. doi: 10.1016/j.bcp.2020.114403
[9] Jiang, J., Huang, Z., Chen, X., Luo, R., Cai, H., Wang, H. … & Zhang Y. (2017). Trifluoperazine Activates FOXO1-Related Signals to Inhibit Tumor Growth in Hepatocellular Carcinoma. *DNA Cell. Biol.,* 36(10), 813-821. doi: 10.1089/dna.2017.3790
[10] Haustova, O. O., & Sinkevich, I. S. (2023). Психофармакотерапія в загальній медичній практиці: психосоматичний підхід (на прикладі амісульприду) [Psychopharmacotherapy in general medical practice: a psychosomatic approach (using the example of amisulpride).] *Міжнародний неврологічний журнал - International Journal of Neurology,* 19(1), 49-58. Taken from: http://inj.zaslavsky.com.ua
[11] Haustova, O. O. (2022). Сучасні підходи до діагностики та терапії шизофренії [Modern approaches to the diagnosis and therapy of schizophrenia]. *Нейроnews психоневрологія та нейропсихіатрія - Neuronews Psychoneurology and Neuropsychiatry.*135(5-6), 12-18. Taken from: https://neuronews.com.ua/uploads/issues/2022/5-6(135)/nn22_5-6_12-18.pdf
[12] Hendriks, D. F. G., Puigvert, L. F., Messner, S., Mortiz, W. & Ingelman-Sundberg, M. (2016). Hepatic 3D spheroid models for the detection and study of compounds with cholestatic liability. *Sci. Rep.*, 6, 35434. doi: 10.1038/srep35434
[13] Lee, W. Y., Lee, W. T., Cheng, C. H., Chen, K. C., Chou, C. M., Chung, C. H. … & Lin, C. W. (2015). Repositioning antipsychotic chlorpromazine for treating colorectal cancer by inhibiting sirtuin 1. *Oncotarget,* 29(6), 27580-2795. doi: 10.18632/oncotarget.4768.
[14] Liang, Z., Zang, Y. Q., Lu, Y., Dong, Q. P, Dong, K. T, & Zhou, H. F. (2021). Chlorpromazine hydrochloride plays a tumor suppressive role in diffuse large B lymphoma by promoting the expression of S1PR2. *Zhonghua Lao Dong Wei Sheng Zhi Ye Bing Za Zhi - Chinese Journal of Industrial Hygiene and Occupational Diseases,* 39(6), 418-423. doi: 10.3760/cma.j.cn121094-20201116-00633
[15] Matteoni, S., Matarrese, P., Ascione, B., Buccarelli, M., Ricci-Vitiani, L., Pallini, R. ... & Abbruzzese, C. (2021). Anticancer Properties of the Antipsychotic Drug Chlorpromazine and Its Synergism with Temozolomide in Restraining Human Glioblastoma Proliferation in Vitro. *Front. Oncol.*, 11, 635472. doi: 10.3389/fonc.2021.635472
[16] Oh, H. A., Kim, Ye-Ji., Moon, K.-S., Seo, J.-W., Jung, B. H., & Woo, D. H. (2022). Identification of integrative hepatotoxicity induced by lysosomal phospholipase A2 inhibition of cationic amphiphilic drugs via metabolomics. *Biochemical and Biophysical Research Communications*, 607, 1-8. doi: 10.1016/j.bbrc.2022.03.038.
[17] Park, S. H., Ko, W., Park, S. H., Lee, S., & Shin, I. (2020). Evaluation of the Interaction between Bax and Hsp70 in Cells by Using a FRET System Consisting of a Fluorescent Amino Acid and YFP as a FRET Pair. *Chem. Biochem.,* 21(1-2), 59-63. doi: 10.1002/cbic.201900293
[18] Rybolovlev, Yu. R. & Rybolovlev, R. S. (1979). Дозирование веществ для млекопитающих по константам биологической активности [Dosing of substances for mammals according to the constants of biological activity]. *Доклад Академии Наук СССР - Report of the Academy of Sciences of the USSR,* 247, 6, 1513-1516.
[19] Rykalo, N. A. (2010). Фрагментація ядерної ДНК гепатоцитів при хронічному токсичному гепатиті у статевонезрілих щурів: патогенетична корекція [Nuclear DNA fragmentation of hepatocytes in chronic toxic hepatitis in sexually immature rats: pathogenetic correction]. *Теоретична і експериментальна медицина - Theoretical and Experimental Medicine,* (4), 49.
[20] Shin, S. Y., Lee, K. S., Choi, Ya.-K., Lim, H. J., Lee, H. G., Lim, Y. & Lee, Y. H. (2013). The antipsychotic agent chlorpromazine induces autophagic cell death by inhibiting the Akt/mTOR pathway in human U-87MG glioma cells. *Carcinogenesis,* 34(9), 2080-2089. doi: 10.1093/carcin/bgt169
[21] Varga, B., Csonka, A., Csonka, A., Molnar, J., Amaral, L. & Spengler, G. (2017). Possible Biological and Clinical Applications of Phenothiazines. *Anticancer Res.,* 37(11), 5983-5993. doi: 10.21873/anticanres.12045
[22] Wu, J., Li, A., Li, Yu., Li, X., Zhang, Q., Song, W. ... & Zhang, F. (2016). Chlorpromazine inhibits mitochondrial apoptotic pathway via increasing expression of tissue factor. *Int. J. Biochem. & Cell. Biol.,* 70, 82-91. doi: 10.1016/j.biocel.2015.11.008.
[23] Xu, F., Xi, H., Liao, M., Zhang, Y., Ma, H., Wu, M. … & Xia, Y. (2022). Repurposed antipsychotic chlorpromazine inhibits colorectal cancer and pulmonary metastasis by inducing G2/M cell cycle arrest, apoptosis, and autophagy. *Cancer Chemother. Pharmacol.,* 89(3), 331-346. doi: 10.1007/s00280-021-04386-z.

ДОСЛІДЖЕННЯ ВМІСТУ ЯДЕРНОЇ ДНК ТА ФАЗ КЛІТИННОГО ЦИКЛУ КЛІТИН ПЕЧІНКИ ЩУРІВ ЗА УМОВ ВВЕДЕННЯ ХЛОРПРОМАЗИНУ

Рикало Н. А., Байло О. В.

Гепатотоксичність антипсихотичних лікарських засобів залишається актуальною проблемою сучасної медицини. Мета роботи - дослідити вміст ядерної ДНК та фази клітинного циклу клітин печінки щурів за умов введення хлорпромазину у

дозах від 3,5 мг/кг до 28 мг/кг впродовж 30 та 60 днів. Дослідження проведено на 60 статевозрілих щурах-самицях. Хлорпромазин вводили один раз на добу щоденно впродовж 30 та 60 діб у дозі 3,5 мг/кг, 7 мг/кг, 14 мг/кг, 21 мг/кг та 28 мг/кг. Вміст ДНК в ядрах клітин печінки щурів визначали методом проточної ДНК-цитометрії. Циклічний аналіз клітин виконували засобами програмного забезпечення FloMax (Partec, Німеччина), де визначали: відсоток ядер в інтервалі G0G1 клітинного циклу, у фазі S, інтервалі G2M, а також показника апоптоза - SUB-G0G1 ділянки на ДНК-гістограмах. Статистична обробка отриманих результатів проведена за допомогою U-критерія Мана-Уітні. Результати проведеного дослідження показали, що хлорпромазин має дозозалежний гепатотоксичний ефект: при збільшенні дози введення даного препарату у щурів від 7 до 28 мг/кг достовірно збільшується відсоток фрагментованих ядер в тканині печінки, що є ознакою загибелі гепатоцитів шляхом апоптоза. Встановлено, що хлорпромазин в дозі 3,5 мг/кг не посилює апоптоз гепатоцитів, тоді як у дозі 21 та 28 мг/кг препарат виявив найбільшу гепатотоксичність, збільшуючи рівень апоптозу у 1,9 та 2,1 ($p<0,05$) рази відповідно. При застосуванні хлорпромазину впродовж 60 днів гепатотоксичний ефект посилюється, що проявляється у достовірному збільшенні фрагментації ядерної ДНК гепатоцитів, що, на нашу думку, варто враховувати при проведенні тривалої терапії пацієнтам.

Ключові слова: *хлорпромазин, апоптоз, фази клітинного циклу, печінка.*

DOI: 10.31393/morphology-journal-2023-29(3)-05 Reports of Morphology, Vol. 29, №3, Pages 32-38

ISSN 1818-1295 eISSN 2616-6194

REPORTS OF MORPHOLOGY

Official Journal of the Scientific Society of Anatomists, Histologists, Embryologists and Topographic Anatomists of Ukraine

journal homepage: https://morphology-journal.com

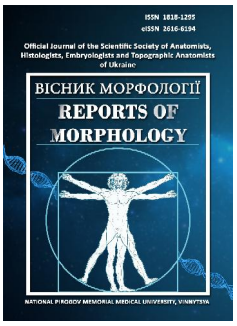

Morphological reasoning of the efficiency of application "Iruksan" in the experiment

Khimich S. D., Rautskis V. P.

Vinnytsia National Pirogov Memorial Medical University, Vinnytsia, Ukraine

ARTICLE INFO

Received: 10 May 2023

Accepted: 09 June 2023

UDC: 616-002.4:615

CORRESPONDING AUTHOR

e-mail: rautskisvik@gmail.com

Rautskis V. P.

CONFLICT OF INTEREST

The authors have no conflicts of interest to declare.

FUNDING

Not applicable.

Treatment of infected and purulent wounds remains an actual problem nowadays. Scientific and practical interest is caused by the use of collagenase enzyme for wound debridement. Aim: to study morphological changes in contaminated and purulent wounds when using "Iruksan" ointment containing collagenase. To reproduce a wound infection, the wound was contaminated with a pathogenic strain of Staphylococcus aureus in combination with Pseudomonas aeruginosa. Microbiological, histological and statistical studies were conducted during the experiment. Control of contamination and identification of pathogens took place in all rats after contamination before use of ointment and at the day of exclusion from experiment. Due to microbiological findings, number of microorganisms in the wounds of animals of the control group remained practically unchanged ($p>0.05$) until the 10th day of observation, and in the experimental group ("Iruksan" ointment was used in the treatment of wounds), the number of microorganisms in the wounds has already decreased by the 7th day of the experiment ($p<0.05$). The obtained data correlate with the results of a morphological findings, especially with the severity of the inflammatory process. We noticed reduction of signs of the inflammatory process and the improvement of epithelization of the wound defect in the group of animals that were treated with "Iruksan" ointment containing collagenase. Due to the results of histological studies, complete coverage of the wound surface with newly formed epithelium was revealed on the 7th day of the experiment in the experimental group, in contrast to the control group where, on the 7th day, typical signs of the wound process for this time period were determined. In the control group of animals, epithelization of wounds was observed on the 10th day. The obtained data demonstrate expedience of use collagenase-based ointment for the treatment of wounds in the first phase of the wound process. It results in faster wound bed cleaning from necrotized tissues and enhance epithelialization.

Keywords: *purulent wound, infected wound, wound process, collagenase, morphological changes in the wound, surgical treatment of the wound.*

Introduction

The problem of diagnosis and treatment of purulent wounds, despite many years of experience and constant attention of scientists, does not lose its relevance. Currently, 30-40 % of patients in surgical departments are patients with purulent-inflammatory diseases. The frequency of purulent-inflammatory complications of postoperative wounds ranges from 2 to 4 % [3]. During operations on organs of the abdominal cavity and abdominal wall, it can reach even 21.1 % [4]. In the general structure of nosocomial infection, almost 45 % of cases are due to postoperative complications, and the mortality rate for purulent infection and its complications has practically not changed over the past 25-30 years and ranges from 35 to 40 % [6, 19]. It is worth taking into account the increase in the number of elderly patients with chronic diseases, namely diabetes, atherosclerosis of the vessels of the lower extremities and chronic venous insufficiency, which contributes to the increase in the number of patients with chronic wounds. A wide range of etiological factors causing the occurrence of chronic contaminated wounds requires a complex approach to treatment, which is based on the principles of pathogeneticity, timeliness and systematicity [5, 9, 17].

It is known that in the treatment of infected wounds, doctors adhere to fundamental principles that involve the use of a combination of surgical and medical treatment methods [13, 14, 15]. The modern approach to wound healing

offers a new therapeutic strategy based on stem cells [12]. At the same time, an important place in the treatment of soft tissue wounds belongs to multicomponent drugs for local use, the choice of which depends on the phase of the wound process. This allows you to ensure the maximum concentration of active substances in the focus of inflammation and stimulate reparative processes. The effectiveness of wound healing is determined not only by time, but also by the achieved aesthetic result. Because even after complete healing of wounds, undesirable consequences for patients may remain, such as, for example, excessive scarring, which in turn has a long-term negative impact and requires additional treatment [10, 18]. To accelerate the process of granulation and shorten the healing time of wounds, preparations of proteolytic enzymes are used, the basis of which is the ability to clean wounds from necrotic tissues and exudate [1]. The use of enzyme preparations as a part of external therapy has features due mainly to their instability, which makes it urgent to improve the existing dosage forms both in terms of stability and efficiency, as well as ease of use.

Collagenases are one of the most effective proteolytic enzymes, as they have the ability to break down collagen, the main component of wounds and scars. Collagen is the strongest protein of tissue detritus [14, 16]. It is also one of the components of the formation of the extracellular matrix of granulation tissue in the proliferative phase of wound healing [8, 11]. According to the results of numerous studies, there is no universal method for performing surgical treatment. Modern approaches combine surgical, mechanical, autolytic and biological methods. At the same time, wounds containing collagen fibers are poorly amenable to cleaning with the help of other proteolytic enzymes - trypsin, chymopsin, streptokinase. It is worth noting that in the United States of America, for example, the above-mentioned enzymes are generally prohibited for use as means for local application. At the same time, collagenase has a selective effect on one protein of wound detritus - collagen, which makes it safe to use as a topical preparation for enzymatic lysis of necrotic tissues [2, 8, 13, 14].

Currently, there are combined medicinal products widely available, the composition of which includes collagenase, which significantly accelerates the purchase of the inflammatory process, accelerates the formation and maturation of granulation tissues with a simultaneous active process of epithelization. However, clear indications for their use and evidence of the effectiveness of use in the treatment of infected and purulent wounds require further research, including morphological.

The purpose of the work: to study the morphological changes in the tissues of contaminated and purulent wounds of rats in the experiment during their treatment with "Iruksan" gel, which contains collagenase.

Materials and methods

Research was carried out on the basis of the department of general surgery, the department of microbiology and the experimental clinic (vivarium) of Vinnytsia National Pirogov Memorial Medical University, Vinnytsia. The Bioethics Committee of the Vinnytsia National Pirogov Memorial Medical University, Vinnytsia, as a result of the examination conducted in accordance with the provisions of the committee, established that the research materials do not contradict the basic bioethical norms of the Council of Europe Convention on the Protection of Vertebrate Animals Used in Experiments and for Other Scientific Purposes dated March 18, 1986, EEC Directive № 609 dated November 24, 1986 and Order of the Ministry of Health of Ukraine № 281 dated November 1, 2000 (Protocol № 6 dated October 3, 2022).

The experimental study was conducted on 32 white laboratory rats (males) with a body weight of 200 to 250 g. The rats were kept in accordance with generally accepted norms. All animals were kept in the same conditions. Before conducting the research, the animals selected for the experiment were quarantined for two weeks on a standard diet, water was not limited. On the day of the experiment, the animals were not fed. After premedication, anesthesia was performed by intramuscular injection of ketamine. In the interscapular area, a standardized wound measuring 1.5 x 1.5 cm was modeled with excision of the skin, subcutaneous tissue, and superficial fascia.

To reproduce a wound infection, the wound was contaminated with a pathogenic strain of Staphylococcus aureus in combination with Pseudomonas aeruginosa at a concentration of 1 billion microbial bodies in 1 ml of liquid. Then the wound was closed with an aseptic gauze bandage. The rats were dynamically observed for 2 days. 2 days after the creation of the experimental wound and its contamination, a macroscopic assessment of local changes and control of the bacterial spectrum of the wound for contamination by the investigated flora was carried out.

Subsequently, the rats were divided into 2 groups of 16 animals each. The distribution of animals was as follows: 0 - control group (without treatment); And - Iruksan gel was used for treatment. The study drug and an aseptic gauze bandage were applied to the wound surface of the animals of the 1st group, in the control group only the replacement of the aseptic bandage was performed. Daily dressings were performed for the next 14 days in all animals. After removing the bandage, local changes in the wound and in the surrounding tissues were evaluated, step-by-step photofixation of the examined wounds was performed.

Four rats from each group were removed from the experiment on the third, seventh, tenth and fourteenth day. Euthanasia was performed by an overdose of intramuscular ketamine anesthesia. Also, on these days of the experiment, bacteriological culture was carried out from the investigated wound. Bacteriological cultures were carried out with the help of Amies transport medium with subsequent identification of the culture at the Department of Microbiology of the National Pirogov Memorial Medical

University, Vinnytsia.

To assess morphological changes, tissues were collected for histological examination by excision of a fragment of the skin with underlying tissues from the location of the wound defect (2.0 x 2.0 cm with a depth of up to 4 mm), departing from its edges by a distance of at least 0.5 cm, with subsequent fixation in 10 % in a solution of neutral buffered formalin for at least 48 hours. The preparations were prepared with further processing in the automatic tissue processor Diapath Donatello TM Series 2 (made in Italy), pouring in paraffin using the pouring dosing console Amos scientific TEC 2800-M (made in Italy). Histological sections with a thickness of 4 μm prepared on an automatic rotary microtome Diapath Galileo AUTO Series 2 (made in Italy) were stained with hematoxylin and eosin.

Microscopy of histological preparations was carried out using an OLIMPUS BX 41 light microscope (Ministry of Health of Ukraine, State Registration Certificate № 8120/ 2008, code 9011800000) using 40, 100, 200, and 400 times magnification. Image visualization and morphometry were performed using the morphometric program Quickphoto micro 2.5 (license agreement № 925113924). During the microscopic examination, the morphological state and composition of the skin tissue at the edges and bottom of the wound defect, the presence of pathological and reparative changes, and their nature were evaluated.

Statistical data analysis was performed using the STATISTICA 64 v12 program. Stat Soft. Inc. and Microsoft Office Excel 2016.

Results

After infection of the simulated wounds, all rats were checked for contamination and identification of the pathogen before the start of the study drug and on the day the rats were removed from the experiment. The results of microbiological research are shown in Table 1.

As can be seen from Table 1, the number of microorganisms in group 0 remained practically unchanged ($p>0.05$) until the 10th day of the experiment. However, in the 1st group, their number decreased ($p<0.05$) until the 7th day, and from the 10th day of the experiment, flora was not sown. The obtained data correlate with the results of a morphological study, namely with the concentration of the pathogen and the severity of the inflammatory process, which gradually decreases up to the 10th day and is completely absent on the 14th day of the experiment in the control group, where complete epithelization of the edges of the wound defect is noted. At the same time, in the 1st (experimental) group, the negative result of the bacteriological examination, associated with complete epithelization of the wound, was present already on the 10th day.

During the morphological study, the following morphometric indicators of tissues in the area of the bottom of the wound defect in animals of both groups were studied: the density (number per 1 mm^2) of blood vessels and the density (number per 1 mm^2) of elements of the inflammatory cell infiltrate (segmented nuclear leukocytes, plasma cells, macrophage elements).

Table 1. Dynamics of changes in the concentration of microorganisms in simulated rat wounds.

Groups of animals	Concentration of pathogens, microbial bodies in 1 ml				
	0 day	3 day	7 day	10 day	14 day
0 group	St. aur. 10^4 Ps. aer. 10^4	St. aur. 10^5	St. aur. 10^5	St. aur. 10^4	-
I group	St. aur. 10^5 Ps. aer. 10^5	St. aur. 10^4	St. aur. 10^2	-	-

Table 2. Density (quantity per 1 mm^2) of blood vessels and leukocyte elements of inflammatory cell infiltration in the tissues of the bottom of the wound defect.

Groups of animals	Morphometric indicators			
	3 day	7 day	10 day	14 day
0 group	vessels - 376 leukocyte - 625	vessels - 538 leukocyte - 332	vessels - 263 leukocyte - 625	epithelialization
I group	vessels - 523 leukocyte - 247	epithelialization	epithelialization	epithelialization

Quantitative results of the obtained data indicate a faster process of epithelization of the wound in animals of the I group, which were treated with gel with collagenase (Table 2).

The results of histological studies showed that on the third day in the control group, inflammatory cell infiltration, signs of unexpressed swelling of tissues, fullness of blood vessels at the edges and bottom of wounds were morphologically determined. The surface layer of necrotized tissues was separated from the underlying tissues by a

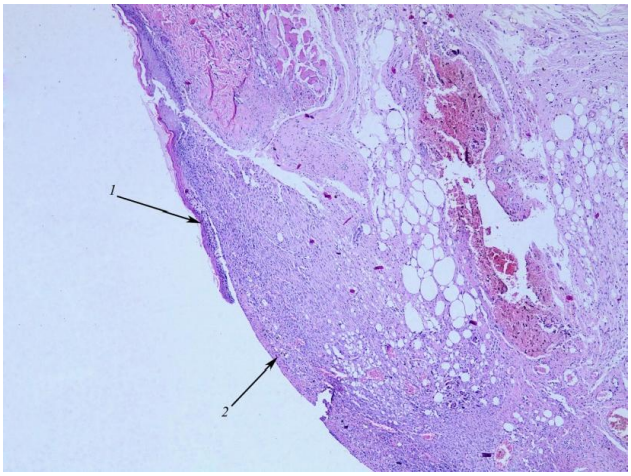

Fig. 1. Morphological changes of tissues in the area of the wound defect. The third day. Control group. The newly formed epidermis at the edge of the wound defect (1), the zone of deposition of fibrinoid substance (2) in the tissues of the wound bed. Hematoxylin-eosin. Ocular 10. Objective 4.

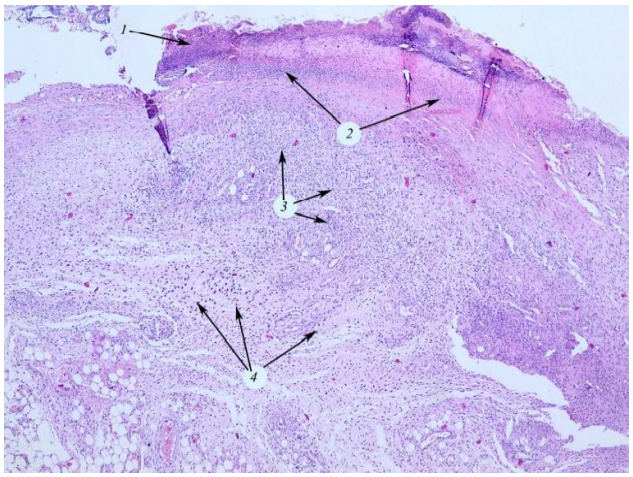

Fig. 2. Morphological changes of tissues in the area of the wound defect. The third day. Control group. Necrotized tissues (1), demarcated by a demarcation leukocyte shaft (2), uneven inflammatory cell infiltration (3), active fibroblasts (4) in the tissues of the wound bed. Hematoxylin-eosin. Ocular 10. Objective 4.

well-defined demarcation leukocyte shaft. On the greater part of the segment of the wound defect, the necrotic tissues were mostly already rejected, only a thin zone of surface deposition of fibrinoid substance remained. In the inflammatory cell infiltrate, neutrophilic and single eosinophilic leukocytes, macrophage elements, and lymphocytes were present. A small number of active fibroblasts were determined in the periwound zone. Regenerative proliferation of multi-layered flat epithelium from the edges of wounds in the form of a thin layer of crawling epitheliocytes was revealed (Figs. 1, 2).

On the third day, the formation of granulation tissue was histologically detected in the I (experimental) group, the presence of areas with a newly formed, thicker than in

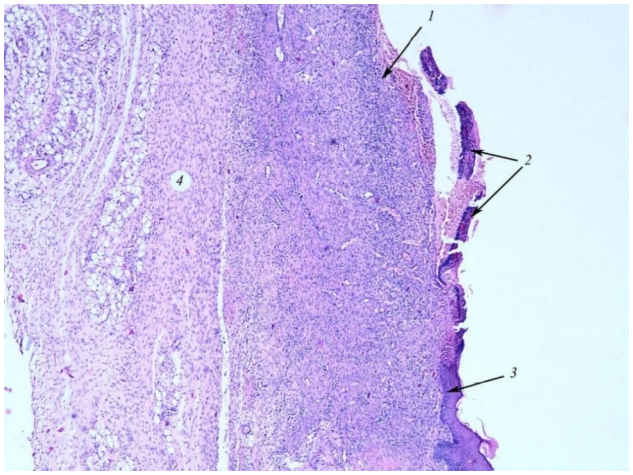

Fig. 3. Morphological changes of tissues in the area of the wound defect. I group. The third day. The tissues of the bottom of the wound (1) are covered with a wound "crust" (2), newly formed epithelium (3) from the edge of the wound. Hematoxylin-eosin. Ocular 10. Objective 4.

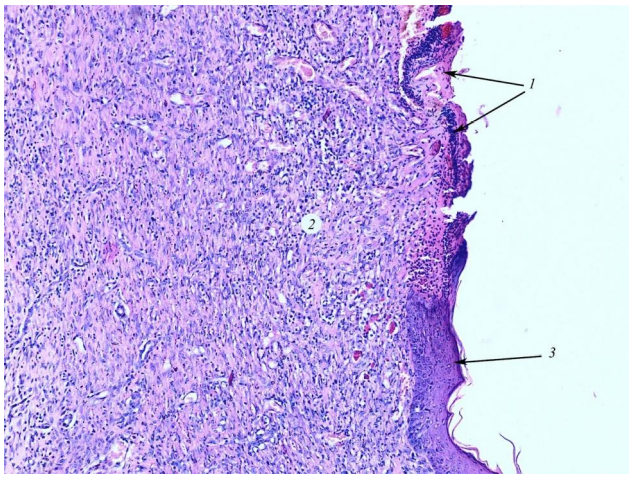

Fig. 4. Morphological changes of tissues in the area of the wound defect. I group. The third day. Wound "crust" (1), covering tissues rich in blood vessels (2), newly formed epithelium (3) from the edge of the wound. Hematoxylin-eosin. Ocular 10. Objective 4.

the previous group, multilayered flat epithelium oriented from the edges of the wound. Non-epithelialized areas of the bottom of the wound were covered with a scab. Within the tissues of the wound bed, leukocyte infiltration remained, with a significant proportion of lymphohistiocytic elements (Figs. 3, 4).

On the seventh day, in the preparations of the zero (control) group, mature granulation tissue was identified, which formed the bottom of the wound defect. This tissue, in addition to numerous blood vessels, contained thin collagen fibers, inflammatory and proliferative cells. From the edges of the wounds, a thin, but considerable in length, epithelial layer was located on the surface of the granulations (Fig. 5).

In contrast to the given data for the zero group, in the 1st (experimental) group, on the seventh day, complete

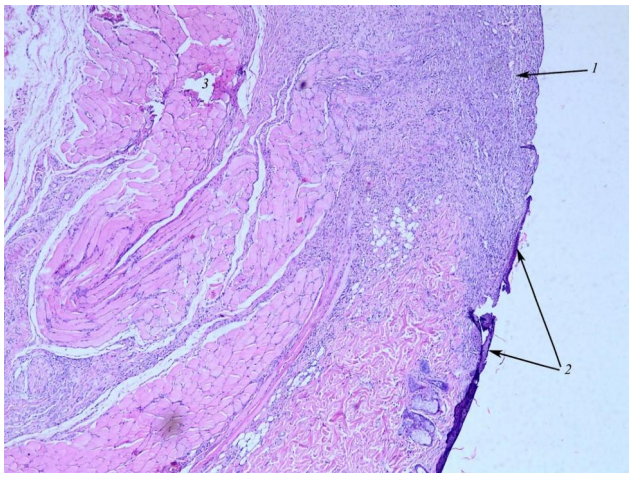

Fig. 5. Morphological changes of tissues in the area of the wound defect. Control group. The seventh day. Mature granulation (1), extensive epithelization (2) of the wound from its edges. Hematoxylin-eosin. Ocular 10. Objective 4.

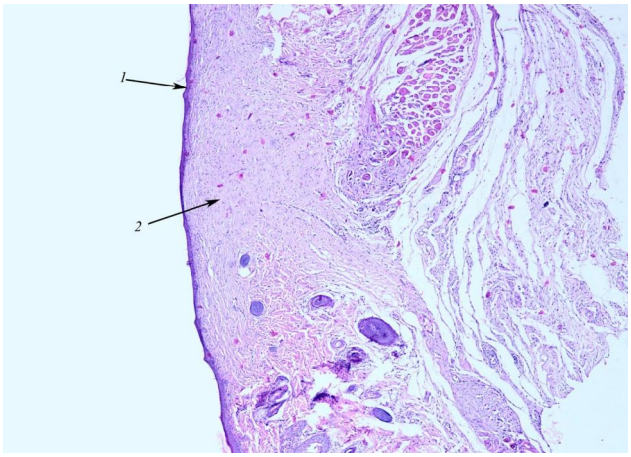

Fig. 6. Morphological changes of tissues in the zone of the bottom of the wound defect. I group. The seventh day. The newly formed epithelium (1) completely covers the scar tissue (2). Hematoxylin-eosin. Ocular 10. Objective 4.

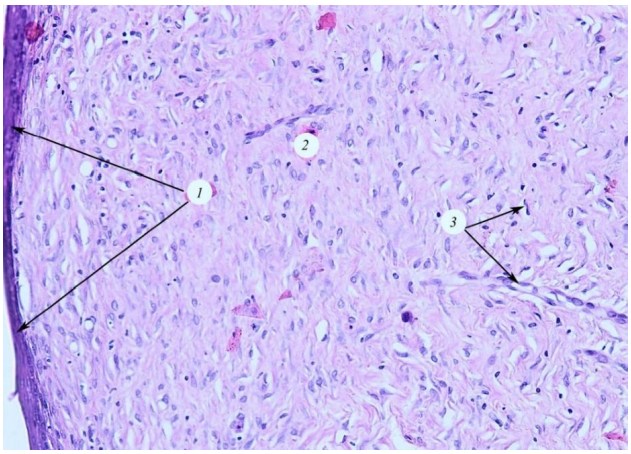

Fig. 7. Morphological changes of tissues in the area of the wound defect. I group. The seventh day. The newly formed epithelium (1) completely covers the scar tissue (2) with thin-walled blood vessels (3). Hematoxylin-eosin. Ocular 10. Objective 4.

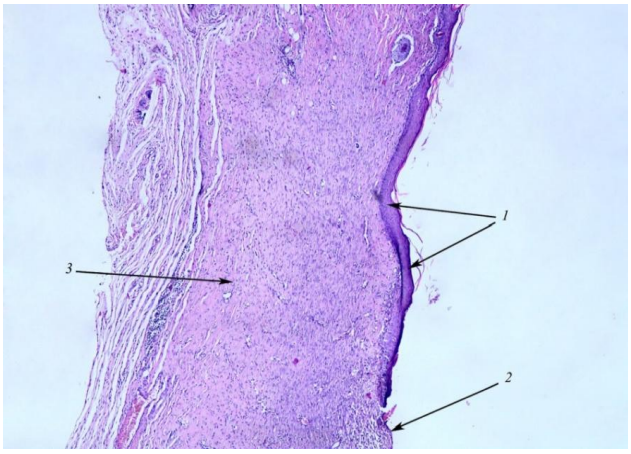

Fig. 8. Morphological changes of tissues in the zone of the bottom of the wound defect. Control group. The tenth day. Newly formed epidermis (1) on the surface of the scar (3), granulation tissue without an epithelial cover (2) in the central parts of the wound. Hematoxylin-eosin. Ocular 10. Objective 4.

coverage of the wound surface with newly formed epithelium was noted. The layer of the epithelium was thin (in some places - only three layers of flattened epitheliocytes), scar tissue with few cells of the lymphohistiocytic series and thin-walled vessels was located under it (Figs. 6, 7).

In the control group of animals, on the tenth day, the wounds were also completely epithelialized. Completion of stratification of the epidermis and maturation of scar tissue was morphologically determined, although in two animals there were centrally small areas without an epithelial cover (Fig. 8).

Discussion

According to the ideas existing today, the wound process after hemostasis takes place in the form of the following phases: inflammation, proliferation and reorganization of the scar with epithelization [22, 23]. In the inflammatory phase, vascular reactions and successive cellular mechanisms of inflammation occur with the participation of neutrophil leukocytes, macrophages, and lymphocytes, and then the wound is cleaned of dead tissues.

In the second phase, the formation of an extracellular matrix of granulation tissue is observed, in which keratinocytes, macrophages, fibroblasts and endothelial cells play a significant role, and collagen is one of the components of this granulation tissue. In the last phase of the wound process, reorganization of scar tissue occurs.

The results of morphological studies obtained by us in the course of experimental work demonstrate some differences in the healing process of contaminated wounds in rats of the control and experimental groups. At the same time, it is important to emphasize that the contamination of wounds in experimental animals was carried out with a pathogenic strain of Staphylococcus aureus in combination with Pseudomonas aeruginosa - pathogens that are typical etiological agents of wound infection in surgical patients.

According to the results of morphometric and histological studies, it was found that the use of the combined drug "Iruksan" has a positive effect on the indicators of the number of leukocyte elements in the focus of inflammation of the wound, which indicates a lower expressiveness of the inflammatory infiltrate when treated with this drug.

Thus, with the help of a histological examination, it was established that on the third day in the control group of animals, inflammatory cell infiltration, signs of unexpressed tissue swelling, blood vessels in the edges and bottom of the wound were found, which is similar to the data highlighted in the work of R. G. Sibbald and co-authors [20]. In the inflammatory cell infiltrate, neutrophilic and single eosinophilic leukocytes, macrophage elements, and lymphocytes were determined, which are characteristic signs of an inflammatory reaction. Regenerative proliferation of multilayered flat epithelium from the edges

of wounds in the form of a thin layer of epitheliocytes was observed. At the same time, on the third day in the experimental group, the formation of granulation tissue, the presence of areas with a thicker, multilayered flat epithelium than in the control group was found. Leukocyte infiltration with a significant proportion of lymphohistiocytic elements remained within the bottom of the wound. The data obtained by us coincide with the data obtained by some scientists [7].

It should be noted that in the dynamics of the experimental group, a faster epithelization of the wound defect was observed: on the 7th day, the wound surface was already completely covered by the newly formed epithelium. These results are significantly different from the indicators of the control group, where mature granulation tissue with proliferative elements was determined on the 7th day, which is a typical manifestation of the course of the wound process in this time period. Later, in the control group of animals, the wounds were also epithelialized on the 10th day of observation.

Thus, a beneficial effect on the early development of granulation tissue and, at the same time, early onset of the phase of wound epithelization in the I (experimental) group compared to the control group was revealed. In our opinion, it is obviously related to the presence of collagenase enzyme in the composition of "Iruksan". After all, it is known that successive changes in the structure of the extracellular matrix require a clear balance between the processes of synthesis and breakdown of collagen [21, 23].

The results of the conducted research form the basis for further study of the role of collagenase in the treatment of contaminated and purulent-necrotic wounds of soft tissues.

Conclusions

1. The combined gel "Iruksan" based on collagenase showed its effectiveness when used at different stages of the wound process compared to the control group, as evidenced by better regenerative activity of tissues in the affected area, which was manifested in the rapid removal of inflammatory cell infiltration and cleansing of the wound from necrotic detritus already on the third day of the experiment and the subsequent accelerated formation and maturation of granulation tissue, simultaneous active process of epithelization of the bottom of the wound defect on the seventh day.

2. The effect was found when using the preparation with collagenase in the treatment of wounds that were contaminated by typical causative agents of wound infection in medical institutions of a surgical profile.

3. The obtained results indicate the expediency of using this drug in the treatment of wounds in the first phase of the wound process, which allows to reduce the time of cleaning the wound surface from purulent-necrotic tissues and epithelization.

References

[1] Ahmed, R., Ray, M. K., Nayak, D., & Mohanta, Y. K. (2023). Microbial Enzymes in Biomedical Applications. In: Microbial Enzymes and Metabolites for Health and Well-Being, 53-74. CRC Press. doi: 10.1201/9781003369295-5

[2] Alipour, H., Raz, A., Zakeri, S., & Dinparast Djadid, N. (2016). Therapeutic applications of collagenase (metalloproteases): A review. *Asian Pacific Journal of Tropical Biomedicine. Hainan Medical University.* doi: 10.1016/j.apjtb.2016.07.017

[3] Berrios-Torres, S. I., Umscheid, C. A., Bratzler, D. W., Leas, B., Stone, E. C., Kelz, R. R., ... & Healthcare Infection Control Practices Advisory Committee. (2017). Centers for disease control and prevention guideline for the prevention of surgical site infection, 2017. *JAMA surgery,* 152(8), 784-791. doi: 10.1001/jamasurg.2017.0904

[4] Carvalho, R. L. R., Campos, C. C., Franco, L. M. C., Rocha, A. M., & Ercole, F. F. (2017). Incidence and risk factors for surgical site infection in general surgeries. *Revista Latino-americana de Enfermagem,* 25, e2848. doi: 10.1590/1518-8345.1502.2848

[5] Falanga, V., Brem, H., Ennis, W. J., Wolcott, R., Gould, L. J., & Ayello, E. A. (2008). Maintenance debridement in the treatment of difficult-to-heal chronic wounds. Recommendations of an expert panel. *Ostomy/wound Management,* (2), 2-13. PMID: 18980069

[6] Fife, C. E., Carter, M. J., Walker, D., & Thomson, B. (2012). Wound care outcomes and associated cost among patients treated in US outpatient wound centers: data from the US Wound Registry. *WOUNDS,* 24(1), 10-17. PMID: 25875947

[7] Ko, U. H., Choi, J., Choung, J., Moon, S. & Shin, J. H. (2019). Physicochemically Tuned Myofibroblasts for Wound Healing Strategy. *Sci. Rep.,* 9, 16070. doi: 10.1038/s41598-019-52523-9

[8] Kumar, V., Abbas, A. K., Fausto, N., & Aster, J. C. (2014). Robbins and Cotran pathologic basis of disease, professional edition e-book. *Elsevier health sciences*. ISBN 978-5-98657-052-5.

[9] Leavitt, T., Hu, M., Marshall, C., Barnes, L., Longaker, M., & Lorenz, P. (2016). Stem cells and chronic wound healing: state of the art. *Chronic Wound Care Management and Research*, 3, 7-27. doi: 10.2147/CWCMR.S84369

[10] Lee, H. J., & Jang, Y. J. (2018). Recent Understandings of Biology, Prophylaxis and Treatment Strategies for Hypertrophic Scars and Keloids. *International Journal of Molecular Sciences,* 19(3), 711. doi: 10.3390/ijms19030711

[11] Mathew-Steiner, S. S., Roy, S., & Sen, C. K. (2021). Collagen in Wound Healing. *Bioengineering,* 8(5), 63. doi: 10.3390/bioengineering8050063

[12] Nourian Dehkordi, A., Mirahmadi Babaheydari, F., Chehelgerdi, M., & Raeisi Dehkordi, S. (2019). Skin tissue engineering: wound healing based on stem-cell-based therapeutic strategies. *Stem Cell Res. Ther.*, 10(1), 111. doi: 10.1186/s13287-019-1212-2

[13] Onesti, M. G., Fioramonti, P., Fino, P., Sorvillo, V., Carella, S., & Scuderi, N. (2016). Effect of enzymatic debridement with two different collagenases versus mechanical debridement on chronic hard-to-heal wounds. *International Wound Journal,* 13(6), 1111-1115. doi: 10.1111/iwj.12421

[14] Patry, J., & Blanchette, V. (2017). Enzymatic debridement with collagenase in wounds and ulcers: a systematic review and meta-analysis. *International Wound Journal,* 14(6), 1055-

1065. doi: 10.1111/iwj.12760
[15] Petrenko, O. M. (2017). Аналіз результатів консервативного та хірургічного лікування пацієнтів із хронічними ранами за традиційною методикою [Analysis of the results of conservative and surgical treatment of patients with chronic wounds according to traditional methods]. *Український медичний часопис - Ukrainian Medical Journal*, 6, 133-135.
[16] Ramundo, J. & Gray, M. (2009). Collagenase for enzymatic debridement: a systematic review. *Journal of Wound, Ostomy, and Continence Nursing: Official Publication of the Wound, Ostomy and Continence Nurses Society,* 36(6 Suppl), S4-S11. doi: 10.1097/WON.0b013e3181bfdf83
[17] Reinke, J. M., & Sorg, H. (2012). Wound repair and regeneration. European surgical research. Europaische chirurgische Forschung. *Recherches chirurgicales europeennes,* 49(1), 35-43. doi: 10.1159/000339613
[18] Sen, C. K. (2019). Human Wounds and Its Burden: An Updated Compendium of Estimates. *Advances in Wound Care,* 8(2), 39-48. doi: 10.1089/wound.2019.0946
[19] Shtanyuk, E. A., Minukhin, V. V., Lyapunov, M. O., Bezugla, O. P., & Purtov, O. V. (2015). Сучасні проблеми та перспективи профілактики та лікування інфекційних ранових ускладнень (огляд літератури) [Modern problems and prospects of prevention and treatment of infectious wound complications (literature review)]. *Експериментальна і клінічна медицина - Experimental and Clinical Medicine,* 66(1), 68-72.
[20] Sibbald, R. G., Elliott, J. A., Persaud-Jaimangal, R., Goodman, L., Armstrong, D. G., Harley, C., … & Somayaji, R. (2021). Wound Bed Preparation 2021. *Advances in skin & wound care,* 34(4), 183-195. doi: 10.1097/01.ASW.0000733724.87630.d6
[21] Singer, A. J. (2022). Healing Mechanisms in Cutaneous Wounds: Tipping the Balance. Tissue engineering. *Part B, Reviews,* 28(5), 1151-1167. doi: 10.1089/ten.TEB.2021.0114
[22] Velnar, T., Bailey, T., & Smrkolj, V. (2009). The wound healing process: an overview of the cellular and molecular mechanisms. *The Journal of International Medical Research,* 37(5), 1528-1542. doi: 10.1177/147323000903700531
[23] Wilkinson, H. N., & Hardman, M. J. (2020). Wound healing: cellular mechanisms and pathological outcomes. *Open Biology,* 10(9), 200223. doi: 10.1098/rsob.200223

МОРФОЛОГІЧНЕ ОБҐРУНТУВАННЯ ЕФЕКТИВНОСТІ ВИКОРИСТАННЯ ЛІКУВАЛЬНОЇ СУМІШІ "ІРУКСАН" В ЕКСПЕРИМЕНТІ

Хіміч С. Д., Рауцкіс В. П.

Лікування інфікованих та гнійних ран залишається актуальною проблемою на сьогоднішній день. Науковий і практичний інтерес викликає застосування ферменту колагенази у препаратах для санації рани. Мета: вивчити морфологічні зміни тканин контамінованих та гнійних ран щурів в експерименті під час їх лікування гелем "Іруксан", що містить колагеназу. Для відтворення ранової інфекції її контамінували патогенним штамом Staphylococcus aureus у комбінації із Pseudomonas aeruginosa, котрі є типовими збудниками ранової інфекції у хірургічних пацієнтів. У процесі експерименту застосовані мікробіологічні, гістологічні, статистичні методи дослідження. Після інфікування модельованих ран у всіх щурів проводили контроль контамінації та ідентифікації збудника перед початком дії досліджуваного препарату та в день виводу щурів з експерименту. За допомогою мікробіологічних досліджень виявлено, що кількість мікроорганізмів у ранах тварин контрольної групи залишалась практично незмінною (p>0,05) до 10 дня спостереження, а у дослідній групі (для лікування ран застосовували гель "Іруксан") кількість мікроорганізмів у ранах зменшувалась (p<0,05) уже до 7-ї доби експерименту. Отримані дані корелюють з результатами морфологічного дослідження, а саме з виразністю запального процесу. Виявлено, що зменшення ознак запального процесу і розвиток епітелізації ранового дефекту відбувався швидше у дослідній групі тварин. За результатами гістологічних досліджень встановлено повне покриття ранової поверхні новоутвореним епітелієм уже на 7-му добу експерименту у дослідній групі, що суттєво відрізняється від показників контрольної групи, де на 7-му добу визначались типові ознаки перебігу ранового процесу для цього часового проміжку. В контрольній групі тварин епітелізація ран спостерігалася на 10-ту добу. Отже, отримані дані свідчать про позитивний ефект використання препарату з колагеназою ("Іруксан") при лікуванні ран, а саме про доцільність його застосування у першій фазі ранового процесу, що дозволяє скоротити терміни очищення поверхні рани від гнійно-некротичних тканин та пришвидшити її епітелізацію.

Ключові слова: *гнійна рана, інфікована рана, рановий процес, колагеназа, морфологічні зміни в рані, хірургічна обробка рани.*

DOI: 10.31393/morphology-journal-2023-29(3)-06 Reports of Morphology, Vol. 29, №3, Pages 39-44

ISSN 1818-1295 eISSN 2616-6194

REPORTS OF MORPHOLOGY

Official Journal of the Scientific Society of Anatomists, Histologists, Embryologists and Topographic Anatomists of Ukraine

journal homepage: https://morphology-journal.com

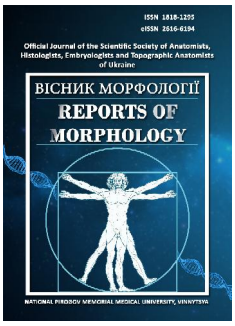

Features of immediate adaptation of the circulatory system to static load in persons with different body mass index

Pastukhova V. A., Bakunovsky O. M., Drozdovska S. B., Filippov M. M., Ilyin V. M., Krasnova S. P., Oliinyk T. M.
National University of Ukraine on Physical Education and Sport, Kyiv, Ukraine

ARTICLE INFO
Received: 24 May 2023
Accepted: 19 June 2023

UDC: 612.13:613.73(045)

CORRESPONDING AUTHOR
e-mail: Pastuhova_V@ukr.net
Pastukhova V. A.

CONFLICT OF INTEREST
The authors have no conflicts of interest to declare.

FUNDING
Not applicable.

In the vast majority of sports, muscle activity is dynamic in nature, however, recently sports physiologists have been paying considerable attention to static exercises. The deep mechanisms of the phenomenon of static efforts have been studied since its discovery, but there are still many gaps in biological knowledge regarding the issue of the impact of static load on the functioning parameters of the circulatory system in individuals with different anthropometric characteristics. The purpose of the work is to study the influence of dosed static load on the parameters of the circulatory system during the early recovery period in people with different body mass indexes. During the study, 36 young men were examined, who were divided into two groups according to the body mass index (BMI) criterion - young men with a normal BMI (nBMI group, the average value of BMI in the group - 21.6), as well as young men with an increased BMI (group iBMI, the average value of BMI in the group is 28.1). Static load (SL) was modeled by maintaining a force equal to 50 % of the maximum static force for 15 seconds on a static dynamometer DS-200. Before exercise and within 3 minutes after its completion, the main parameters of central hemodynamics were measured in the examined persons using tetrapolar thoracic rheoplethysmography on the computerized diagnostic complex "Cardio+" (Ukraine). Statistical data processing was carried out using the computer program IBM SPSS Statistics (version 26), using non-parametric methods of evaluating the obtained results. We have established that in the initial state, young men with a normal body mass index differ from persons with an increased body mass index by a lower value of heart rate, total peripheral resistance and blood pressure, as well as higher values of stroke and minute blood volumes, stroke and cardiac indices. The dosed static load leads to the same nature of changes in the parameters of the circulatory system in all examined persons, regardless of the body mass index. Differences in body mass index affect only the degree of manifestation of certain changes. A more significant manifestation of the Lingard phenomenon was recorded in young men with an increased body mass index, as evidenced by a greater degree of deviation of the measured parameters of the circulatory system in response to static exercise.

Keywords: *circulatory system, early recovery, static load.*

Introduction

In 2020, 100 years have passed since Lingard discovered the phenomenon of static effort. The deep nature of the phenomenon named after the discoverer was also studied by physiologists in the following decades. However, sports physiologists pay much more attention to physical exercises of a dynamic nature [3, 14]. In the vast majority of sports, muscle activity is dynamic in nature, but recently there has been a growing interest in health physical culture in static exercises [5, 15], to the study of which a significant contribution was made by the domestic scientist O. R. Radzievsky. They are an effective tool not only for developing strength, but also for endurance and flexibility. In strength fitness, programs have been developed based on the use of static exercises for body weight correction, etc. [2, 10, 12, 13, 18, 24].

However, we should note that there are still relatively few special works aimed at researching the impact of static loads on the parameters of the blood circulation system in modern scientific development [6, 11, 16]. The question of the relationship between static physical load and

anthropometric parameters attracts even less attention of researchers [1, 14]. We could not find scientific publications devoted to the study of the influence of body composition on the course of short-term adaptation to dosed static load in the available literature.

The purpose of our work was to study the effect of dosed static load on the parameters of the circulatory system during the early recovery period in people with different body mass indexes.

Materials and methods

The work is a fragment of the research work of the department of medical and biological disciplines of the National University of Physical Education and Sports of Ukraine "The influence of exogenous and endogenous factors on the course of adaptive reactions of the body to physical exertion of various intensities" (state registration number 012U108187). 42 untrained young men (20 years old) who had no bad habits, were practically healthy and had no acute diseases or chronic pathology were examined. Martine's test was used for preliminary selection and formation of groups. For the next stage of work, from the total number of examined persons, those in whom the reaction to the Martine test was normotonic (36 persons) were selected. In the future, to study the reaction of the circulatory system to static load, body weight and length were determined (using a floor height meter with mechanical scales RPV 2000), body mass index (BMI) according to the Quetelet formula, (the Quetelet index, QI = body weight(kg)/height^2(cm), maximum standing strength (using a standing dynamometer DS-200). For further analysis of the obtained results, the examined young men were divided into 2 groups according to the BMI criterion in accordance with WHO recommendations - persons with a normal BMI (nBMI group, n=18, young men with BMI from 18.8 to 24.9; group mean - 21.6), individuals with increased BMI (iBMI, n=18, examined with BMI from 27.4 to 30.0; group mean - 28.1). Individuals with BMI below the norm, and with a BMI considered as obesity, there were no subjects examined in our study.

The Bioethics Committee of the National University of Physical Education and Sports of Ukraine (protocol № 3 dated 22.01.2021) established that the research does not contradict the basic bioethical standards of the Helsinki Declaration, the Council of Europe Convention on Human Rights and Biomedicine (1977), the relevant WHO resolutions and the laws of Ukraine.

Static load (SL) was modeled by holding on a static dynamometer DS-200 for 15 seconds a force that was 50 % of the maximum static force. Before and at the 1st, 2nd and 3rd minutes after the end of the exercise, blood pressure was measured in a standing position (according to the Korotkov method), heart rate was counted for 10 seconds by palpation on the left carotid artery. At the same time, a tetrapolar thoracic rheoplethysmogram was recorded in a standing position using the computerized diagnostic complex "Cardio+". The following parameters were analyzed - heart rate (HR), stroke and minute blood volumes (SV and MBV, respectively), stroke and cardiac indices (SI and CI, respectively), total peripheral vascular resistance (TPR), systolic and diastolic blood pressure (sAT and dAT, respectively). We analyzed the pumping function of the heart and the state of peripheral resistance of blood vessels by indicators normalized to the body surface area of the examinees (SI, CI), and not by the absolute values of systolic and cardiac output and TPR, with the aim of leveling anthropometric differences between individuals from different groups.

Statistical data processing was carried out using the computer program IBM SPSS Statistics (version 26), using non-parametric methods of evaluating the obtained research results.

Results

A total of 36 young men were examined, the height of the subjects was in the range of 170-193 cm (average height - 179.8 cm), body weight - in the range of 60-103 kg (average value - 78.4 kg), BMI - from 19.8 to 28.9 (on average - 24.2). Changes in central hemodynamic parameters in examined young men with different body mass indexes before static exercise and in the early recovery period after it are presented in Table 1.

At rest, the heart rate in individuals of the nBMI group (76.01±3.12 beats/min) is significantly lower by 10.27 % compared to representatives of the iBMI group (83.82±3.42 beats/min). Static load causes an initial decrease in heart rate in individuals of both groups (by 6.14 % and 8.11 %, all with $p<0.05$) compared to the initial state. However, already 1 minute after the end of the load, the heart rate increases in young men of both groups, but to a different extent - by 5.01 % in the nBMI group, and by 7.48 % in the iBMI group (all with $p<0.05$). In the future, a tendency to restore the initial level of heart rate was recorded. This was more effective in young men with a normal BMI, because at the last follow-up period, the difference in heart rate with resting state was 1.46 % in them, while in individuals from the iBMI group it was 3.23 %.

The value of SV in individuals of the nBMI group at rest was 66.70±2.89 ml/min, which is 15.10 % higher than the value of SV in the iBMI group (56.63±2.67 ml/min). Changes in the value of SV after static loading are characterized by similar dynamics in individuals of both groups - immediately after SL, the SV parameter decreases, and after one minute it increases compensatory, followed by a gradual recovery to the initial state. Thus, the initial decrease in SV immediately after SL was 6.43 % ($p<0.05$) in the nBMI group, and 9.57 % ($p<0.05$) in the iBMI group. After 1 min. after the cessation of exercise, a compensatory increase in SV occurs in individuals of both groups - by 14.20 % ($p<0.05$) in the nBMI group and by 19.83 % ($p<0.05$) in the iBMI group. As in the case of heart rate changes, the SV parameter recovered faster in individuals of the nBMI group because, at the end of

Table 1. Changes in parameters of cardiac pumping function and central hemodynamics in response to static load.

Parameter	Group	Before SL	First minute after SL	Second minute after SL	Third minute after SL
HR, beats/s	nBMI	76.01±3.12	71.34±3.01*	79.82±3.23*	77.12±3.09
	iBMI	83.82±3.42^	77.02±3.38*^	90.09±3.55*^	86.53±3.41^
SV, ml	nBMI	66.70±2.89	62.41±2.32*	76.17±3.31*	69.24±2.91
	iBMI	56.63±2.67^	51.21±2.81*^	67.86±2.81*^	58.91±2.85
MBV, l/min	nBMI	5.071±0.362	4.452±0.314*	6.082±0.411*	5.344±0.381
	iBMI	4.753±0.291^	3.942±0.191*^	5.926±0.394*^	5.102±0.364*^
SI, ml/m^2	nBMI	36.05±1.42	33.74±1,20*	41.17±1.73*	37.43±1.50
	iBMI	28.89±1.21^	26.13±1.11*^	34.62±1.40*^	30.06±1.35^
CI, l/min/m^2	nBMI	2.742±0.228	2.418±0.215*	3.291±0.262*	2.890±0.233
	iBMI	2.421±0.174^	2.017±0.153*^	3.125±0.213*^	2.601±0.187^
TPR, dynes/sec/cm^{-5}	nBMI	1421±98	1871±114*	1302±109*	1391±102
	iBMI	1549±104^	2205±183*^	1329±121*	1519±142^
sAT, mmHg.	nBMI	120.0±2.3	136.3±4.7*	132.9±3.8*	123.7±2.6
	iBMI	122.4±3.4	141.9±4.8*	134.7±4.0*	126.9±2.8
dAT, mmHg.	nBMI	75.14±2.01	88.00±3.14*	82.00±3.02*	77.45±2.76
	iBMI	77.25±2.45	92.00±4.05*	84.88±3.92*	81.88±3.51

Notes: * - statistically significant compared to resting state, ^ - statistically different from the values of the nBMI group in the same observation period.

the observation period, the SV difference with the initial state was 3.81 % in them, in contrast to the iBMI group, in which the SV differed by 4.03 %.

The value of the MBV parameter in the nBMI group at rest was 5.071±0.362 l/min, which is statistically significantly higher than the MBV value in the iBMI group (4.753± 0.291 l/min) by 6.37 %. Static loading with respect to changes in MBV causes the same dynamics as in the case of HR and SV. Thus, in the first minute after SL, a decrease in MBV was recorded in both groups, but to a different extent - in the nBMI group by 12.81 % ($p<0.05$), in the iBMI group by 16.91 % ($p<0.05$). The second minute after the load is characterized by a compensatory increase in MBV, which changes the initial decrease of this parameter immediately after SL. In the nBMI group, the degree of growth was 19.92 % ($p<0.05$), whereas in the iBMI group it was 28.79 % ($p<0.05$). The third minute after exercise is characterized by a gradual recovery of the MBV value in both groups, but to a different extent - more effectively in individuals with a normal BMI (the difference with the resting state was 5.32 %, while in the iBMI group it was 7.39 % ($p<0.05$).

The value of SI in the nBMI group at baseline was 36.05±1.42 ml/m^2, which is 19.86 % higher than the value of the same parameter in the iBMI group (28.89±1.21 ml/m^2). The first minute after SL is characterized by a decrease in SI in both groups - by 6.43 % ($p<0.05$) in the nBMI group, and by 9.57 % ($p<0.05$) in the iBMI group. The second minute after SL is characterized by a compensatory significant increase in SI values in both groups - in the nBMI group by 14.20 % ($p<0.05$), in the iBMI group by 19.83 % ($p<0.05$). Just as in the case of changes in heart rate, SV and MBV, the third minute after exercise is characterized by the recovery of the value of SI to the values of the resting state, but this happens faster in individuals of the nBMI group - in them by 3 minutes. after SL, the difference with the resting state is 3.81 %, while in the iBMI group it is 4.03 %.

The value of the cardiac index in individuals of the nBMI group at rest is 2.742±0.228 l/min/m^2, which is 11.63 % higher than the similar parameter in the iBMI group (2.421±0.174 l/min/m^2). Static load causes a decrease in the CI parameter, which was recorded in the first minute after the end of SL in both groups - by 12.18 % ($p<0.05$) in the nBMI group, and by 16.91 % ($p<0.05$) in the iBMI group. The second minute after SL is characterized by a compensatory increase in CI at the level of 19.92 % ($p<0.05$) in individuals with normal BMI, and by 28.79 % ($p<0.05$) in the iBMI group. The course of the third minute after static loading is characterized by a decrease in CI, but reaching the value of the initial state does not occur in any of the groups. However, it is more effective to restore CI in the nBMI group because the difference with the resting state in them is 3 min is 5.32 %, and in the iBMI group - 7.39 %. At all follow-up periods, the value of CI in individuals from the nBMI group was statistically significantly greater than that in individuals from the iBMI group.

The value of TPR in persons with a normal BMI is 1421±98 dynes/sec/cm^{-5}, which is 8.97 % less than the value of the same parameter in the iBMI group (1549± 104 dynes/sec/cm^{-5}). Static load leads to the opposite changes compared to previously considered parameters - there is a strong increase in TPR in both groups, to a lesser extent - in the nBMI group (by 31.64 %, $p<0.05$), to a greater

extent - in individuals from the iBMI group (by 42.38 %, p <0.05). The second minute after the end of SL is characterized, on the contrary, by a decrease in the value of TPR compared to the initial state - by 8.41 % (p<0.05) in the nBMI group, and by 14.21 % (p<0.05) in individuals from the iBMI group. Later, a tendency to recovery of TPR was recorded in both groups, but to a different extent.

The values of systolic and diastolic pressure at rest in the individuals of both groups are not statistically significantly different. The dynamics of sAT and dAT in both groups in response to static load are very similar - the values of both types of pressure immediately after SL increase (to a greater extent in individuals from the iBMI group), gradually return to resting values in later periods. However, the degree of initial increase in sAT and dAT immediately after SL is greater in the iBMI group. The restoration of the initial value of sAT and dAT occurs more efficiently in the nBMI group because the percentage of deviation of the values of both types of pressure at 3 minutes after SL in individuals with a normal BMI is smaller compared to the iBMI group.

Discussion

According to the data of our study, the parameters of central hemodynamics are characterized by a number of differences depending on BMI and differ in individuals of different groups both in a state of rest and in the nature of urgent adaptation to static load. At rest, heart rate in both groups met the criteria for normocardia, but in the iBMI group it was significantly higher than in the nBMI group. The value of MBV in the initial state in individuals with a normal BMI exceeded the value of the similar parameter in the iBMI group due to a higher value of SV. Such a conclusion can be made in view of the lower value of the HR parameter in persons with a normal BMI compared to young men in whom the BMI is elevated. They also have higher parameters of the cardiac and shock indices at rest compared to individuals of the iBMI group. Against the background of higher values of SV and MBV in young men with a normal BMI, this may be evidence of higher functional reserves of the heart and a greater level of tolerance to physical exertion (in particular, static) compared to individuals with an increased BMI. Values of both measured types of blood pressure in the initial state did not have a statistically significant difference between the groups. However, the values of both types of pressure were more significant in young men with increased BMI both at rest and at all times after static exercise, which is consistent with the data of other researchers [17]. The greater value of total peripheral resistance in individuals from the iBMI group indicates an increased tone of pre- and post-capillary resistance vessels, which is most likely caused by increased basal sympathetic influences [19, 22].

Static load causes the same nature of changes in the parameters of the circulatory system, regardless of BMI; the difference in BMI determined only the degree of manifestation of one or another reaction of the cardiovascular system. The initial decrease in HR, SV, and MBV values immediately after SL, present in both groups, is a strain effect. It is caused by maintaining a powerful tonic effort, increasing intrathoracic, intrapulmonary pressure, and as a result, increasing compression on the heart [5, 6]. Under conditions of compression of blood vessels inside skeletal muscles during static effort, the volume of venous return of blood to the heart decreases [4, 20, 21]. As a result of the implementation of myogenic mechanisms of heart activity, this leads to a decrease in the value of the main parameters of its work, which was recorded by us immediately after SL. Further growth of the pumping function of the heart in individuals of both groups has a compensatory nature and is characterized by the desire to restore blood circulation in vessels that were compressed during static stress [7, 25]. The increase in both types of blood pressure under the influence of SL can be explained by the increase in pressure inside the aorta during the maintenance of static tension, which, according to the logic of the Anrep phenomenon (loading the heart with outflow), leads to an increase in the force of heart contraction, and as a result - to an increase in the value of sAT and dAT [8, 9].

Taking into account the greater degree of reactivity of the circulatory system in the early period of adaptation to static load in individuals with increased BMI, as well as the fact that at the last follow-up period the difference between the values of the measured parameters was smaller in the nBMI group, it can be argued that a more balanced and effective course of recovery after SL occurred in individuals with a normal body mass index.

Summarizing all of the above, it is worth noting that a greater degree of manifestation of the Lingard phenomenon in our study was recorded in young men with an increased body mass index. It can be assumed that this is connected with an increased volume of circulating blood, a greater load on the heart and stronger sympathetic influences on the activity of the heart and blood vessels. In our opinion, for more detailed conclusions, the study of changes in central hemodynamics during static exercise depending on BMI should be supplemented by the study of the reaction of the circulatory system to SL with mandatory consideration of fat and muscle components in the body composition. This will open the possibility to more accurately reveal the deep mechanisms of differences in the reactions of central hemodynamics of persons with different BMIs to different regimes of physical exertion.

Conclusion

1. At rest, young men with a normal body mass index differ from persons with an increased body mass index by a lower heart rate, total peripheral resistance and blood pressure, as well as by higher values of stroke and minute blood volumes, stroke and heart indices.

2. The dosed static load leads to the same nature of changes in the parameters of the circulatory system in all

examined persons, regardless of the body mass index. Differences in body mass index affect only the degree of manifestation of certain changes.

3. A more significant manifestation of the Lingard phenomenon was recorded in young men with an increased body mass index, as evidenced by a greater degree of deviation of the measured parameters of the circulatory system in response to static load.

4. The results obtained by us allow us to predict the reaction of the circulatory system to static load depending on the value of the body mass index, which can be of practical importance during strength training.

References

[1] Aragon, A., Brad, J., Schoenfeld, R., & Wildman, A. (2017). International society of sports nutrition position stand: diets and body composition. *J. Int. Soc. Sports Nutr.,* 14, 14-16. doi: 10.1186/s12970-017-0174-y

[2] Areta, J., Burke, L., Camera, D., West, D., Crawshay, S., & Moore D. (2014). Reduced resting skeletal muscle protein synthesis is rescued by resistance exercise and protein ingestion following short-term energy deficit. *Am. J. Physiol. Endocrinol. Metab.,* 306(8), 989-997. doi: 10.1152/ajpendo.00590.2013

[3] Bakunovsky, O. M., Lukyantseva, H. V., & Kotlyarenko, L. T. (2021). Different features of changes in central hemodynamics during early recovery after different exercise regimes. *Fiziol. Zh.,* 67(6), 13-20. doi: 10.15407/fz67.06.013

[4] Beaumont, A., Grace, F., Richards, J., Hough, J., Oxborough, D., & Sculthorpe, N. (2017) Left ventricular speckle tracking-derived cardiac strain and cardiac twist mechanics in athletes: a systematic review and meta-analysis of controlled studies. *Sports Med.,* 47(6), 1145-1170. doi: 10.1007/s40279-016-0644-4

[5] Bracamonte, J. H., Saunders, S. K., Wilson, J. S., Truong, U. T., & Soares, J. S. (2022). Patient-Specific Inverse Modeling of In Vivo Cardiovascular Mechanics with Medical Image-Derived Kinematics a Input Data: Concepts, Methods, and Applications. *Appl. Sci.* (Basel), 12(8), 3954. doi: 10.3390/app12083954

[6] Bracamonte, J. H., Wilson, J. S., & Soares, J. S. (2022). Quantification of the heterogeneous effect of static and dynamic perivascular structures on patient-specific local aortic wall mechanics using inverse finite element modeling and DENSE MRI. *J. Biomech.*, 138, 111119. doi: 10.1016/j.jbiomech.2022.111119

[7]. Chen, H., Chen, C., Spanos, M., Li, G., Lu, R., Bei, Y., & Xiao, J. (2022). Exercise training maintains cardiovascular health: signaling pathways involved and potential therapeutics. Signal Transduct. *Target Ther.,* 7(1), 1-18. doi: 10.1038/s41392-022-01153-1

[8] D'Andrea, A., Formisano, T., Riegler, L., Scarafile, R., America, R., Martone, F., ... & Calabro, R. (2017). Acute and chronic response to exercise in athletes: the "supernormal heart". *Exercise for Cardiovascular Disease Prevention and Treatment: From Molecular to Clinical,* Part 1, 21-41. doi: 10.1007/978-981-10-4307-9_2

[9] DeLorey, D. S., & Clifford, P. S. (2022). Does sympathetic vasoconstriction contribute to metabolism: Perfusion matching in exercising skeletal muscle? *Front. Physiol.*, 13, 980524. doi: 10.3389/fphys.2022.980524

[10] Evaristo, S., Moreira, C., & Lopes, L. (2019). Muscular fitness and cardiorespiratory fitness are associated with health-related quality of life: Results from labmed physical activity study. *Exerc. Sci. Fit.*, 20(2), 55-61. doi: 10.1016/j.jesf.2019.01.002

[11] Figueroa, A., Hooshmand, S., Figueroa, M., & Bada, A. M. (2010). Cardiovagal baroreflex and aortic hemodynamic responses to isometric exercise and post-exercise muscle ischemia in resistance trained men. *Scand. J. Med. Sci. Sports,* 20(2), 305-309. doi: 10.1111/j.1600-0838.2009.00927.x

[12] Hackett, D. A., & Chow, C. M. (2013). The Valsalva maneuver: its effect on intra-abdominal pressure and safety issues during resistance exercise. *J. Strength Cond. Res.*, 27(8), 2338-2345. doi: 10.1519/JSC.0b013e31827de07d

[13] Howe, L., Read, P., & Waldron, M. (2017). Muscle Hypertrophy: A Narrative Review on Training Principles for Increasing Muscle Mass. *Strength and Condit. J.*, 39(5), 72-81. doi: 10.1519/SSC.0000000000000330

[14] James, L. J., Funnell, M. P., James R. M., & Mears, S. A. (2019). Does Hypohydration Really Impair Endurance Performance? Methodological Considerations for Interpreting Hydration Research. *Sports Med.*, 49(2), 103-114.

[15] Joshi, H., & Edgell, H. (2019). Sex differences in the ventilatory and cardiovascular response to supine and tilted metaboreflex activation. *Physiol. Rep.,* 7(6), e14041. doi: 10.14814/phy2.14041

[16] Larson-Meyer, D. E., Woolf, K., & Burke, L. (2018). Assessment of Nutrient Status in Athletes and the Need for Supplementation. *Int. J. Sport Nutr. Exerc. Metab.,* 28(2), 139-158. doi: 10.1123/ijsnem.2017-0338

[17] Lee, B. S., Kim, K. A., Kim, J. K., & Nho, H. (2020). Augmented Hemodynamic Responses in Obese. *Int. J. Environ. Res. Public Health,* 176, 7321-7335. doi: 10.3390/ijerph17197321

[18] Liokaftos, D. (2019). Natural bodybuilding: An account of its emergence and development as competition sport. *Int. Review Sociol. Sport,* 54(6), 753-770. doi: 10.1177/1012690217751439

[19] Longstrom, J. M., Colenso-Semple, L. M., Waddell, B. J., Mastrofini, G., Trexler, E. T., & Campbell, B. I. (2020). Physiological, Psychological and Performance-Related Changes Following Physique Competition: A Case-Series. *J. Funct. Morphol. Kinesiol.*, 25(5), 2-27. doi: 10.3390/jfmk5020027

[20] Maden-Wilkinson, T. M., Balshaw, T. G., Massey, G. J., & Folland, J. P. (2020). What makes long-term resistance-trained individuals so strong? A comparison of skeletal muscle morphology, architecture, and joint mechanics. *J. Appl. Physiol.,* 128(4), 1000-1011. doi: 10.1152/japplphysiol.00224.2019

[21] Moore, J. P., Simpson, L. L., & Drinkhill, M. J. (2022). Differential contributions of cardiac, coronary and pulmonary artery vagal mechanoreceptors to reflex control of the circulation. *J. Physiol.,* 600(18), 4069-4087. doi: 10.1113/JP282305

[22] Notarius, C. F., Millar, P. J., & Floras, J. S. (2015). Muscle sympathetic activity in resting and exercising humans with and without heart failure. *Appl. Physiol. Nutr. Metab.,* 40(11), 1107-1115. doi: 10.1139/apnm-2015-0289

[23] Perry, B. G., & Lucas, S. J. (2021). The Acute Cardiorespiratory and Cerebrovascular Response to Resistance Exercise. *Sports Med. Open,* 27, 7(1), 36. doi: 10.1186/s40798-021-00314-w

[24] Rossow, L. M., Fukuda, D. H., Fahs, C. A., Loenneke, J. P., & Stout, J. R. (2013). Natural bodybuilding competition preparation and recovery: A 12-month case study. *Int. J. Sports Physiol. and Performance,* 8(5), 582-592. doi: 10.1123/ijspp.8.5.582

[25] Schuttler, D., Clauss, S., Weckbach, L. T., & Brunner, S. (2019). Molecular mechanisms of cardiac remodeling and regeneration in physical exercise. *Cells,* 8(10), 11-28. doi: 10.3390/cells8101128

ОСОБЛИВОСТІ ТЕРМІНОВОЇ АДАПТАЦІЇ СИСТЕМИ КРОВООБІГУ ДО СТАТИЧНОГО НАВАНТАЖЕННЯ В ОСІБ З РІЗНИМ ІНДЕКСОМ МАСИ ТІЛА

Пастухова В. А., Бакуновський О. М., Дроздовська С. Б., Філіппов М. М., Ільїн В. М., Краснова С. П., Олійник Т. М.

В переважній більшості видів спорту м'язова діяльність відрізняється динамічним характером, втім, останнім часом спортивні фізіологи приділяють значну увагу статичним вправам. Глибинні механізми феномену статичних зусиль вивчають з моменту його відкриття, але до цих пір лишається багато лакун у біологічному знанні стосовно проблематики впливу статичного навантаження на параметри функціонування системи кровообігу у осіб з різними антропометричними характеристиками. Мета роботи - дослідження впливу дозованого статичного навантаження на параметри системи кровообігу в період раннього відновлення у осіб з різним індексом маси тіла. Під час дослідження було обстежено 36 юнаків, яких за критерієм індексу маси тіла (ІМТ) було розподілено на дві групи - юнаки з нормальним ІМТ (група нІМТ, середнє значення ІМТ в групі - 21,6), а також юнаки з підвищеним ІМТ (група пІМТ, середнє значення ІМТ в групі - 28,1). Статичне навантаження (СН) моделювали шляхом утримання на становому динамометрі ДС-200 протягом 15 секунд зусилля, що складало 50 % від максимальної станової сили. Перед навантаженням та протягом 3 хвилин після його завершення у обстежених осіб вимірювали основні параметри центральної гемодинаміки за допомогою тетраполярної грудної реоплетизмографії на комп'ютеризованому діагностичному комплексі "Кардіо+" (Україна). Статистичну обробку даних проведено за допомогою комп'ютерної програми IBM SPSS Statistics (версія 26), із використанням непараметричних методів оцінки отриманих результатів. Нами встановлено, що у вихідному стані юнаки з нормальним індексом маси тіла відрізняються від осіб з підвищеним індексом маси тіла меншою величиною частоти серцевих скорочень, загального периферичного опору і артеріального тиску, а також більшими значеннями ударного і хвилинного об'ємів крові, ударного і серцевого індексів. Дозоване статичне навантаження призводить до однакового характеру змін параметрів системи кровообігу у всіх обстежених осіб, незалежно від індексу маси тіла. Відмінності в індексі маси тіла впливають лише на ступінь прояву тих або інших змін. Більш значний прояв феномену Лінгарда був зафіксований у юнаків з підвищеним індексом маси тіла, про що свідчить значніший ступінь відхилення виміряних параметрів системи кровообігу у відповідь на статичне навантаження.

Ключові слова: *система кровообігу, раннє відновлення, статичне навантаження.*

DOI: 10.31393/morphology-journal-2023-29(3)-07 Reports of Morphology, Vol. 29, №3, Pages 45-51

ISSN 1818-1295 eISSN 2616-6194

REPORTS OF MORPHOLOGY

Official Journal of the Scientific Society of Anatomists, Histologists, Embryologists and Topographic Anatomists of Ukraine

journal homepage: https://morphology-journal.com

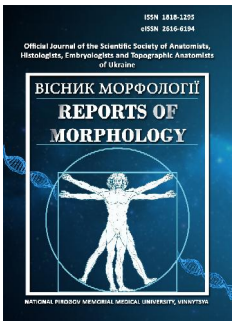

Changes in the microscopic organisation of rat adrenal glands under the influence of *Vipera berus berus* venom

Niyazmetov T. S.
Bogomolets National Medical University, Kyiv, Ukraine

ARTICLE INFO
Received: 02 June 2023
Accepted: 05 July 2023

UDC: 61:612.4:615.9.616.4:616-099

CORRESPONDING AUTHOR
e-mail: timur_X007@icloud.com
Niyazmetov T. S.

CONFLICT OF INTEREST
The authors have no conflicts of interest to declare.

FUNDING
Not applicable.

Snakebite envenoming is a common but neglected public health problem worldwide. Annual mortality as a result of snakebites exceeds 138,000. The organs of the endocrine system are among the first to react to the effects of snake and viper toxins. Under these conditions, the adrenal glands are involved in the pathological process and contribute to the formation of the adaptation syndrome, undergoing complex structural changes. The research aims to study the changes in the microscopic organization of the adrenal glands of rats under the influence of Vipera berus berus venom. Experimental studies were carried out on white non-linear male rats. The animals were conditionally divided into a control and an experimental group of 10 individuals. Experimental rats were injected intraperitoneally in a saline solution with a semi-lethal dose (LD50) (1.576 mg/g^{-1}) of Vipera berus berus venom. Animals of the control group were injected intraperitoneally with only saline solution. Rats were removed from the experiment 24 hours after exposure to the venom and anaesthetized by decapitation. Adrenal gland samples were taken for microscopic examination. Fixation of the material and preparation of paraffin blocks were carried out according to generally accepted methods. Histological preparations of the adrenal glands were stained with hematoxylin and eosin. Histological preparations were studied using an SEO SCAN light microscope. Under the influence of Vipera berus berus venom in zona glomerulosa of the adrenal cortex, moderately pronounced pathological changes were found, including vacuolization and granularity of the cytoplasm of endocrinocytes, loss of precise contours of nuclei, their hyperchromasia, expansion of lumens of sinusoidal capillaries, accumulation of erythrocytes in them. Under these conditions, zona fasciculata is characterized by significant cell granularity and perinuclear edema. Less pronounced structural organization changes were noted in the zona reticularis of the adrenal cortex. Endocrinocytes of this zone had small sizes, eosinophilic cytoplasm and dark nuclei. In the medulla of the adrenal glands, the cells were large in size and had indistinct contours, the cytoplasm was characterized by basophilic granularity, and the nuclei were light due to the predominance of euchromatin. The most pronounced effect of Vipera berus berus venom was on the zona glomerulosa and zona fasciculata of the adrenal cortex; most of the morphological signs of pathology in which were caused by a violation of protein metabolism in the cells of the parenchymal and stromal elements of this organ.

Keywords: *vipers, venom, adrenal glands, endocrinocytes, rats.*

Introduction

Snakebite envenoming is a common but neglected public health problem worldwide, especially in tropical countries. Annual mortality due to snake bites exceeds 138,000 [14, 17, 18]. It is believed that this problem is underestimated, and in many countries, individual cases of bites are not subject to proper fixation [5, 16]. In India, about 58,000 people die each year from complications caused by snake and viper venom [12, 15, 22].

About 200 species of venomous snakes are known, most of which belong to the *Elapidae* and *Viperidae* families (sometimes the *Lamprophiidae* family and the *Atractaspidinae* subfamily). They differ in the venom's chemical composition and the venomous apparatus's structure [6, 7, 8].

It is known that the toxins of snakes and vipers are a complex mixture of proteins, peptides, low molecular weight substances, and salts in the water environment [3]. Usually, the venom has a neurotoxic effect, local destruction of soft tissues in the places of its inoculation, or a vasohemotoxic effect. Clinical manifestations are diverse and include local (edema, tissue necrosis) and systemic [1, 2]. The latter manifests in neuromuscular paralysis, rhabdomyolysis, hypotension, collapse, and DIC syndrome [24, 25]. In recent years, scientists have reported the development under these conditions of endocrine and metabolic disorders due to pituitary dysfunction, adrenal gland damage, dysglycemia, electrolyte disturbances, and renal tubular acidosis [19, 20, 23].

The organs of the endocrine system are among the first to react to the effects of snake and viper toxins. The consequences of their bites can be acute or chronic in nature but cause a violation of the structure and functions of almost all central and peripheral organs of the specified system. Under these conditions, the adrenal glands are involved in the pathological process and contribute to the formation of the adaptation syndrome, undergoing complex structural changes. To date, the histological changes of the adrenal glands in the case of snake and viper bites are not sufficiently covered in the available scientific sources. In addition, there is a complete lack of data on morphological changes in the organ's structure under conditions of poisoning with toxins of the most common European vipers, namely *Vipera berus berus*, which determines the relevance of the chosen topic.

The aim of the research is to study the changes in the microscopic organization of the adrenal glands of rats under the influence of *Vipera berus berus* venom.

Materials and methods

Experimental studies were carried out on white non-linear male rats. For preliminary acclimatization, the animals were kept for seven days in the animal facility of Taras Shevchenko National University of Kyiv. Then they were kept in laboratory conditions at constant temperature (22±3°C), humidity (60±5 %) and light (12 h light/12 h dark cycle), being fed standard rodent food and water *ad libitum* [9]. All experiments were conducted by the National Institutes of Health Guidelines for the Care and Use of laboratory animals and the European Council Directive of 24 November 1986 for the Care and Use of Laboratory Animals (86/609/EEC). The research was approved and confirmed by the Bioethics Commission of the NSC "Institute of Biology and Medicine" of the Taras Shevchenko National University of Kyiv (protocol No. 2, dated August 19, 2021).

Vipera berus berus venom was obtained from the V. N. Karazin Kharkiv National University. The lyophilized crude venom was stored at -20°C and dissolved in a saline solution immediately before the experiment.

The animals were conditionally divided into a control and an experimental group of 10 individuals. Experimental rats were injected intraperitoneally in a saline solution with a semi-lethal dose (LD50) (1.576 mg/g^{-1}) of *Vipera berus berus* venom. Animals of the control group were injected intraperitoneally with only saline solution. Rats were removed from the experiment 24 hours after exposure to the venom and anaesthetised by decapitation.

Adrenal gland samples from animals of all groups were taken for microscopic examination. The pieces were fixed in a 10 % formalin solution for one day. Further, the pieces were dehydrated in alcohols of increasing concentration and embedded in paraffin blocks. Histological preparations of adrenal glands were stained with hematoxylin and eosin [13]. Histological specimens were studied using an SEO SCAN light microscope and photo-documented using a Vision CCD Camera with a system of image output from histological specimens.

Results

When exposed to *Vipera berus berus* venom, significant changes in their typical microscopic organization were observed in the adrenal glands of experimental rats.

Zona glomerulosa of the adrenal cortex of rats exposed to *Vipera berus berus* venom shows signs of moderate pathological changes. Parenchyma cells form rounded clusters separated by stroma elements. Nuclei sometimes lose precise contours (Fig. 1A), many of them are hyperchromic, and those that retain a light color are characterized by the formation of heterochromatin lumps that often accumulate under the nucleolem. Hyperchromic nuclei, in turn, have an uneven contour with signs of the early stages of karyopyknosis, which is a logical reaction of the cell to intoxication. The cytoplasm of endocrinocytes is characterized by vacuolization; in some areas, it is stained unevenly, and it also has granularity (Fig. 1D). The presence of such granularity may be associated with proteolytic processes in the cytoplasm, which lead to the accumulation of eosinophilic lumps of protein in the cytoplasm.

Stromal elements are not subject to significant changes - fibroblast nuclei are dark and flattened, as in the control group. However, the structure of the collagen fibers of the capsule appears to be loose and has unclear boundaries of both cells and extracellular elements (Fig. 1B, 1C). Such changes are generally characteristic of the stromal elements of the adrenal cortex under negative influences. If we talk about vascularization, then in contrast to the single erythrocytes inherent in the sinusoidal capillaries of the adrenal glands of animals from the control group, zona glomerulosa from this experimental group is characterized by a cluster of aggregated erythrocytes that "clog" the lumens of the sinusoids and lead to their expansion (see Fig. 1B). The presence of hollow vacuoles is also noted in the vessel lumens. Such characteristics of the microcirculatory channel can be explained by the effect of snake venom on blood plasma proteins, which can lead to its coagulation and aggregation of formal elements.

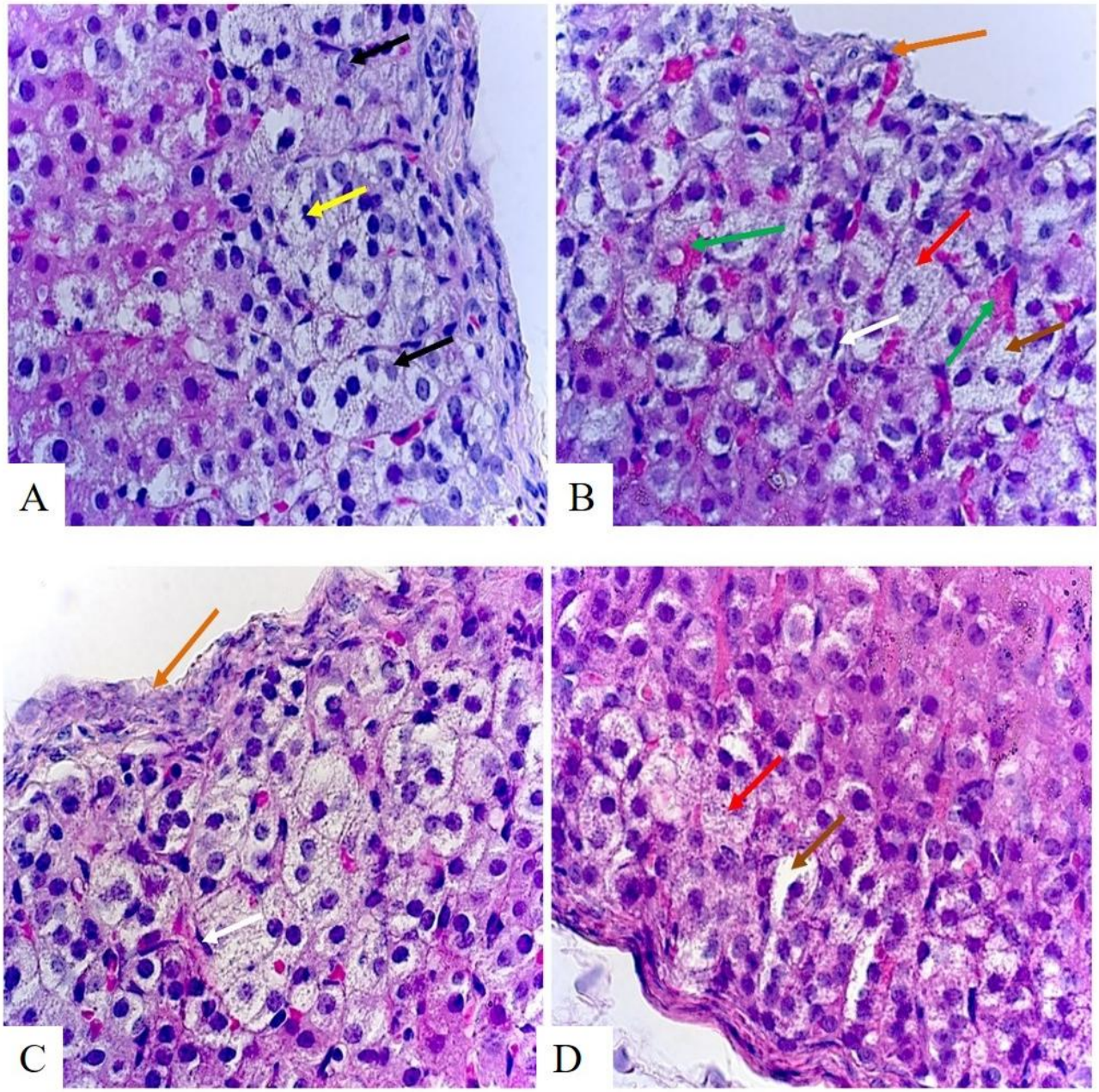

Fig. 1. Capsule and zona glomerulosa of the adrenal glands of rats from the experimental group with the injection of *Vipera berus berus* venom. A: unclear and uneven contours of nuclei (black arrows); shrunken nuclei (yellow arrows). B: accumulation of erythrocytes and vacuoles in the sinusoids (green arrows). B, C: flattened nuclei of fibroblasts (white arrows); loose collagen fibers (orange arrows). B, D: cytoplasmic vacuolization (brown arrows); cytoplasmic granularity (red arrows). Staining with hematoxylin and eosin; x1000.

Zona fasciculata of the adrenal cortex of rats from this group is characterized by columns of intensively eosinophilic cells. Their cytoplasm is characterized by pronounced granularity; cell boundaries somewhat lose clarity and become blurred. Stratification in white lumens with uneven edges on an eosinophilic background is observed in the cytoplasm, which is not the usual appearance of fat inclusions for further hormone synthesis. The number of perinuclear swellings increases; the nuclei themselves are intensively stained and have clear borders and a regular shape with smooth borders without signs of wrinkling. Quite large extracellular vacuoles are sometimes observed between the cells (Fig. 2A).

Sinusoidal capillaries in the zona fasciculata, similar to the zona glomerulosa, are filled with numerous aggregated erythrocytes, which leads to the expansion of their lumen. Single erythrocytes are challenging to distinguish, and the color of aggregated groups is uneven. Vacuoles are also sometimes observed between groups of red blood cells (Fig. 2B). The nuclei of interstitial fibroblasts remain

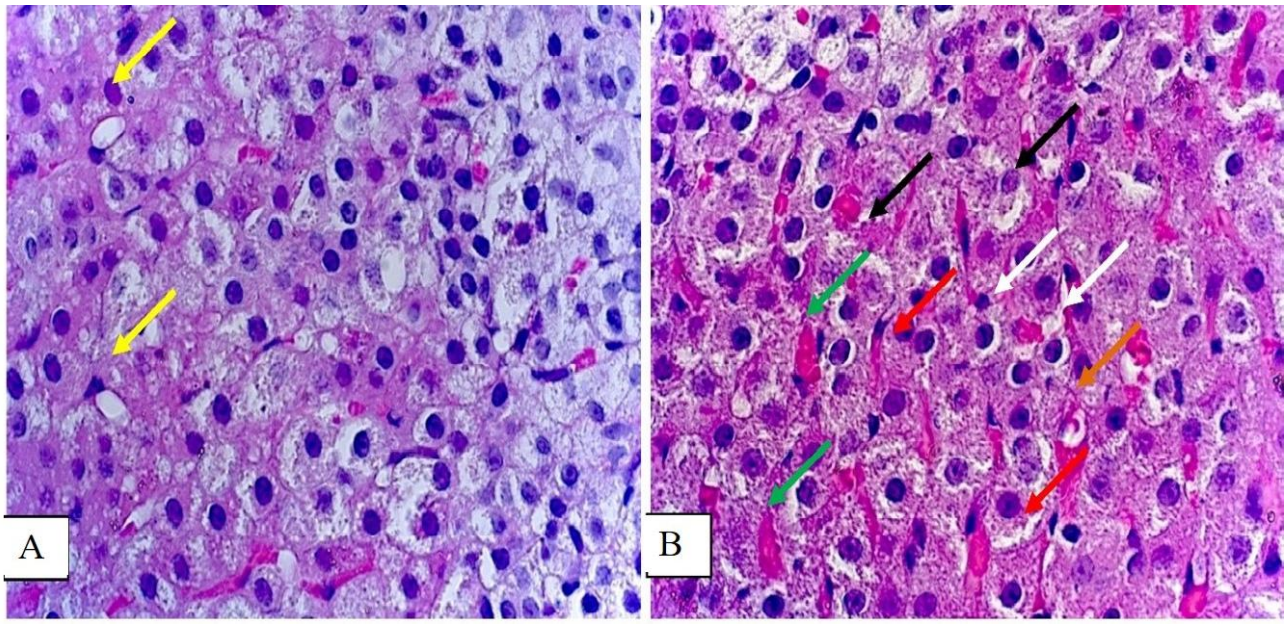

Fig. 2. Zona fasciculata of the adrenal glands of rats from the experimental group with the introduction of *Vipera berus berus* venom. A: extracellular vacuoles (yellow arrows). B: cytoplasmic granularity (red arrows); lumens in the cytoplasm (black arrows); perinuclear edema (white arrows); accumulation of erythrocytes in the sinusoids (green arrows); vacuole in the vessel lumen (orange arrow). Staining with hematoxylin and eosin; x1000.

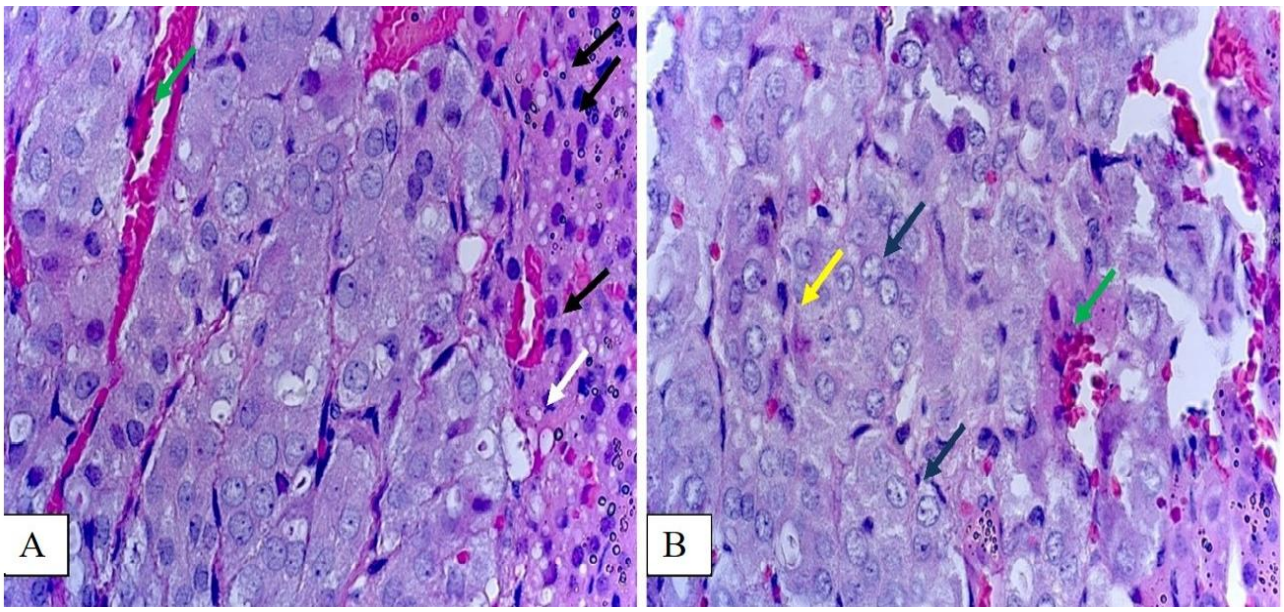

Fig. 3. Zona reticularis of the cortex (A) and the medulla (A, B) of the adrenal glands of rats from the experimental group injected with *Vipera berus berus* venom. A: elongated hyperchromic nuclei (black arrows); fat vacuole (white arrow). B: basophilic granularity (yellow arrow); euchromatic nuclei (blue arrows). A, B: vessels with aggregated erythrocytes (green arrows). Staining with hematoxylin and eosin; x1000.

flattened and dark.

Compared to other areas of the cortex of animals from this experimental group, the zona reticularis has undergone the most minor changes. Smaller sizes characterize the cells than in other zones, dark nuclei, which sometimes have an elongated shape, and eosinophilic cytoplasm with minor inclusions of fatty vacuoles (Fig. 3A, 3B).

The stroma of this zone is characterized by the presence of fibroblasts with dark, flattened nuclei, which is a typical characteristic of both other zones of the cortex of animals from this group and the control group. Dilated vessels direct to the large venous sinuses of the medulla.

Similar to the zona reticularis, the medulla of the adrenal glands does not undergo significant changes under the influence of *Vipera berus berus* venom, which is generally confirmed by the literature - the cortex reacts much more

reactively to the acute effects of poisons than the medulla. Large sizes, basophilic granularity and indistinct borders characterize the cells. The nuclei are very bright due to the predominance of euchromatin and have regular clear borders (see Fig. 3B).

The stroma of the medulla is characterized by the presence of thin interstitial connective tissue layers with elongated dark nuclei of fibroblasts and large-diameter vessels that ensure the outflow of blood from this organ, filled with formal blood elements.

Discussion

Among the known complications associated with damage of the adrenal glands in snake and viper bites are hemorrhage and acute adrenal insufficiency. Hemorrhages were recorded during numerous autopsies. In most cases, a hematoma of the adrenal glands is characteristic, and in 25 % of cases, bilateral hemorrhage was recorded, and in 6% of cases, had ischemic necrosis. Like the pituitary gland, the adrenal glands have a good blood supply, and therefore the etiology of hemorrhagic complications is equated to the Waterhouse-Friderichsen syndrome. Since the venom contains both active procoagulant components and those that cause bleeding, the development of DIC syndrome, hemorrhages and necrosis of the adrenal glands are characteristic phenomena [4].

H. J. Finol et al. [10] investigated the effect of *Bothrops venezuelensis* venom on morphological changes in the adrenal glands of experimental animals. Their results demonstrate that under these conditions, a violation of the integrity of the endothelial lining and protrusion of epithelial cells into the lumen of the capillaries were detected in the vessels of the adrenal cortex. Adrenocorticocytes contained round and oval tubular formations, which probably belonged to smooth ER. There are swollen mitochondria with a small number of crystals. Cell nuclei had vague contours enriched with heterochromatin; the perinuclear space was significantly expanded. The presence of the Golgi complex, swollen rough ER, and autophagosomes was determined. Lipid droplets with different electron densities were noticeable. Granules of lipofuscin were observed near mitochondria. 6 hours after the injection of the venom; studies showed the presence of fibroblasts with elongated nuclei in the cells of the adrenal cortex. These cells were located between the plasmalemma of adrenocorticocytes and the capillary wall. Swelling of cisterns of rough ER was detected. Mitochondria are disorganized, and lipid inclusions are visible in the cytoplasm. Chimeric formations in the cytoplasm, similar in structure to the nucleus, surrounded by a shell, were observed. Lipid inclusions had high electron density. After 24 hours of the experiment, the presence of fenestrae and individual areas with a violation of integrity were noted in the endothelial lining of the adrenal vessels. A small number of lipid droplets characterized the adrenal cortex cells, the presence of cisterns and tubules of smooth ER, numerous swollen mitochondria, multivesicular bodies, and lysosomes. In some nuclei of these cells, the perinuclear space was expanded. In some places, nuclei without heterochromatin and those containing electron-dense bodies, which probably correspond to nucleoli, were observed, but their characteristic structure was lost. The authors associate these morphological changes in the structural organization of the adrenal glands with the influence of the main components of the venom, namely proteases, PLA, and numerous non-enzymatic toxins.

According to researchers, the venom of the *Crotalus pifanorum* causes a violation of the normal histoarchitectonics of the adrenal glands of rats. It was established that 3 hours after its administration to experimental animals, swelling of mitochondrial cristae, cisterns of smooth ER, presence of Weibel-Palade bodies, and electron-dense lipid droplets are found in the cells of the organ's cortex. At the same time, individual mitochondria had tubular cristae. After 6 hours of research, capillaries were found in the cortical substance of the adrenal glands, inside which a significant number of erythrocytes were concentrated. An increase in secretory activity was observed in some endocrinocytes, manifested in an increase in organelles responsible for production and synthesis. Mitochondria had increased electron density. Lipid droplets are present in a significant amount, and smooth ER has undergone reduction. Nuclei had different electron densities and heterochromatin content, and karyolemma had signs of swelling. In some places, cells were identified where swelling or loss of mitochondrial cristae or those undergoing autophagy were observed. After 24 hours of the experiment, a violation of the structural organization of the capillary walls was detected. The latter had a detachment of the endothelium from the basement membrane. The lumen of the capillaries was filled with erythrocytes. Endotheliocytes lost the electron density of the cytoplasm; mitochondria did not have cristae. In the cytoplasm of adrenocorticocytes, there were lipid droplets, lysosomes and mitochondria with degenerative changes of the cristae. The nuclear membrane of adrenal cortex cells is swollen; degenerative processes are also visible in them. Some cells in the cytoplasm contained smooth ER and had initial signs of necrosis. It should be noted that during this study, scientists paid particular attention to structural changes in mitochondria. Thus, during their ultrastructural analysis, after 3 hours of the experiment, an increase in the intermembrane space of mitochondria, signs of their autophagy, and a violation of the integrity of the cristae were observed. In some places, there were areas of absence of the inner mitochondrial membrane. After 6 hours, organelle membrane damage and matrix vacuolization were characteristic. At the 24th hour, the research noted an even more significant expansion of the intermembrane space, an increase in the electron density of the mitochondrial matrix, ruptures, destruction of membranes, disappearance of cristae, and those

remaining cristae were swollen. The authors believe that the venom of these vipers has a toxic effect on organelles through the action of proteases and PLA [11].

Conclusions

1. Under the influence of *Vipera berus berus* venom in the zona glomerulosa of the adrenal cortex, moderately pronounced pathological changes were found, including vacuolization and granularity of the cytoplasm of endocrinocytes, loss of precise contours of nuclei, their hyperchromia, expansion of lumens of sinusoidal capillaries, accumulation of erythrocytes in them. Under these conditions, the zona fasciculata is characterized by significant cell granularity and perinuclear edema. Less pronounced structural organization changes were noted in the zona reticularis of the adrenal cortex. Endocrinocytes of this zone had small sizes, eosinophilic cytoplasm and dark nuclei.

2. In the medulla of the adrenal glands, the cells were large in size. They had indistinct contours, the cytoplasm was characterized by basophilic granularity, and the nuclei were light due to the predominance of euchromatin.

3. The venom of *Vipera berus berus* had a more pronounced effect on the zona glomerulosa and zona fasciculata of the adrenal cortex; most of the morphological signs of pathology in which were caused by a violation of protein metabolism in the cells of the parenchymal and stromal elements of this organ.

References

[1] Abd El-Aziz, T. M., Shoulkamy, M. I., Hegazy, A. M., Stockand, J. D., Mahmoud, A., & Mashaly, A. M. A. (2020). Comparative study of the in vivo toxicity and pathophysiology of envenomation by three medically important Egyptian snake venoms. *Arch Toxicol,* 94(1), 335-344. doi: 10.1007/s00204-019-02619-y

[2] Alangode, A., Rajan, K., & Nair, B. G. (2020). Snake antivenom: Challenges and alternate approaches. *Biochem. Pharmacol.,* 81, 114135. doi: 10.1016/j.bcp.2020.114135

[3] Almeida, J. R., Resende, L. M., Watanabe, R. K., Carregari, V. C., Huancahuire-Vega, S., da S Caldeira, C. A., … & Da Silva, S. L. (2017). Snake venom peptides and low mass proteins: Molecular tools and therapeutic agents. *Curr. Med. Chem.,* 4(30), 3254-3282. doi: 10.2174/0929867323666161028155611

[4] Bhattacharya, S., Krishnamurthy, A., Gopalakrishnan, M., Kalra, S., Kantroo, V., Aggarwal, S., … & Surana, V. (2020). Endocrine and metabolic manifestations of snakebite envenoming. *Am. J. Trop. Med. Hyg.,* 103(4), 1388-1396. doi: 10.4269/ajtmh.20-0161

[5] Bolon, I., Durso, A. M., Mesa, S. B., Ray, N., Alcoba, G., Chappuis, F., … & Ruiz de Castaneda, R. (2020). Identifying the snake: first scoping review on practices of communities and healthcare providers confronted with snakebite across the world. *PLoS One,* 15(3), e0229989. doi: 10.1371/journal.pone.0229989

[6] Casewell, N. R., Jackson, T. N. W., Laustsen, A. H., & Sunagar, K. (2020). Causes and consequences of snake venom variation. *Trends Pharmacol. Sci.*, 41(8), 570-581. doi: 10.1016/j.tips.2020.05.006

[7] Damm, M., Hempel, B. F., & Sussmuth, R. D. (2021). Old world vipers - a review about snake venom proteomics of viperinae and their variations. *Toxins* (Basel), 13(6), 427. doi: 10.3390/toxins13060427

[8] Di Nicola, M. R., Pontara, A., Kass, G. E. N., Kramer, N. I., Avella, I., Pampena, R., … & Paolino, G. (2021). Vipers of major clinical relevance in Europe: Taxonomy, venom composition, toxicology and clinical management of human bites. *Toxicology,* 453, 152724. doi: 10.1016/j.tox.2021.152724

[9] Dobrelia, N. V., Boitsova, L. V. & Danova, I. V. (2015). Правова база для проведення етичної експертизи доклінічних досліджень лікарських засобів з використанням лабораторних тварин [Legal basis for ethical examination of preclinical studies of drugs using laboratory animals]. *Фармакологія та лікарська токсикологія - Pharmacology and drug toxicology,* (2), 95-100.

[10] Finol, H. J., Garcia, E., Gonzalez, R., Sanchez, E. E., & Rodriguez-Acosta, A. (2020). Qualitative and quantitative ultrastructural analysis of the mitochondria from adrenal gland cortex under the action of Viperidae family snake venoms. *Int. J. Morphol.,* 38(5), 1271-1280. doi: 10.4067/S0717-95022020000501271

[11] Finol, H. J., Garcia-Lunardi, E., Gonzalez, R., Giron, M. E., Uzcategui, N. L., & Rodriguez-Acosta, A. (2020). Qualitative and quantitative study of the changes in the ultrastructure of mammalian adrenal cortex caused by the venezuelan Tigra Mariposa (Bothrops venezuelensis) snake venom. *J. Microsc. Ultrastruct.,* 8(3), 104-114. doi: 10.4103/JMAU.JMAU_49_19

[12] George, T. K., Toms, A. G., Fenn, B. N., Kumar, V., Kavitha, R., Georgy, J. T., … & Zachariah, A. (2019). Renal outcomes among snake-envenomed patients with acute kidney injury in southern India. *Natl. Med. J. India,* 32(1), 5-8. doi: 10.4103/0970-258X.272106

[13] Horalskyi, L. P., Khomych, V. T., & Kononskyi, O. I. (2011). *Основи гістологічної техніки і морфофункціональні методи досліджень у нормі та при патології [Fundamentals of histological technique and morphofunctional research methods in normal and pathology].* Житомир: Полісся - Zhytomyr: Polissya.

[14] Jayakrishnan, M. P., Geeta, M. G., Krishnakumar, P., Rajesh, T. V., & George, B. (2017). Snake bite mortality in children: beyond bite to needle time. *Arch. Dis. Child.,* 102(5), 445-449. doi: 10.1136/archdischild-2016-311142

[15] Kalita, B., Patra, A., Das, A., & Mukherjee, A. K. (2018). Proteomic analysis and immune-profiling of Eastern India Russell's Viper (Daboia russelii) venom: correlation between RVV composition and clinical manifestations post RV bite. *J. Proteome Res.,* 17(8), 2819-2833. doi: 10.1021/acs.jproteome.8b00291

[16] Longbottom, J., Shearer, F. M., Devine, M., Alcoba, G., Chappuis, F., Weiss, D. J., … & Pigott, D. M. (2018). Vulnerability of snakebite envenoming: a global mapping of hotspots. *Lancet,* 392(10148), 673-684. doi: 10.1016/S0140-6736(18)31224-8

[17] Minghui, R., Malecela, M. N., Cooke, E., & Abela-Ridder, B. (2019). WHO's snakebite envenoming strategy for prevention and control. *Lancet Glob. Health*, 7(7), 837-838. doi: 10.1016/S2214-109X(19)30225-6

[18] Paolino, G., Di Nicola, M. R., Pontara, A., Didona, D., Moliterni, E., Mercuri, S. R., … & Pampena, R. (2020). Vipera snakebite in Europe: a systematic review of a neglected disease. J. Eur. Acad. Dermatol. *Venereol.,* 34(10), 2247-2260. doi: 10.1111/jdv.16722

[19] Pucca, M. B., Knudsen, C., S. Oliveira, I., Rimbault, C., A. Cerni, F., Wen, F. H., … & Monteiro, W. M. (2020). Current knowledge

on snake dry bites. *Toxins* (Basel), 12(11), 668. doi: 10.3390/toxins12110668

[20] Seifert, S. A., Armitage, J. O., & Sanchez, E. E. (2022). Snake envenomation. *N. Engl. J. Med.,* 386(1), 68-78. doi: 10.1056/NEJMra2105228

[21] Simoes-Silva, R., Alfonso, J., Gomez, A., Holanda, R. J., Sobrinho, J. C., Zaqueo, K. D., ... & Soares, A. M. (2018). Snake venom, a natural library of new potential therapeutic molecules: challenges and current perspectives. *Curr. Pharm. Biotechnol.,* 19(4), 308-335. doi: 10.2174/1389201019666180620111025

[22] Sunil, K. K., Joseph, J. K., Joseph, S., Varghese, A. M., & Jose, M. P. (2020). Cardiac involvement in vasculotoxic and neurotoxic snakebite - a not so uncommon complication. *J. Assoc. Physicians India,* 68(11), 39-41.

[23] Ullah, A. (2020). Structure-function studies and mechanism of action of snake venom L-amino acid oxidases. *Front Pharmacol,* 11, 110. doi: 10.3389/fphar.2020.00110

[24] Variawa, S., Buitendag, J., Marais, R., Wood, D., & Oosthuizen, G. (2021). Prospective review of cytotoxic snakebite envenomation in a paediatric population. *Toxicon,* 190, 73-78. doi: 10.1016/j.toxicon.2020.12.009

[25] Waiddyanatha, S., Silva, A., Siribaddana, S., & Isbister, G. K. (2019). Long-term effects of snake envenoming. *Toxins* (Basel), 1(4), 193. doi: 10.3390/toxins11040193

ЗМІНИ МІКРОСКОПІЧНОЇ ОРГАНІЗАЦІЇ НАДНИРКОВИХ ЗАЛОЗ ЩУРІВ ПРИ ДІЇ ОТРУТИ VIPERA BERUS BERUS

Ніязметов Т. С.

Отруєння внаслідок укусів змій є частою, але занедбаною проблемою охорони здоров'я в усьому світі. Щорічна смертність, як наслідок зміїних укусів, перевищує 138 000. Органи ендокринної системи одними з перших реагують на дію токсинів змій та гадюк. Надниркові залози за даних умов залучаються до патологічного процесу та сприяють формуванню адаптаційного синдрому, зазнаючи, однак, складних структурних перебудов. Метою дослідження є вивчення змін мікроскопічної організації надниркових залоз щурів при дії отрути Vipera berus berus. Експериментальні дослідження проводили на білих нелінійних щурах самцях. Тварин умовно розподіляли на дві групи - контрольну і дослідну по 10 особин в кожній. Дослідним щурам внутрішньоочеревинно вводили напівлетальну дозу (LD50) (1,576 мг/г$^{-1}$) отрути Vipera berus berus на фізіологічному розчині. Тваринам контрольної групи внутрішньоочеревинно вводили лише фізіологічний розчин. Виводили щурів з експерименту через 24 години після впливу отрути, знеживлюючи шляхом декапітації. Для мікроскопічного дослідження забирали зразки надниркових залоз. Фіксацію матеріалу та виготовлення парафінових блоків проводили за загальноприйнятими методиками. Забарвлення гістологічних препаратів надниркових залоз здійснювали гематоксиліном та еозином. Гістологічні препарати вивчали за допомогою світлового мікроскопа SEO SCAN. При впливі отрути Vipera berus berus в клубочковій зоні кори надниркових залоз виявлено помірно виражені патологічні зміни, серед яких вакуолізація та зернистість цитоплазми ендокриноцитів, втрата чітких контурів ядер, їх гіперхромія, розширення просвітів синусоїдних капілярів, скупчення в них еритроцитів. Пучковій зоні за даних умов притаманні значна зернистість клітин та перинуклеарний набряк. У сітчастій зоні кори надниркових відмічали менш виражені зміни структурної організації. Ендокриноцити цієї зони мали невеликі розміри, еозинофільну цитоплазму й темні ядра. В мозковій речовині надниркових залоз клітини були великих розмірів, мали нечіткі контури, цитоплазма характеризувалась базофільною зернистістю, ядра були світлими внаслідок переважання еухроматину. Найбільш виражений вплив отрута Vipera berus berus чинила саме на клубочкову та пучкову зони кори надниркових, більшість з морфологічних ознак патології в яких була спричинена порушенням білкового обміну у клітинах паренхіматозних та стромальних елементів даного органу.

Ключові слова: *гадюки, отрута, надниркові залози, ендокриноцити, щури.*

DOI: 10.31393/morphology-journal-2023-29(3)-08 Reports of Morphology, Vol. 29, №3, Pages 52-57

ISSN 1818-1295 eISSN 2616-6194

REPORTS OF MORPHOLOGY

Official Journal of the Scientific Society of Anatomists, Histologists, Embryologists and Topographic Anatomists of Ukraine

journal homepage: https://morphology-journal.com

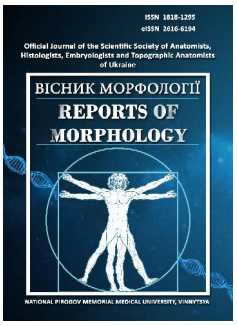

Physical and mathematical modeling of the distribution of load forces on the feminal component of an endoprosthesis of the hip joint under real conditions

Torchynskyi V. P.[1], Nizalov T. V.[1], Shmelyova L. V.[2], Suprun, A. D.[2]

[1]State University "Institute of Traumatology and Orthopedics of the National Academy of Medical Sciences of Ukraine", Kyiv, Ukraine
[2]Department of Theoretical Physics, Faculty of Physics, Taras Shevchenko Kyiv National University, Kyiv, Ukraine

ARTICLE INFO
Received: 30 June 2023
Accepted: 31 July 2023

UDC: 616.728.2-089.843-76

CORRESPONDING AUTHOR
e-mail: vtorch@ua.fm
Torchynskyi V. P.

CONFLICT OF INTEREST
The authors have no conflicts of interest to declare.

FUNDING
Not applicable.

Determination of the factors causing the development of aseptic instability of endoprosthesis components is one of the main tasks of modern traumatology and orthopedics. It is important from a scientific and medical point of view to carry out physical and mathematical modeling of the distribution of load forces and their moments on the femoral component of a hip endoprosthesis. The purpose of the study: to conduct a physical and mathematical modeling of the distribution of load forces on the femoral component of a hip endoprosthesis under real conditions of incomplete axially symmetrical contact of the femoral component of the endoprosthesis and the femur, when the surface of the lower end of the endoprosthesis is not in contact with the surface of the bone. In the work, mathematical modeling of the distribution of point load forces and their moments on the contact surface between the femoral endoprosthesis stem and the bone marrow canal of the femur in real conditions is carried out. For qualitative estimates of point distributions of the load force, based on the analysis of previous results, an estimated empirical formula was obtained for these distributions: $g(\lambda,\lambda 1)=P(\lambda,\lambda 1) / 140\lambda^{7/2}$, in which the pressure $P(\lambda,\lambda 1)$ is taken in kilograms per square centimeter (kg/cm2), and the point force $g(\lambda,\lambda 1)$ is in kilograms (kg). It was determined that the best, from the point of view of minimizing the harmful mechanical impact of the prosthesis on the femur, is the situation when the length of the prosthesis stem is not less than half the length of the femur ($\lambda \geq 0.5$). In this case, the values of the point load forces do not exceed 0.1 kg, at least for the length of the area of real contact, which is not less than half the length of the prosthesis stem ($\lambda 1 \geq 0.5\lambda$). It has been proven that the use of a prosthesis stem that is less than a third of the length of the femur is not advisable. Since already at the length of the prosthesis stem, which is 30 % of the length of the femur ($\lambda=0.3$), point loads increase rapidly and can reach from 0.55 to 1.5 kg depending on the length of the contact area. Such point loads are undesirable for the femur in the area of contact with the prosthesis in terms of the integrity of the femur.

Keywords: *bone tissue, femoral implant, point distribution of load force, mathematical model in real conditions.*

Introduction

The need to perform total hip arthroplasty is steadily increasing both in the world and in Ukraine, which is associated with traumatic cases, an increase in cases of degenerative-dystrophic diseases of the hip joint, and the general aging of the population [6, 12, 16, 21].

At the same time, cases of aseptic instability of endoprosthetic components 5-10 years after surgery account for 25-60 % of the total number of performed endoprostheses, which requires re-endoprosthetics with the use of large material costs and is a major social and medical problem [7, 17, 18, 19]. Therefore, determining the factors causing the development of aseptic instability of endoprosthesis components is one of the main tasks of modern traumatology and orthopedics.

One of the main causes of micromobility in the endoprosthesis-bone system, which leads to aseptic instability of endoprosthesis components, independent of the surgical technique, is the development of adaptive porosity of dense bone tissue and, as a result, its functional underloading or overloading [10, 14]. Today, there are no

optimal indicators of the load on the implanted femoral component of the endoprosthesis. This leads in the early postoperative period during rehabilitation loads to underloading or overloading of the bone-femoral component of the endoprosthesis system with impaired osseointegration of bone tissue.

The adaptive properties of bone tissue, depending on its external load, are a powerful means for the body to restore impaired functions of the bone system [3, 5]. However, in diagnostic studies used today, these properties are taken into account subjectively. The reason for this provision is the complexity of the adaptation process and the lack of technical means of control over the adaptive change in the structure and mechanical characteristics of living bone. Currently, the only means of predicting the reaction of bone tissue to changes in external mechanical load is biomechanical modeling [8, 20]. The method of mathematical modeling makes it possible to eliminate the need for the production of bulky physical models associated with material costs; to reduce the time of determining the characteristics (especially when calculating mathematical models using computer technologies and effective computational methods and algorithms); study the behavior of the modeling object at different parameter values, predicting the nature of its changes from the analysis of the mathematical model; analyze the possibility of using different elements; obtain characteristics and indicators that are difficult to obtain experimentally (correlation, frequency, parametric sensitivity) [15]. Therefore, it is important from a scientific and medical point of view to carry out physical-mathematical modeling of the distribution of load forces and their moments on the femoral component of the endoprosthesis of the hip joint.

The main attention in the work is focused on the calculations and analysis of the dependence of the distribution of elastic load forces on the length of the endoprosthesis stem in real conditions of incomplete contact of the femoral component of the endoprosthesis and the femur and the absence of defects in the proximal part of the femur. The distribution of forces corresponding to such a real contact can occur immediately after the operation and be a quantitative measure of the quality of its execution. Deviation from such distributions is also a quantitative measure, but of pathological changes. Therefore, knowledge of these distributions in real conditions is the task that will be implemented in this work.

The purpose of the research is to carry out physical and mathematical modeling of the distribution of load forces on the femoral component of the endoprosthesis of the hip joint under real conditions of incomplete axially symmetrical contact of the femoral component of the endoprosthesis and the femur, when the surface of the lower end of the endoprosthesis is not in contact with the surface of the bone.

Materials and methods

The article was carried out with the funds of the state budget of Ukraine, the research was carried out within the framework of the State Institution "Institute of Traumatology and Orthopedics of the National Academy of Medical Sciences of Ukraine" "Develop new and improve existing methods of diagnosis and treatment of patients with coxarthrosis with accompanying spinal pathology" (2019-2021) Subject code CF.2020.1.NAMSU (applicable), state registration № 0119U001022.

The experimental research plan was approved by the Bioethics Committee of the State Institution "Institute of Traumatology and Orthopedics of the National Academy of Medical Sciences of Ukraine" (Protocol № 198 dated 10.05.2020).

Description of the model and preliminary calculations

1. Modification of the model.

The femur is elongated along the z axis and has a length L_0=40 cm (Fig. 1). The radius of the cylindrical medullary canal of the femur is assumed to be equal to R_0=1 cm. Figure 1 shows the idealized situation for the length of the stem prosthesis Λ=20 cm length, but here too this value is used as one of the main variable parameters, the influence of which on the distribution of forces is studied [11].

The conical contact surface is modeled by a hyperboloid of rotation:

$$z(r)=\frac{L_0}{R_0}\sqrt{r^2+\frac{R_0^2}{L_0^2}\left(L_0 - \text{L}\right)^2}\quad , \qquad (1)$$

bounded from above by a horizontal plane: $z(r)=L_0$.

In a real situation, it is taken into account that the lower part of the stem prosthesis is not in contact with the inner surface of the femur. Only the upper part of the prosthesis stem is in contact Λ1 long. It is obvious that the inequality always holds Λ1≤Λ. That is, only that part of the surface (1) that satisfies the condition is considered L_0-Λ1≤ $z(r)$≤L_0.

Figure 2 shows the same situation as Figure 1, but for the case of real contact. Value Λ1 chosen equal to 15 cm. That is, in relation to the value selected in Figure 1 Λ=20 cm, Figure 2 shows a case Λ1=0.75 .

2. Determination of the real contact area of the prosthesis stem and the medullary canal of the femur.

Now the task is to find the area of the surface shown in Figure 2 and bounded from below and above by horizontal planes $z(r)=L_0$-Λ1 and $z(r)=L_0$, respectively. That is, the surface (1) we are considering is limited by inequalities:

$$\left(L_0 - \text{L}1\right) \text{£}\, z(r) \text{£}\, L_0 . \qquad (2)$$

As before [14], we first find an infinitesimally small element of the surface (1). In accordance with the definition of G. Korn and T. Korn. [9] its projection on the plane (x,y) (or (r,φ) in cylindrical coordinates) is determined by the ratio:

$$dS=\sqrt{1+\left(z\text{¢}_x\right)^2+\left(z\text{¢}_y\right)^2}\,dxdy=\sqrt{1+\left(z\text{¢}_x\right)^2+\left(z\text{¢}_y\right)^2}\,r\,dr\,d\text{j} \qquad (3)$$

where $z\text{¢}_x, z\text{¢}_y$ - partial derivatives of the surface equation (1), which here must first be used in the form:

$$z(x,y)=\frac{L_0}{R_0}\sqrt{x^2+y^2+\frac{R_0^2}{L_0^2}\left(L_0 - \text{L}\right)^2}$$

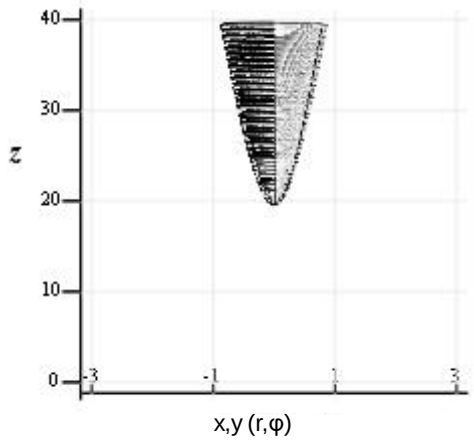

Fig. 1. General view of the contact area of the inner surface of the femur with the prosthesis stem in the ideal situation of their complete conical contact.

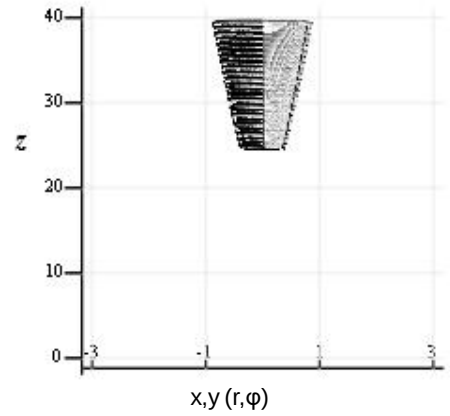

Fig. 2. The shape of the contact surface of the stem prosthesis with the inner surface of the femur in real conditions. Contact area Λ1=15 cm at Λ=20 cm. That is, Λ1=0.75Λ.

For partial derivatives can be found:

$$z_x'(x,y)=\frac{l_0 x}{\sqrt{x^2+y^2+R_0^2(1-\lambda)^2}}\cdot\frac{l_0 r\cos(\varphi)}{\sqrt{r^2+R_0^2(1-\lambda)^2}}=z_x'(r,\varphi); \quad (4)$$

$$z_y'(x,y)=\frac{l_0 y}{\sqrt{x^2+y^2+R_0^2(1-\lambda)^2}}\cdot\frac{l_0 r\sin(\varphi)}{\sqrt{r^2+R_0^2(1-\lambda)^2}}=z_y'(r,\varphi), \quad (5)$$

where $l_0 = L_0/R_0$ - dimensionless femur length in units of radius R_0, and $\lambda = L/L_0$ - the dimensionless length of the stem prosthesis relative to the length of the femur. As you can see here l_0=40, and λ varies within 0<λ<1. In accordance with definitions (3), (4) and (5) for the differential element *dS* of the considered surface in both representations - both Cartesian and cylindrical - can be found:

$$dS(x,y)=\sqrt{1+\frac{l_0^2(x^2+y^2)}{x^2+y^2+R_0^2(1-\lambda)^2}}\,dx\,dy\cdot$$

$$\cdot\sqrt{1+\frac{l_0^2 r^2}{r^2+R_0^2(1-\lambda)^2}}\,r\,dr\,d\varphi = dS(r,\varphi)$$

To find the area S of the surface contact, it is most convenient to use the cylindrical representation:

$$dS(r,\varphi)=\sqrt{1+\frac{l_0^2 r^2}{r^2+R_0^2(1-\lambda)^2}}\,r\,dr\,d\varphi\ . \quad (6)$$

In this representation of integration over the angular variable φ from 0 to 2π can be performed immediately, since nothing depends on it. That is, such an integral will give simply a factor 2π. As for integration by variable *r*, then here the integration is performed within the range of values that now depends on two parameters. From the dimensionless length of the prosthesis stem λ and the length of the contact area $\lambda 1 = L1/L_0$ and are determined by condition (2). To find the limits of integration, we will substitute (1) in (2) and solve the obtained relation *r* for both parts of inequality (2). As a result, we will have a value R_λ and $R_{\lambda 1}$, respectively, for the upper and lower limits of integration:

$$R_\lambda = R_0\sqrt{1-(1-\lambda)^2}\ ;\ \ R_{\lambda 1}=R_0\sqrt{(1-\lambda 1)^2-(1-\lambda)^2}, \quad (7)$$

and the integral itself for determining the required area is reduced to the form:

$$S(\lambda,\lambda 1)=\pi R_0^2\int_{(1-\lambda 1)^2-(1-\lambda)^2}^{1-(1-\lambda)^2}\sqrt{1+\frac{l_0^2 x}{\left(x+(1-\lambda)^2\right)}}\,dx \quad (8)$$

In the last entry, it is emphasized that the dependence of the area *S* is investigated not only on the dimensionless length of the prosthesis stem: $\lambda = L/L_0$, and from the dimensionless length of the contact region: $\lambda 1 = L1/L_0$. Figure 3 shows the dependence *S*(λ,λ1), calculated according to formula (8). The highest curve (λ1=λ) in Figure 3 corresponds to the ideal situation of full surface contact [11]. From the graphs in Figure 3, it can be seen that when the area of real contact is not less than 75 % of the length of the prosthesis stem (λ1-0.75λ), then the value of the area differs little from the ideal situation. The contact area decreases significantly when the length of the contact area decreases λ1 (in Figure 3 are curves λ1=0.5λ and λ1=0.25λ).

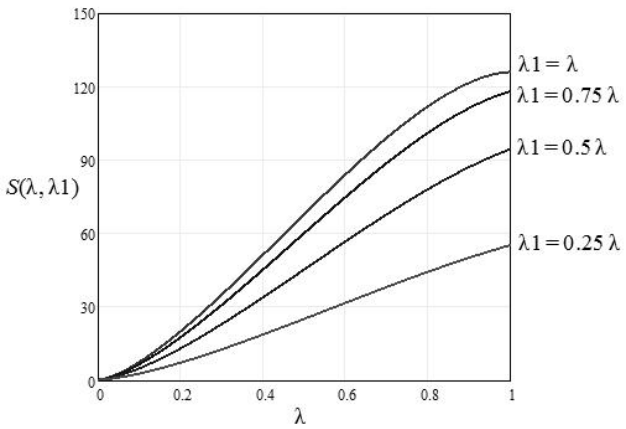

Fig. 3. Accurate dependence of the area *S*(λ,λ1) from the dimensionless length of the prosthesis stem λ for different values of the dimensionless length of the real contact region λ1 surfaces of the prosthesis stem and bone marrow canal of the femur (cm²).

Results

Determination of pressure and point distribution of load forces in the "prosthesis-femur" system under real conditions and analysis of its influence on mechanical stability.

Now, knowing the contact area (8), it is necessary to find the basic characteristics - the pressure on the contact surface of the stem prosthesis and the femur and point distributions of load forces.

Pressure is defined as the ratio of the magnitude of the load force F_0 to the contact area $S(\lambda,\lambda 1)$: $P(\lambda,\lambda 1)=F_0/S(\lambda,\lambda 1)$, where the area is defined by the integral (8). As before, the basic load force is assumed to be equal: F_0=40kg. Dependence of pressure on dimensionless length λ prosthesis stem for different values of the contact area λ1 shown in Figure 4.

Here, the lowest curve 1 corresponds to the ideal case [11] (λ1=λ). Curve 2, which corresponds to the contact area, which is 75 % of the length of the prosthesis stem (λ1=0.75λ) is quite closely adjacent to it. As can be seen from the figure, the area: $0{,}75\lambda \le \lambda 1 \le \lambda$ (when the length of the contact surface exceeds 75 % of the total length of the stem of the prosthesis) is the best, as it provides the least pressure on the femur from the side of the prosthesis. Further, with the reduction of the contact area, the pressure increases quite quickly, which is already undesirable from the point of view of the integrity of the femur.

For qualitative estimates of point distributions of the load force, based on the analysis of previous results of T. V. Nizalov and co-authors [11], an estimated empirical formula was obtained for these distributions:

$$g(l,l1)=\frac{P(l,l1)}{140\,l^{7/2}},$$

in which the pressure $P(\lambda,\lambda 1)$ is taken in kilograms per square centimeter (kg/cm^2), and point force $g(\lambda,\lambda 1)$ - in kilograms (kg). The distribution of this force is shown in Figure 5.

Figure 5 shows that the best situation, from the point of view of minimizing the harmful mechanical impact of the prosthesis on the femur, is when the length of the stem of the prosthesis is not less than half the length of the femur ($\lambda \ge 0.5$). In this case, the values of point load forces do not exceed 0.1 kg, at least for the length of the area of real contact, which is not less than half the length of the stem prosthesis ($\lambda 1 \ge 0.5\lambda$). As can be seen from Figure 5 (curve 4), already for the length of the contact area, which is a quarter of the length of the prosthesis stem (λ1=0.25λ) the point force can reach 0.15 kg for the stem length of the prosthesis, which is half the length of the femur (λ=0.5). From the graphs in Figure 5, it is also clear that the length of the prosthesis stem, which is less than one third of the length of the femur, is undesirable. Because already at the length of the prosthesis stem, which is 30 % of the length of the femur (λ=0.3), point loads grow rapidly and, as can be seen from the graphs in Figure 5, can reach from 0.55 to 1.5 kg, depending on the length of the contact area. Such

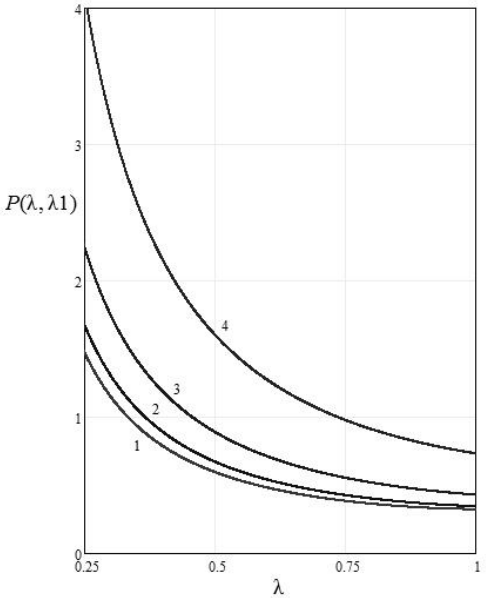

Fig. 4. Dependence of pressure distributions on the dimensionless length of the prosthesis stem for different values of the real contact length (kg/cm^2). 1 - (л1=л); 2 - (л1=0.75л); 3 - (л1=0.5л); 4 - (л1=0.25л).

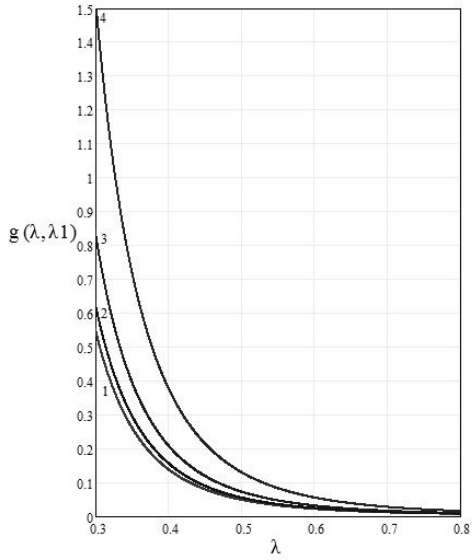

Fig. 5. Dependence of point distributions of load forces on the dimensionless length of the prosthesis stem for different values of the real contact length (kg). 1 - (л1=л); 2 - (л1=0.75л); 3 - (л1=0.5л); 4 - (л1=0.25л).

point loads are undesirable for the femur in the area of contact with the prosthesis in terms of the integrity of the femur.

Discussion

Mathematical models of the theory of reliability are models that take into account mechanical, physical and other real processes that entail a change in the properties of the object and its constituent parts. These are mechanics

models that are widely used in structural calculations. Force and kinematic interactions of elements and structures are complex. The behavior of these objects significantly depends on their interaction with the environment, the nature and intensity of operational processes [4].

To predict the behavior of structural elements, it is necessary to take into account the processes of loading, deformation, wear, accumulation of damage and destruction under variable loads and other external influences. It is possible to evaluate system reliability indicators theoretically and computationally based on physical models and statistical data on material properties, loads and impacts [1].

On the basis of previously developed methods of mathematical modeling of load forces for stem endoprosthesis of the hip joint under conditions of ideal contact, similar calculations were carried out under conditions of real contact for pressure on the femur from the side of the stem endoprosthesis and point distributions of load forces. Namely, under conditions when the area of the top of the femoral component of the endoprosthesis is not in contact with the femur.

The area of real contact between the stem prosthesis and the medullary canal of the femur, when the contact surface is not completely dense in the area of the distal end of the stem prosthesis, was modeled in the form of a truncated hyperboloid of rotation, which is the closest geometric shape of this part of the prosthesis in real conditions. The truncation plane was considered perpendicular to the axis of the femoral component of the endoprosthesis. The main attention was focused on the analysis of the dependence of the real contact area, the pressure on the femur from the endoprosthesis, and the point distributions of load forces on the length of the stem prosthesis and the contact area. Deviations in the distribution of pressure and point load forces under conditions of real contact due to changes in the contact area caused by disturbances in different zones in accordance with the classification of W. G. Paproski and co-authors [13] is a quantitative measure of pathological changes during the operation of the endoprosthesis.

Comparison of the observed changes in the contact area with the results of pressure calculations and point distributions of load forces for such changes may in the future provide an opportunity to develop a diagnostic and treatment algorithm and determine the need for additional surgical intervention.

The conducted research will contribute to the development of a diagnostic and treatment algorithm, the implementation of which will increase the effectiveness of the treatment of this severe orthopedic pathology.

Conclusion

1. In the work, mathematical modeling of the distribution of point load forces and their moments on the contact surface between the femoral endoprosthesis stem and the medullary canal of the femur under real conditions is carried out.

2. It was determined that the best situation, from the point of view of minimizing the harmful mechanical impact of the prosthesis on the femur, is the situation when the length of the stem of the prosthesis is not less than half the length of the femur ($\lambda \geq 0.5$). In this case, the values of point load forces do not exceed 0.1 kg, at least for the length of the area of real contact, which is not less than half the length of the prosthesis stem ($\lambda 1 \geq 0.5\lambda$).

3. It has been proven that the use of a stem prosthesis that is less than a third of the length of the femur is not advisable. Because already at the length of the prosthesis stem, which is 30 % of the length of the femur ($\lambda=0.3$), point loads grow rapidly and can reach from 0.55 to 1.5 kg, depending on the length of the contact area. Such point loads are undesirable for the femur in the area of contact with the prosthesis in terms of the integrity of the femur.

References

[1] Diagne, H. R., Tchoumi, S. Y., & Tchuenche J. M. (2021). A mathematical model of COVID-19 with vaccination and treatment. *Computational and Mathematical Methods in Medicine,* 2, 16. doi: 10.1155/2021/1250129

[2] Goncalves, P. T., Arteiro, A., Rocha, N., & Pina, L. (2022). Numerical Analysis of Micro-Residual Stresses in a Carbon/ Epoxy Polymer Matrix Composite during Curing Process. *Polymers,* 14, 2653. doi: 10.3390/polym14132653

[3] Guzhevsky, I. V., & Solodei, I. I. (2017). Питання побудови сучасних математичних моделей біомеханіки при вирішенні проблем ендопротезування кульшового суглоба [The question of building modern mathematical models of biomechanics when solving the problems of hip joint replacement]. *Опір матеріалів і теорія споруд - Resistance of Materials and Theory of Structures,* 99, 106-122.

[4] Hameed, A. Z., Aravind Raj, S., Kandasamy, J., Shahzad, M. A., & Baghdadi, M.A. (2022) 3D Printing Parameter Optimization Using Taguchi Approach to Examine Acrylonitrile Styrene Acrylate (ASA) Mechanical Properties. *Polymers,* 14, 3256. doi: 10.3390/polym14163256

[5] Heckmann, N. D., Yang, J.-W., Ong, K. L., Lau, E. C., Brian, C. F., Bohl, D. D., & Della Valle, C. J. (2021). Revision Surgery for Instability After Total Hip Arthroplasty: Does Timing Matter? *J. Arthroplasty,* 36(5), 1779-1783. doi: 10.1016/ j.arth.2020.12.035

[6] Huang, Ch.-H., Aydemir, B., & Foucher, Kh. C. (2023). Split-Belt Treadmill Training Improves Mechanical Energetics and Metabolic Cost in Women with Unilateral Hip Osteoarthritis: A Proof-of-Concept Study. *Biomechanics,* 3(2), 220-230. doi: 10.3390/biomechanics3020019

[7] Kawai, T., Shimizu, T., Goto, K., Kuroda, Y., Okuzu, Y., Otsuki, B., Fujibayashi, S., & Matsuda, S. (2022). The impact of spinopelvic parameters on hip degeneration after spinal fusion. *Spine,* 47(15), 1093-102. doi: 10.1097/ BRS.0000000000004340

[8] Kelsey, A., Rankin, B. A. Logan, P., Nasreddine, A., Minotti, P., Leslie M., & Wiznia, D. H. (2022) Computer-assisted Navigation for Complex Revision of unstable Total Hip Replacement in a patient with Post-traumatic arthritis. *Arthroplasty today,* 15, 153-158. doi: 10.1016/j.artd.2022.03.015

[9] Korn, G., & Korn, T. (Eds.) (1984). *Справочник по математике для научных работников и инженеров. Определения, теоремы, формулы [Handbook of mathematics for scientists and engineers. Definitions, theorems, formulas].* M.: Наука - M.: Science.

[10] Martino, A. D., Brunello, M., Bordini, B., Rossomando, V., Tassinari, L., D'Agostino, C., & Faldini, F. R. C. (2023). Unstable Total Hip Arthroplasty: Should It Be Revised Using Dual Mobility Implants? A Retrospective Analysis from the R.I.P.O. Registry. *J. Clin. Med.,* 12(2), 440. doi: 10.3390/jcm12020440

[11] Nizalov, T. V., Torchynskyi, V. P., Shmelyova, L. V., & Suprun, A. D. (2016). Фізико-математичне моделювання розподілу сил навантаження та цих моментів на стегновому компоненті ендопротеза кульшового суглоба [Physico-mathematical modeling of the distribution of load forces and these moments on the femoral component of the hip joint endoprosthesis]. *Вісник ортопедії, травматології та протезування - Bulletin of Orthopedics, Traumatology and Prosthetics,* 3, 17-26.

[12] Pantha, B., Agusto, F. B., & Elmojtaba, I. M. (2020). Optimal control applied to a visceral leishmaniasis model. *Electronic Journal of Differential Equations*, 80, 1-24.

[13] Paprosky, W. G., Perona, G. P., & Lawrence, M. J. (1984). Acetabular defect classification and surgical reconstruction in revision arthoplasty, a 6 year follou-up evaluation. *J. Arthroplasty,* 9(1), 33-43. doi: 10.1016/0883-5403(94)90135-x

[14] Perticarini, L., Rossi, S., & Benazzo, F. (2020). Unstable total hip replacement: why? Clinical and radiological aspects. *HIP Int.,* 30(2), 37-41. doi: 10.1177/1120700020971725

[15] Tymanyuk, V. O., Kokody, M. G., Penkin, Y. M., Ryzhov, A. A., & Zhuk, V. A. (Eds.). (2010). *Компьютерное моделирование в курсах физики и биофизики [Computer modeling in physics and biophysics courses].* Запорожье: Издательство Запорожского государственного медицинского университета - Zaporozhye: Publishing House of Zaporozhye State Medical University.

[16] Voloshyna, O., Balashova, I., Ducova, O., Lysyi, I., Buheruk, V., Naidonova, O., … & Ukrainska, K. (2023). Possibilities of using combined kinesiotherapy in patients with coxarthrosis. *Journal of Physical Education and Sport,* 23(2), 492-501. doi: 10.7752/jpes.2023.02061

[17] Walter, N., Hinterberger, T., Szymski, D., & Alt, V. (2023). Psychological comorbidities in osteoarthritis in Germany. *Sci. Rep.,* 13, 2905. doi: 10.1038/s41598-023-29867-4

[18] Yasuda, T., Matsunaga, K., Hashimura, T., Tsukamoto, Y., Sueyoshi, T., Ota, S., … & Onishi, E. (2020). Characterization of rapidly progressive osteoarthritis of the hip in its early stage. *Eur. J. Rheumatol.*, 7(3), 130-134. doi: 10.5152/eurjrheum.2020.19159

[19] Yin, Y., Yu, Z., Wang, J., & Junzhi, S. (2022). Effectiveness of the Rehabilitation Training Combined with Maitland Mobilization for the Treatment of Chronic Ankle Instability: A Randomized Controlled Trial. *Int. J. Environ. Res. and Public Health*, 19(22), 15328. doi: 10.3390/ijerph192215328

[20] Zagrevsky, V. I., & Zagrevsky, O. I. (Eds.) (2018). *Биомеханика физических упражнений [Biomechanics of physical exercises].* Томск: Издательский дом Томского государственного университета - Tomsk: Tomsk State University Publishing House.

[21] Zhang, Q., Cai, W. W., Wang, G. H., & Shen, X. J. (2020). Prevalence and contributing factors of osteoporosis in the elderly over 70 years old: an epidemiological study of several community health centers in Shanghai. *Ann. Palliat. Med.,* 9(2), 231-238. doi: 10.21037/apm.2020.02.09

ФІЗИКО-МАТЕМАТИЧНЕ МОДЕЛЮВАННЯ РОЗПОДІЛУ СИЛ НАВАНТАЖЕННЯ НА СТЕГНОВОМУ КОМПОНЕНТІ ЕНДОПРОТЕЗА КУЛЬШОВОГО СУГЛОБА ЗА РЕАЛЬНИХ УМОВ

Торчинський В. П., Нізалов Т. В., Шмельова Л. В., Супрун А. Д.

Визначення факторів, що зумовлюють розвиток асептичної нестабільності компонентів ендопротезу є одним з основних завдань сучасної травматології та ортопедії. Важливим в науковому та медичному плані є проведення фізико-математичного моделювання розподілу сил навантаження та їх моментів на стегновому компоненті ендопротеза кульшового суглоба. Мета дослідження - провести фізико-математичне моделювання розподілу сил навантаження на стегновому компоненті ендопротеза кульшового суглоба за реальних умов неповного аксіально-симетричного контакту стегнового компоненту ендопротеза і стегнової кістки, коли поверхня нижнього кінця ендопротезу знаходиться не в контакті з поверхнею кістки. У роботі проведене математичне моделювання розподілу точкових сил навантаження та їх моментів на поверхні контакту між ніжкою стегнового ендопротезу та кістково-мозкового каналу стегнової кістки в реальних умовах. Для якісних оцінок точкових розподілів сили навантаження, на основі аналізу попередніх результатів, для цих розподілів було отримано оціночну емпіричну формулу: $g(\lambda,\lambda1)=P(\lambda,\lambda1) / 140\lambda^{7/2}$, у якій тиск $P(\lambda,\lambda1)$ береться у кілограмах на сантиметр квадратний (кг/см^2), а точкова сила $g(\lambda,\lambda1)$ - у кілограмах (кг). Визначено, що найкращою, з точки зору мінімізації шкідливого механічного впливу протезу на стегнову кістку, є ситуація, коли довжина ніжки протезу не менша половини довжини стегнової кістки ($\lambda \geq 0,5$). У цьому разі значення точкових сил навантаження не перевищують 0,1 кг принаймні для довжини області реального контакту не меншого за половину довжини ніжки протезу ($\lambda1 \geq 0,5\lambda$). Доведено, що використання ніжки протезу, меншої за третину довжини стегнової кістки не доцільно. Оскільки вже при довжині ніжки протезу, що складає 30 % від довжини стегнової кістки ($\lambda=0,3$), точкові навантаження стрімко зростають і можуть, досягати від 0,55 до 1,5 кг в залежності від довжини області контакту. Такі точкові навантаження небажані для стегнової кістки в області контакту з протезом у розумінні цілісності стегнової кістки.

Ключові слова: *кісткова тканина, стегновий імплант, точковий розподіл сили навантаження, математична модель в реальних умовах.*

DOI: 10.31393/morphology-journal-2023-29(3)-09 Reports of Morphology, Vol. 29, №3, Pages 58-66

ISSN 1818-1295 eISSN 2616-6194

REPORTS OF MORPHOLOGY

Official Journal of the Scientific Society of Anatomists, Histologists, Embryologists and Topographic Anatomists of Ukraine

journal homepage: https://morphology-journal.com

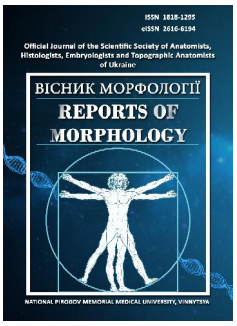

Peculiarities of correlations between spirometric and anthropometric indicators in practically healthy young women of mesomorphic somatotype

Kyrychenko Yu. V., Sarafyniuk L. A., Khapitska O. P., Dus S. V., Yakusheva Yu. I.
National Pirogov Memorial Medical University, Vinnytsia, Ukraine

ARTICLE INFO
Received: 04 July 2023
Accepted: 03 August 2023

UDC: 616.24-073.173-053.7(477.44)

CORRESPONDING AUTHOR
e-mail: lsarafinyuk@gmail.com
Sarafyniuk L. A.

CONFLICT OF INTEREST
The authors have no conflicts of interest to declare.

FUNDING
Not applicable.

The issue of studying the relationships between indicators of the external structure of the body and spirographic parameters in persons of a certain sex, age, ethno-territorial zoning remains relevant, especially from the point of view of the need to determine the reference values of indicators of external breathing. The purpose of the study was to determine the peculiarities of the relationship between spirographic parameters and indicators of the external structure of the body in practically healthy young women of the mesomorphic constitutional type of the Podilia region of Ukraine. We conducted a complex clinical and laboratory study of young women aged 16 to 20 years, which corresponds to the youthful period of ontogenesis. 109 practically healthy young women were selected, in whom no deviations in the state of health were detected according to the results of radiography, echocardiography, tetrapolar rheovasography and rheoencephalography, sonographic examination of parenchymal organs of the abdominal cavity and thyroid gland, general and biochemical blood analysis. For this group of subjects, we performed a spirographic examination using the Medgraphics Pulmonary Function System 1070 series according to the methodology of the American Pulmonology Association and the European Respiratory Society (2019). The anthropometric study was carried out according to the method of V. V. Bunak (1941), the somatotypological study - according to the calculated modification of the Heath-Carter method (1990). The assessment of the component composition of body weight was carried out according to Matiegka method (1921). After somatotyping, it was found that 32 young women had a mesomorphic type of constitution, for which Spearman's correlation analysis was conducted in the licensed software package "Statistica 5.5". It was established that the majority of spirographic indicators in practically healthy young women of the mesomorphic somatotype had isolated statistically significant correlations with anthropo-somatotypological parameters, with the exception of parameters that reflect lung capacities. Vital capacity at rest, had the largest number and strength of correlations, was significantly associated with the value of 24 anthropo-somatotypological indicators. Total, longitudinal and girth body dimensions, the ectomorphic component of the somatotype, muscle, bone and fat mass of the body were most often correlated with the capacity indicators of external respiration. All speed spirographic indicators and maximum peak expiratory flow were correlated with the skinfold thickness. The study of correlations is the basis of further mathematical modeling to determine the appropriate spirographic indicators in an individual representative of the female sex of the juvenile age of the mesomorphic somatotype.

Keywords: *spirometry, anthropometry, mesomorphic somatotype, correlation, young women, youth.*

Introduction

The modern human body is characterized by a large spectrum of phenotypic variability of anatomical and physiological features. The use of correlation analysis, as one of the main methods of assessing the harmony of physical development, allows you to comprehensively consider the interrelationships of parameters that reflect

the functions and structure of our body. Over the past decades, convincing experience has been accumulated in identifying relationships between individual morphofunctional indicators and somatometric parameters that characterize the external structure of the body [10, 19, 21, 22]. The issue of studying the relationship between indicators of the external structure of the body and spirographic parameters in persons of a certain sex, age, ethno-territorial zoning remains relevant, especially from the point of view of the need to determine the reference values of indicators of external respiration [5, 8, 15] and an individual approach to their determination [1, 14]. Which, in turn, is due to the significant progression and prevalence of respiratory diseases among the population of different countries [7, 17, 18, 25]. In particular, in Ukraine, it is the most widespread pathology, which creates a global problem for the health care of the country due to a large percentage of the impression of the working population, comorbidity of the pathologies of the lungs themselves and the negative impact on concomitant diseases [4, 13].

Currently, in scientific research, there is information about the connection of certain indicators of the external structure of the body (most often - height while standing and sitting, body weight) with spirometric indicators [9]. An inverse relationship between the characteristics of fat deposition (the amount of fat and fat-free mass, the total amount of water in the human body, the anterior-posterior size of the abdomen) and the indicators of pulmonary ventilation was found [5, 8, 15, 24]. Unfortunately, there is little data on correlations of rapid spirographic indicators, lung volumes and capacities with total and different groups of partial body sizes in practically healthy individuals of a certain sex, age, and region of Ukraine. Therefore, the solution of this scientific question is relevant and has undeniable practical significance.

The purpose of the study was to determine the peculiarities of the relationship between spirographic parameters and indicators of the external structure of the body in practically healthy young women of the mesomorphic constitutional type in the Podilia region of Ukraine.

Materials and methods

On the basis of the research center of the National Pirogov Memorial Medical University, Vinnytsia, we conducted a comprehensive clinical and laboratory study of women aged 16 to 20 years, which corresponds to the youthful period of ontogenesis. 109 practically young women (YW) were selected, in which no deviations in health were detected according to the results of radiography, echocardiography, tetrapolar rheovasography and rheoencephalography, sonographic examination of parenchymal organs of the abdominal cavity and thyroid gland, general and biochemical blood analysis. All subjects (according to the results of the questionnaire) were residents of the Podilia region of Ukraine. We performed a spirographic examination of this group of subjects using the Medgraphics Pulmonary Function System 1070 series according to the American Pulmonology Association and the European Respiratory Society method [6]. Lung volumes and capacities and speed spirographic indicators were evaluated [11].

The anthropometric study was carried out according to the method of V. V. Bunak [2], during which 49 parameters of the external structure of the body were determined. The somatotypological study was carried out according to the calculated modification of the Heath-Carter method [3]. The assessment of the component composition of body weight was carried out according to the Matiegka method [12]. After somatotyping, it was found that 32 YW had a mesomorphic type of constitution, and Spearman's correlation analysis was performed for them in the licensed software package "Statistica 5.5".

The research was carried out within the framework of the university-wide topic "Somato-viscerometric features of the human body in different periods of ontogenesis" (state registration № 0121U113772) and was approved at a meeting of the bioethics commission (Protocol № 4 dated May 18, 2023).

Results

Analyzing the interrelationships of spirographic parameters reflecting lung capacities in practically healthy YW mesomorphic somatotype with total and partial body dimensions, it is necessary to note a large number of revealed reliable correlations and unreliable connections of medium strength. Thus, *the forced vital capacity of the lungs* had significant only direct connections with constitutional characteristics, in particular with all total and almost all longitudinal dimensions of the body, girths of the stressed shoulder, waist, hips and feet, acromial diameter and external conjugate, skinfold thickness on the forearm (Table 1). The value of the *forced capacity of the lungs on inspiration* also had direct correlations of medium strength with all total and longitudinal dimensions of the body, the width of the distal epiphysis of the shoulder, the girth dimensions of the segments of the upper and lower limbs, chest, waist and hips, the external conjugate, the size of the muscle and bone mass of the body. *Vital capacity*, determined at rest, had the largest number and strength of reliable connections with indicators of the external structure of the body (see Table 1). A direct strong relationship was found with the height of the pubic point and this spirometric indicator. In addition, vital capacity was correlated with all total and longitudinal dimensions of the body, the width of the distal epiphysis of the shoulder, girth dimensions of the stressed arm, hip, lower leg in the upper third, neck, waist, hand, foot, chest, acromial diameter, ectomorphic component of the somatotype, and all components body weight composition. *Inspiratory capacity* in practically healthy YW mesomorphic somatotypes had correlations of medium strength with all total body dimensions and height of all anthropometric points, the width of the distal

Table 1. Values of correlation coefficients (r) of anthropometric dimensions with volumes spirographic indicators in mesomorph YW.

Anthropometric indicators	Lung capacity				Lung volumes	
	FVC	FIVC	SVC	IC	FEV1	ERV
body weight	**0.45**	**0.48**	**0.59**	**0.48**	**0.32**	**0.37**
body length	**0.47**	**0.50**	**0.52**	**0.39**	**0.33**	**0.30**
body surface area	**0.47**	**0.51**	**0.58**	**0.44**	**0.33**	**0.35**
height of suprasternal point	**0.42**	**0.51**	**0.57**	**0.49**	0.28	**0.32**
pubic point height	**0.45**	**0.59**	**0.62**	**0.44**	0.27	**0.42**
acromial point height	**0.39**	**0.53**	**0.55**	**0.44**	0.23	**0.31**
finger point height	0.29	**0.41**	**0.44**	**0.30**	0.06	**0.32**
height trochanter point	**0.33**	**0.43**	**0.54**	**0.40**	0.18	**0.36**
the width of the shoulder epiphysis	0.22	**0.38**	**0.32**	0.08	0.13	**0.34**
width of the epiphysis of the forearm	0.13	0.18	0.24	0.19	0.06	0.17
width of femoral epiphysis	-0.27	-0.01	-0.16	-0.04	-0.24	-0.10
the width of crus epiphysis	0.07	-0.25	0.16	**0.30**	0.15	0.01
the girth of the tense shoulder	**0.30**	0.24	**0.30**	0.27	0.25	0.06
the girth of the relaxed shoulder	0.29	0.16	0.27	**0.36**	0.25	-0.06
forearm girth in the upper part	0.02	**0.34**	0.19	0.19	0.06	0.05
forearm girth in the lower part	0.02	**-0.31**	0.01	0.29	0.09	-0.24
thigh girth	0.09	**0.40**	**0.36**	0.25	-0.03	0.22
crus girth in the upper part	0.19	**0.32**	**0.47**	**0.38**	-0.02	**0.33**
crus girth in the lower part	-0.02	-0.17	0.05	-0.01	-0.03	0.11
neck girth	0.23	0.27	**0.39**	0.28	0.17	0.19
waist girth	**0.30**	**0.55**	**0.44**	0.28	0.18	0.20
girth of the thighs	**0.38**	**0.44**	0.19	0.13	0.29	0.08
hand girth	0.14	-0.10	**0.32**	0.23	0.07	**0.32**
foot circumference	0.31	**0.46**	**0.32**	0.09	0.18	0.28
chest girth (inhale)	0.12	**0.41**	**0.51**	**0.37**	0.06	**0.32**
chest girth (exhalation)	0.07	**0.38**	**0.45**	**0.35**	0.04	0.26
chest girth (pause)	0.09	**0.37**	**0.50**	**0.45**	0.05	0.28
sagittal mid-thoracic diameter	0.12	0.11	0.26	**0.37**	0.09	-0.04
acromial diameter	**0.33**	0.25	**0.42**	0.29	0.28	0.28
interspinous distance	-0.01	0.15	-0.03	0.10	0.03	-0.10
intercristal distance	0.05	0.26	0.07	0.14	-0.02	-0.11
intertrochanteric distance	0.02	0.16	0.05	0.10	0.06	-0.01
external conjugate	**0.37**	**0.32**	0.01	-0.11	0.25	0.05
skinfold thickness on the forearm	**0.31**	0.16	0.13	0.01	0.28	0.08
skinfold thickness under the scapula	0.27	-0.02	-0.02	0.17	0.21	-0.29

Continuation of table 1.

Anthropometric indicators	Lung capacity				Lung volumes	
	FVC	FIVC	SVC	IC	FEV1	ERV
skinfold thickness on the stomach	-0.04	-0.18	0.21	0.20	-0.14	0.11
skinfold thickness on the side	-0.08	-0.05	0.26	0.19	-0.10	0.18
skinfold thickness on the thigh	0.05	0.06	0.25	0.27	-0.05	0.13
skinfold thickness on the crus	0.04	0.02	0.08	0.16	-0.03	-0.04
endomorphic component	0.01	-0.05	0.15	0.13	-0.05	0.03
mesomorphic component	-0.20	-0.18	-0.24	-0.20	-0.16	-0.21
ectomorphic component	0.14	0.11	**0.34**	**0.31**	0.11	**0.31**
muscle mass of the body	0.26	**0.45**	**0.46**	**0.37**	0.15	0.25
body bone mass	0.14	**0.30**	**0.37**	0.25	0.03	**0.32**
body fat mass	0.23	0.23	**0.40**	**0.35**	0.11	0.17

Notes: here and in the following, reliable correlations of average strength are highlighted in blue, unreliable correlations of average strength in pink, reliable strong correlations in green; FVC - forced vital capacity; FIVC - forced inspiratory vital capacity; SVC - slow vital capacity (at rest); IC - inspiratory capacity; FEV1 - forced expiratory volume in the first second; ERV - expiratory reserve volume.

epiphysis of the tibia, the girth of the relaxed shoulder and the upper third of the tibia, the chest, the sagittal midthoracic diameter, the ectomorphic component of the somatotype and muscular and body fat mass.

Spirometric indicators, which reflected lung volumes, had a small number of reliable correlations with anthropo-somatotypological indicators in YW mesomorphs. Thus, *forced expiratory volume in the first second* did not have any significant correlation, but with all total body dimensions, non-significant average strength direct relationships were established. *Expiratory residual volume* had only 4 significant correlations with constitutional characteristics, but it should be noted that direct mean ligament strength was recorded with all total and longitudinal body dimensions, width of the distal epiphysis of the shoulder, girths in the upper third of the leg, hand and chest on inhalation, the ectomorphic component of the somatotype and the bone mass of the body (see Table 1).

Speed spirographic indicators in practically healthy YW of mesomorphic somatotype had isolated statistically significant correlations with body structure parameters (Table 2). *The expiratory volume rate, respectively, at 25 % of the forced vital capacity of the lungs* (FVC) had only an unreliable direct mean correlation with the skinfold thickness under the scapula. *Volumetric velocity of exhalation at 50 % of FVC*, respectively, had inverse, non-reliable average strength relationships with hip girth, transverse lower thoracic diameter, and skinfold thickness on the abdomen. *Expiratory volume, respectively, at 75 % of FVC* also had only inverse correlations, reliable - with skinfold thickness on the side and abdomen, unreliable -

Table 2. Values of correlation coefficients (r) of anthropometric dimensions with speed spirographic indicators in mesomorph YW.

Anthropometric indicators	Speed spirographic indicators				
	FEF 25 %	FEF 50 %	FEF 75 %	FEF 25-75 %	FEF 75-85 %
body weight	-0.07	-0.03	0.06	0.05	0.2
body length	0.02	-0.05	-0.01	0.02	0.1
body surface area	0.01	-0.03	0.01	0.04	0.17
height of suprasternal point	-0.11	-0.03	0.07	0.03	0.27
pubic point height	-0.01	0.05	0.11	0.11	0.21
acromial point height	-0.10	-0.09	0.04	0.01	0.23
finger point height	-0.14	-0.18	-0.08	-0.14	0.10
height trochanter point	-0.04	-0.07	-0.05	-0.04	0.12
the width of the shoulder epiphysis	0.04	-0.10	-0.08	-0.09	-0.02
width of the epiphysis of the forearm	-0.04	-0.10	0.01	-0.06	-0.01
width of femoral epiphysis	-0.15	-0.19	-0.12	-0.21	0.02
the width of crus epiphysis	0.02	-0.11	0.08	0.06	0.22
the girth of the tense shoulder	0.03	0.02	0.04	0.08	0.10
the girth of the relaxed shoulder	-0.04	0.10	0.08	0.11	0.20
forearm girth in the upper part	-0.16	-0.14	-0.02	-0.10	0.12
forearm girth in the lower part	0.10	0.08	0.09	0.08	0.16
thigh girth	-0.18	**-0.30**	**-0.30**	-0.29	-0.13
crus girth in the upper part	-0.18	-0.21	-0.24	-0.25	-0.06
crus girth in the lower part	-0.05	0.05	0.27	0.19	0.16
neck girth	-0.06	-0.13	-0.04	-0.02	0.07
waist girth	-0.12	-0.21	-0.14	-0.14	0.06
girth of the thighs	0.09	0.10	0.20	0.12	0.28
hand girth	-0.14	-0.17	-0.03	-0.07	0.12
foot circumference	0.12	-0.02	-0.08	0.01	-0.07
chest girth (inhale)	-0.04	-0.27	-0.31	-0.19	-0.15
chest girth (exhalation)	-0.06	-0.28	-0.27	-0.19	-0.11
chest girth (pause)	-0.03	-0.24	-0.25	-0.15	-0.10
transverse mid-thoracic diameter	-0.19	-0.17	-0.03	-0.13	0.03
transverse lower-thoracic diameter	-0.14	**-0.31**	-0.29	**-0.32**	-0.14
sagittal mid-thoracic diameter	-0.14	-0.10	-0.03	-0.02	0.16
acromial diameter	-0.02	0.06	0.13	0.14	0.18
interspinous distance	0.19	0.07	0.15	0.10	0.15
intercristal distance	0.18	-0.05	-0.10	-0.07	-0.07
intertrochanteric distance	-0.01	-0.05	0.15	0.03	0.18
external conjugate	0.24	0.20	0.18	0.21	0.12
skinfold thickness on the back surface of the shoulder	0.14	-0.01	-0.01	0.03	-0.05
skinfold thickness on the front surface of the shoulder	0.15	0.07	0.18	0.15	0.19
skinfold thickness on the forearm	0.27	0.14	0.22	0.24	0.15
skinfold thickness under the scapula	**0.33**	0.19	0.15	0.20	0.03
skinfold thickness on the stomach	-0.09	**-0.33**	**-0.40**	**-0.33**	**-0.37**
skinfold thickness on the side	-0.03	-0.27	**-0.35**	-0.25	-0.29
skinfold thickness on the thigh	0.12	0.01	-0.24	-0.12	-0.22

Continuation of table 2.

Anthropometric indicators	Speed spirographic indicators				
	FEF 25 %	FEF 50 %	FEF 75 %	FEF 25-75 %	FEF 75-85 %
skinfold thickness on the crus	0.18	0.06	-0.15	-0.06	-0.20
endomorphic component	0.09	-0.19	-0.25	-0.17	-0.26
mesomorphic component	0.23	-0.12	-0.29	-0.19	**-0.35**
ectomorphic component	-0.11	0.09	0.18	0.10	**0.31**
muscle mass of the body	-0.24	-0.18	-0.01	-0.08	0.22
body bone mass	-0.14	-0.21	-0.10	-0.16	0.05
body fat mass	0.08	-0.11	-0.14	-0.08	-0.09

Notes: FEF 25% - forced expiratory flow in 25 % of FVC; FEF 50 % - forced expiratory flow respectively in 50 % of FVC; FEF 75% - forced expiratory flow respectively in 75 % of FVC; FEF 25-75% - forced mid-expiratory flow; FEF 75-85% - forced expiratory flow respectively from 75 % to 85 % exhalation from FVC.

Table 3. Values of correlation coefficients (r) of anthropometric dimensions with spirographic indicators in mesomorph YW.

Anthropometric indicators	Spirographic indicators				
	MVV	FEF max	FIF 50 %	FEV1 FVC	FEF50 FIF
body weight	-0.17	0.01	0.11	-0.14	-0.15
body length	-0.09	0.04	0.29	-0.24	-0.27
body surface area	-0.11	0.05	0.24	-0.23	-0.22
height of suprasternal point	-0.22	-0.03	0.12	-0.11	-0.15
pubic point height	-0.18	0.03	-0.08	-0.19	-0.03
acromial point height	-0.23	0.01	-0.03	-0.15	-0.10
finger point height	**-0.30**	-0.18	-0.04	-0.25	-0.24
height trochanter point	-0.07	0.08	0.02	-0.12	-0.12
the width of the shoulder epiphysis	-0.07	0.12	0.15	-0.19	-0.17
width of the epiphysis of the forearm	0.01	-0.04	-0.05	-0.16	-0.02
width of femoral epiphysis	**-0.36**	-0.12	0.05	0.08	-0.11
the width of crus epiphysis	0.09	0.12	**-0.38**	0.20	0.25
the girth of the tense shoulder	0.17	0.14	**0.40**	-0.14	-0.17
the girth of the relaxed shoulder	0.12	-0.01	0.27	0.04	-0.08
forearm girth in the upper part	0.06	-0.16	0.26	0.05	-0.18
forearm girth in the lower part	0.26	0.03	-0.14	0.20	0.25
thigh girth	-0.13	-0.17	0.18	**-0.37**	-0.11
crus girth in the upper part	-0.23	-0.13	-0.03	**-0.33**	-0.05
crus girth in the lower part	0.15	-0.11	-0.23	0.07	-0.03
neck girth	0.15	0.08	0.23	-0.21	-0.18
waist girth	-0.14	-0.02	0.17	-0.22	-0.20
girth of the thighs	-0.06	-0.01	0.29	-0.02	-0.31
hand girth	0.12	-0.20	0.13	-0.20	-0.16
foot circumference	-0.05	0.29	0.13	**-0.32**	-0.18
chest girth (inhale)	0.10	0.08	0.05	-0.26	-0.01
chest girth (exhalation)	0.07	0.06	0.06	-0.19	-0.03
chest girth (pause)	0.04	0.06	0.05	-0.18	-0.03
transverse mid-thoracic diameter	-0.09	-0.16	0.06	-0.25	-0.22
transverse lower-thoracic diameter	-0.12	-0.14	-0.19	-0.29	0.10
sagittal mid-thoracic diameter	0.11	-0.06	-0.15	0.05	0.14

Continuation of table 3.

Anthropometric indicators	Spirographic indicators				
	MVV	FEF max	FIF 50 %	FEV1 FVC	FEF50 FIF
acromial diameter	**0.30**	0.06	0.25	-0.08	-0.03
interspinous distance	0.07	0.21	0.21	0.21	-0.11
intercristal distance	-0.03	0.22	-0.16	-0.13	0.09
intertrochanteric distance	-0.07	-0.14	0.09	0.15	-0.11
external conjugate	-0.18	0.28	0.35	-0.02	**-0.40**
skinfold thickness on the back surface of the shoulder	0.17	0.20	-0.03	-0.17	-0.12
skinfold thickness on the front surface of the shoulder	0.19	0.13	0.23	-0.03	-0.20
skinfold thickness on the forearm	0.17	**0.31**	**0.30**	-0.07	-0.19
skinfold thickness under the scapula	0.09	**0.44**	-0.01	-0.10	0.18
skinfold thickness on the stomach	-0.03	0.09	0.05	**-0.38**	-0.06
skinfold thickness on the side	0.10	0.14	0.10	-0.28	0.03
skinfold thickness on the thigh	0.03	0.21	0.14	-0.21	0.10
skinfold thickness on the crus	0.09	0.20	0.08	-0.22	0.05
endomorphic component	0.07	**0.34**	-0.04	-0.28	0.19
mesomorphic component	0.22	**0.32**	0.25	-0.20	-0.08
ectomorphic component	-0.11	-0.04	**-0.33**	0.12	0.28
muscle mass of the body	-0.18	-0.21	0.09	-0.14	-0.17
body bone mass	-0.26	-0.06	-0.02	-0.13	-0.15
body fat mass	0.01	0.18	0.16	-0.28	-0.06

Notes: MVV - maximum voluntary ventilation; FEF max - maximum forced expiratory flow; FIF 50% - forced inspiratory flow at 50 % of FVC; FEV1/FVC - Tiffeneau-Pinelli index; FEF50/FIF - the ratio of the forced air flow in the middle of exhalation to the middle of inhalation.

with thigh girth. *The average expiratory flow*, which characterizes the expiratory volumetric rate, respectively, in 25-75 % of FVC, had only two unreliable inverse average relationships: with skinfold thickness on the abdomen and transverse lower thoracic diameter. The *value of expiratory volume velocity, respectively, from 75 % to 85 % of exhalation from FVC* in YW of the mesomorphic somatotype had reliable inverse correlations of average strength with skinfold thickness on the abdomen and the mesomorphic component of the somatotype, while a direct and unreliable relationship of average strength was found with the ectomorphic component.

We established that the *maximum voluntary ventilation* of the lungs in YW mesomorphic somatotype had only one reliable inversely proportional correlation with the width of the distal epiphysis of the thigh, and an unreliable feedback of medium strength was with the height of the finger anthropometric point, a direct one with the acromial diameter (Table 3). *The maximum peak exhalation flow* had direct connections of medium strength with indicators of subcutaneous fat deposition on the forearm and under the shoulder blade, as well as with the value of the endomorphic and mesomorphic components of the somatotype. An inverse reliable relationship was recorded *between the volumetric inspiratory rate, which is 50 % of FVC*, and the width of the distal epiphysis of the lower leg, and direct relationships with the girth of the stressed shoulder and skinfold thickness on the forearm. *The Tiffeneau-Pinelli index* was inversely proportional to the average strength of correlation with the size of girths (thighs, lower third of the legs, feet) and skinfold thickness on the abdomen. *The indicator of the ratio of the forced air flow in the middle of exhalation to the middle of inhalation* in YW of the mesomorphic somatotype had only one inverse, reliable correlation - with the value of the external conjugate (see Table 3).

Discussion

Scientific studies convincingly show that individuals of different sexes have different strength and direction of correlations between visceral and anthropo-somatotypological indicators of the body [16]. In addition, the number of modern epidemiological studies on sex differences in the prevalence and course of respiratory diseases is increasing [25], in particular, mortality in chronic obstructive pulmonary disease is now higher in women than in men [17]. Women have a greater tendency to develop chronic bronchitis [23]. Therefore, the study of the features of spirometric indicators, their interrelationships with the features of the body structure in women of a certain age and a separate constitutional type will be a reasonable basis for determining their proper values.

Based on the results of the analysis of the peculiarities of the relationships between spirographic indicators and parameters of the external structure of the body in practically healthy teenage girls of the mesomorphic constitutional type of the Podilia region of Ukraine, it was found that the largest number and strength of significant correlations had spirographic parameters reflecting lung capacities. In particular, vital capacity at rest had the largest number and strength of correlations, was significantly associated with the value of 24 anthropo-somatotypological indicators (48.98 % of all other body dimensions that were determined in this study), all correlations were direct, of medium strength, except for a strong correlation with the height of the pubic point. The forced vital capacity of the lungs was significantly associated with the value of 14 (28.57 %) indicators of the external structure of the body; it is the only capacitive spirographic parameter that did not correlate with any component of somatotype or body weight. Forced inspiratory lung capacity was correlated with 44.89 % of the anthropo-somatotypological body dimensions determined in this study, in particular with all total and longitudinal dimensions, as well as with the vast majority of body girth dimensions, muscle and bone mass of the body. The inspiratory capacity was significantly related to the value of 18 (36.73 %) indicators of the external structure of the body.

It is noteworthy that all lung capacities had correlations of moderate strength (closer to strong) with all total (length, mass, and body surface area) and longitudinal body dimensions (height of anthropometric points). Most of the spirographic indicators of this group had relationships with individual girth measurements, in particular hips, legs, waist, hips, feet, chest, ectomorphic component of the somatotype, muscle, bone and fat mass of the body. Thus, in YW with a mesomorphic somatotype, an increase in the longitudinal dimensions and weight of the body and its individual components will lead to an increase in indicators of the vital capacity of the lungs and inspiratory capacity at rest and under stress. Our results do not contradict the data of the study by M. Jibril and co-authors [9], where it is stated that spirographic parameters that reflect lung function are interrelated with body length and weight, the component composition of body weight.

Lung volumes determined by spirography in YW of mesomorphic somatotype had non-numerical significant correlations (all correlations are direct, of medium strength, closer to weak) with indicators of external body structure. In particular, the volume of forced exhalation in the first second had only unreliable average correlations with total body dimensions, and the residual volume of exhalation was correlated with the value of 14 (28.57 %) indicators of external body structure, of which only 4 were reliable.

Rapid spirographic indicators in practically healthy adolescent YW of mesomorphic somatotype had isolated statistically significant correlations with anthropo-somatotypological parameters. The vast majority of significant correlations were inverse. Unlike the previous group of spirometric parameters, all speed indicators were correlated with skinfold thickness. Skinfold thickness on the abdomen was interrelated with the value of almost all indicators of this group, with the exception of volumetric expiratory velocity, respectively, at 25 % of FVC. Scientists discovered a relationship between spirometric indicators and body fat mass, anterior-posterior abdominal size, and the amount of water in the human body [5, 15, 24]. According to the results of our research, it can be predicted that an increase in subcutaneous fat deposition, in particular, skinfold thickness on the abdomen in mesomorph YW will lead to a decrease in high-speed spirometric indicators.

It should be noted that the maximum peak exhalation flow in YW mesomorphs is directly related to the value of skinfold thickness under the shoulder blade and on the forearm, as well as to the value of the endomorphic and mesomorphic components of the somatotype. In a study by X. Tang and co-authors [23] among adults who do not smoke, it was found that obesity does not affect most spirometric indicators, except for the maximum peak expiratory flow, which was also confirmed by the results of our study.

Thus, the correlations established by us between indicators of external respiration and somatometric parameters confirm the previously known facts of the relationship between visceral indicators and constitutional features, which is important for establishing reference values of individual structural components of human body systems [9, 10, 19, 20].

Thus, an integral part of the scientific and practical monitoring of the state of health should be the assessment of respiratory function, the peculiarities of the relationship between spirographic and anthropometric indicators, which will make it possible to conduct statistical modeling in the future in order to establish the proper parameters of external breathing in persons of a certain sex and somatotype.

Conclusion

1. Established relationships between anthropo-somatotypological parameters and spirographic indicators in practically healthy YW mesomorphic constitutional type Podilia of the region of Ukraine.

2. Among the spirographic indicators, lung capacity had the greatest strength (r = 0.30 - 0.62) and the number (from 28.57 % to 48.98 % of all possible) of significant correlations with constitutional characteristics. Vital capacity at rest had the largest number and strength of correlations. Total, longitudinal and girth body dimensions, the ectomorphic component of the somatotype, muscle, bone and fat mass of the body were most often correlated with the capacity indicators of external respiration.

3. Other spirographic indicators in practically healthy YW mesomorphic somatotype had isolated statistically significant correlations with anthropo-somatotypological parameters. All speed spirographic indicators and maximum peak expiratory flow were correlated with skinfold thickness.

References

[1] Bajo, J. M. (2010). Relationship Between the Lung Function and Anthropometric Measures and Indexes in Adolescents from Cordoba, Argentina. *American Journal of Human Biology,* 22(6), 823-829. doi: 10.1002/ajhb.21090

[2] Bunak, V. V. (1941). *Антропометрия [Anthropometry].* M.: Наркомпрос РСФСР - M.: People's Commissariat of the RSFSR.

[3] Carter, J. L., & Heath, B. H. (1990). *Somatotyping - development and applications.* Cambridge University Press.

[4] Chorna, V. V., Khliestova, S. S., Gumeniuk, N. I., Makhniuk, V. M., & Sydorchuk, T. M. (2020). Показники захворюваності і поширеності та сучасні погляди на профілактику хвороб [Morbidity indicators and dissemination and modern attitudes on disease prevention]. *Вісник Вінницького національного медичного університету - Reports of Vinnytsia National Medical University,* 24(1), 158-164. doi: 10.31393/reports-vnmedical-2020-24(1)-31

[5] Fahmy, W. A., Khairy, S. A., & Anwar, G. M. (2013). The effects of obesity on pulmonary function tests among children and adolescents. *Researcher,* 5(1), 55-59. doi: 10.7813/2075-4124.2013/5-6/A.23

[6] Graham, B. L., Steenbruggen, I., Miller, M. R., Barjaktarevic, I. Z., Cooper, B. G. & Hall, G. L. (2019). Standardization of Spirometry 2019 Update. An Official American Thoracic Society and European Respiratory Society Technical Statement. American *Journal of Respiratory and Critical Care Medicine*, 200(8), 70-88. doi: 10.1164/rccm.201908-1590S

[7] Imad, H., & Yasir, G., (2015). Epidemiological and clinical characteristics, spirometric parameters and response to budesonide/formoterol in patients attending an asthma clinic: an experience in a developing country. *Pan African Medical Journal,* 21(1), 154. doi: 10.11604/pamj.2015.21.154.5404

[8] Ishikawa, C., Barbieri, M. A, Bettiol, H., Bazo, G., Ferraro, A. A., & Vianna, E. O. (2021). Comparison of body composition parameters in the study of the association between body composition and pulmonary function. *BMC Pulmonary Medicine,* 21(1), 178. doi: 10.1186/s12890-021-01543-1

[9] Jibril, M., Saadatu, M., & Farida, S. (2015). Relationship between anthropometric variables and lung function parameters among primary school children. *Annals of Nigerian Medicine,* 9(1), 20.

[10] Khapitska, O. P. (2017). Взаємозв'язки реографічних показників гомілки з соматометричними характеристиками легкоатлетів мезоморфного соматотипу [Relationships of rheographic indicators of the lower leg with somatometric characteristics of mesomorphic somatotype track and field athletes]. *Вісник проблем біології та медицини - Bulletin of Problems Biology and Medicine*, 4, 2(140), 205-207.

[11] Marushko, Yu. V., & Borysyuk, M. V. (2021). Спірометрія [Spirometry]. *Педіатрія - Pediatrics*, 4(60), 26-28.

[12] Matiegka, J. (1921). The testing of physical effeciecy. Amer. J. Phys. Antropol., 2(3), 25-38. doi: 10.1002/ajpa.1330040302

[13] Mishchenko, M. M. (2022). Національні тренди поширеності захворювань серед мешканців України та Харківської області [National trends in the prevalence of diseases among residents of Ukraine and the Kharkiv region]. *Клінічна та профілактична медицина - Clinical and Preventive Medicine,* 4(22), 80-87. doi: 10.31612/2616-4868.4(22).2022.12

[14] Mozun, R, Berger, F, & Singer, F. (2022). One size does not fit all-Why do pediatric spirometry estimates vary across populations "down under"? *Pediatric Pulmonology*, 57(2), 345-346. doi: 10.1002/ppul.25751

[15] Ogunlana, M, O., Oyewole, O. O., Lateef, A. I., & Ayodeji, A. F. (2021). Anthropometric determinants of lung function in apparently healthy individuals. *South African Journal of Physiotherapy,* 77(1), 1509. doi: 10.4102/sajp.v77i1.1509

[16] Piliponova, V. V. (2014). Статевий диморфізм кореляцій між показниками кардіоінтервалографії та антропо-соматотипологічними параметрами в юнаків і дівчат Поділля мезоморфного соматотипу [Gender dimorphism of correlations between cardiointervalography indicators and anthropo-somatotypological parameters in boys and girls of the Podillia mesomorphic somatotype]. *Вісник морфології - Reports of Morphology*, 20(1), 26-29.

[17] Raghavan, D., & Jain, R. (2016). Increasing awareness of sex differences in airway diseases. *Respirology,* 21(3), 449-459.doi: 10.1111/resp.12702

[18] Raghavan, D., Varkey, A., & Bartter, T. (2017). Chronic obstructive pulmonary disease: the impact of gender. *Current Opinion in Pulmonary Medicine,* 23(2), 117-123. doi: 10.1097/MCP.0000000000000353

[19] Sarafyniuk, L. A., Syvak, A. V., Yakusheva, Yu. I. & Borejko, T. I. (2019). Correlations of cardiointervalographic indicators with constitutional characteristics in athletes of mesomorphic somatotype. *Biomedical and Biosocial Anthropology,* 35, 17-22. doi: 10.31393/bba34-2019-03

[20] Semenchenko, V. V. (2018). Correlation of anthropo-somatometric parameters of the body of practically healthy women of the ectomorphic somatotype with cerebral blood circulation indicators. *Biomedical and Biosocial Anthropology,* 30, 27-35.

[21] Semenchenko, V. V., Serebrennikova, O. A., & Gunas, I. V. (2018). Зв'язки конституціональних параметрів тіла практично здорових жінок ендо-мезоморфного соматотипу з реоенцефалографічними показниками [Relationships of the constitutional parameters of the body of practically healthy women of the endo-mesomorphic somatotype with rheoencephalographic indicators]. *Вісник наукових досліджень - Herald of Scientific Research*, 1(90), 151-155.

[22] Sergeta, I. V., Gunas, I. V., Kovalchuk, V. V. & Shipitsina, O. V. (2017). Особливості зв'язків показників варіабельності серцевого ритму з антропо-соматотипологічними параметрами тіла практично здорових дівчат з різними типами гемодинаміки [Features of correlation of heart rate variability with anthropo-somatotypologic body parameters of healthy healthy girls with different types of hemodynamics]. *Вісник морфології - Reports of Morphology,* 23(2), 327-331.

[23] Tang, X., Lei, J., Li, W., Peng, Y., Wang, C., Huang, K., & Yang, T. (2022). The Relationship Between BMI and Lung Function in Populations with Different Characteristics: A Cross-Sectional Study Based on the Enjoying Breathing Program in China. *International Journal of Chronic Obstructive Pulmonary Disease,* 17, 2677-2692. doi: 10.2147/COPD.S378247

[24] Yildiran, H., K?ksal, E., Ayyildiz, F., & Ayhan, B. (2021). Relationship between pulmonary function and anthropometric measurements and body composition in young women. *Cukurova Medical Journal Cilt.,* 46(4), 1379-1386. doi: 10.17826/cumj.978037

[25] Zakaria, R., Harif, N., Al-Rahbi, B., Aziz, C. B. A., & Ahmad, A. H. (2019). Gender Differences and Obesity Influence on Pulmonary Function Parameters. *Oman Medical Journal,* 34(1), 44-48. doi: 10.5001/omj.2019.07

ОСОБЛИВОСТІ ВЗАЄМОЗВ'ЯЗКІВ МІЖ СПІРОМЕТРИЧНИМИ ТА АНТРОПОМЕТРИЧНИМИ ПОКАЗНИКАМИ У ПРАКТИЧНО ЗДОРОВИХ ДІВЧАТ МЕЗОМОРФНОГО СОМАТОТИПУ

Кириченко Ю. В., Сарафинюк Л. А., Хапіцька О. П., Дусь С. В., Якушева Ю. І.

Актуальним залишається питання вивчення взаємозв'язків між показниками зовнішньої будови тіла та спірографічними параметрами в осіб певної статі, віку, етно-територіального районування, особливо з позиції необхідності визначення референтних значень показників зовнішнього дихання. Метою дослідження було визначення особливостей взаємозв'язків між спірографічними параметрами та показниками зовнішньої будови тіла у практично здорових дівчат юнацького віку мезоморфного конституціонального типу Подільського регіону України. Провели комплексне клініко-лабораторне дослідження осіб жіночої статі у віці від 16 до 20 років, що відповідає юнацькому періоду онтогенезу. Було відібрано 109 практично здорових дівчат, у яких не виявлені відхилення у стані здоров'я за результатами рентгенографії, ехокардіографії, тетраполярної реовазографії та реоенцефалографії, сонографічного дослідження паренхіматозних органів черевної порожнини та щитоподібної залози, загального та біохімічного аналізу крові. Даній групі досліджуваних ми провели спірографічне обстеження на апараті Medgraphics Pulmonary Function System 1070 series за методикою Американської асоціації пульмонологів та Європейського респіраторного товариства (2019). Антропометричне дослідження провели за методом В. В. Бунака (1941), соматотипологічне - за розрахунковою модифікацією метода Heath-Carter (1990). Оцінку компонентного складу маси тіла провели за методом Матейко (1921). Після соматотипування було виявлено, що у 32 дівчат був мезоморфний тип конституції, для них був проведений кореляційний аналіз за Спірменом у ліцензійному програмному пакеті "Statistica 5.5". Встановлено, що більшість спірографічних показники у практично здорових дівчат юнацького віку мезоморфного соматотипу мали поодинокі статистично значущі кореляції з антропо-соматотипологічними параметрами, за винятком параметрів, які відображають легеневі ємності. Показник життєвої ємності в стані спокою мав найбільшу кількість і силу кореляцій, він був значуще пов'язаний із величинами 24 антропо-соматотипологічних показників. Найчастіше з ємнісними показниками зовнішнього дихання корелювали тотальні, поздовжні та обхватні розміри тіла, ектоморфний компонент соматотипу, м'язова, кісткова та жирова маси тіла. Всі швидкісні спірографічні показники та максимальний піковий потік видиху корелювали з товщиною шкірно-жирових складок. Вивчення кореляційних зв'язків є підґрунтям подальшого математичного моделювання для визначення належних спірографічних показників у окремої представниці жіночої статі юнацького віку мезоморфного соматотипу.

Ключові слова: *спірометрія, антропометрія, мезоморфний соматотип, кореляція, дівчата, юнацький вік.*

DOI: 10.31393/morphology-journal-2023-29(3)-10 Reports of Morphology, Vol. 29, №3, Pages 67-72

ISSN 1818-1295 eISSN 2616-6194

REPORTS OF MORPHOLOGY

Official Journal of the Scientific Society of Anatomists, Histologists, Embryologists and Topographic Anatomists of Ukraine

journal homepage: https://morphology-journal.com

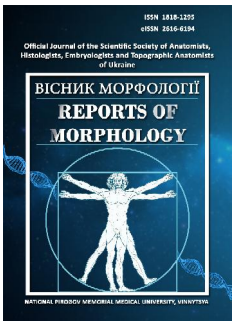

Features of anthropometric indicators and dimensions of the coronary sinus and relationships between these indicators in patients without coronary artery pathology

Liulka Ye. M., Bilash S. M.
Poltava State Medical University, Poltava, Ukraine

ARTICLE INFO
Received: 12 June 2023
Accepted: 11 July 2023

UDC: 611.142.06+572]:616-071.3-027.44

CORRESPONDING AUTHOR
e-mail: 0509539343@ukr.net
Liulka Ye. M.

CONFLICT OF INTEREST
The authors have no conflicts of interest to declare.

FUNDING
Not applicable.

Recently, in Ukraine, there has been a significant increase in the possibilities of invasive treatment of cardiovascular pathologies, the number of open-heart cardiosurgical operations and endovascular interventions is increasing. Each of these interventions requires endovascular catheterization of the coronary venous sinus of the heart, the variety of anatomical features of which requires a detailed study of the anatomy of the venous system of the heart. The purpose of the work is to establish the features of the coronary sinus dimensions and anthropometric indicators in men and women without coronary artery pathology, as well as the relationships between these indicators. Weight, body length, body mass index, anterior-posterior size of the chest, as well as the dimensions of the coronary sinus were determined (the length of the coronary sinus from the mouth to the oblique atrial vein, the transverse size of the coronary sinus in the area of the mouth in the sagittal and axial planes, the transverse size of the coronary sinus in the middle third in the sagittal and axial plane, the transverse dimension of the coronary sinus at the level of the oblique vein of the atrium in the sagittal and axial plane) in 15 men and 9 women aged 44 to 60 years (average age according to the age classification of the World Health Organization) without pathology of the coronary arteries, who underwent CT coronary angiography at the "Amosov National Institute of Cardiovascular Surgery NAMS of Ukraine". Statistical processing of the obtained results was carried out in the license package "Statistica 6.0" using non-parametric estimation methods. As a result of the conducted research, the limits of the percentile range of anthropometric indicators and the size of the coronary sinus in men and women without coronary artery pathology were established. When analyzing the value of these indicators between men and women, only significantly higher values of body mass and length were established in men. Therefore, when analyzing the relationship between the dimensions of the coronary sinus and the anthropometric parameters of the body, the distribution of indicators by sex was not carried out. When analyzing the correlations between age, sex, weight, body length, body mass index, signs of body mass index (indicates underweight, equivalent to normal body weight, indicates the presence of excess weight, or is a sign of obesity) and the anterior-posterior size of the chest with almost all dimensions of the coronary sinus, multiple reliable direct strong (r=0.64 and r=0.67) and medium strength (r=0.44 and r=0.47), as well as unreliable medium strength direct correlations with the anterior-posterior size of the chest were established (r=0.40 in both cases). In addition, multiple nonreliable average strength direct correlations of more than half of coronary sinus dimensions were established with body weight (r= from 0.32 to 0.35). When analyzing the correlations between the sizes of the coronary sinus, multiple reliable direct strong (r= from 0.60 to 0.65) and medium strength (r= from 0.41 to 0.59), as well as unreliable medium strength direct (r= from 0.30 to 0.40) correlations were established with half the size of these indicators.

Keywords: *coronary sinus, CT coronary angiography, morphometry, anthropometry, correlations, men and women without coronary artery pathology, sex differences.*

Introduction

Diseases of the cardiovascular system continue to occupy the first place in the mortality structure of the population of most countries of the world. Recently, in our country, there has been a significant increase in the possibilities of invasive treatment of cardiovascular pathologies, the number of open-heart cardiosurgical operations and endovascular interventions is increasing. As of the middle of 2023, there are 17 electrophysiological laboratories in Ukraine, which perform invasive electrophysiological interventions for heart rhythm disorders. Each of these interventions requires endovascular catheterization of the coronary venous sinus of the heart using an electrophysiological catheter to study the electrical activity of the heart. In addition, in certain cardiovascular diseases, resynchronization three-chamber artificial pacemakers are implanted, in which restoration of the synchronous contractility of the heart cavities is realized due to stimulation of the left parts of the heart through one of the tributaries of the coronary venous sinus. The variety of anatomical features of the coronary venous sinus requires a detailed study of the anatomy of the venous system of the heart, as well as the determination of certain regularities in the size of its individual parts in order to create tools for catheterization of the coronary venous sinus and its tributaries [1, 5, 7]. For a long time, the possibilities of anatomical research methods were limited to the analysis of sectional material, including after its fixation with formalin [11, 17, 21]. Coronary venous sinus size measurements on sectioned material differ from those in vivo, which is explained by the absence of intravital hemodynamic turgor [14]. For this purpose, some researchers used X-ray contrast angiography, which was first performed in 1951 [20], including retrograde filling of the coronary venous sinus, which made a significant contribution to the understanding of the morphology of the venous system of the heart [6, 10]. With the introduction of the technique of multispiral computer tomography - a method of obtaining spatial three-dimensional models of individual body structures, researchers gained the opportunity not only to assess the linear dimensions of the coronary venous sinus during life, but also other morphometric indicators that cannot be assessed on sectional material [4, 8, 13, 15, 18, 22]. In our opinion, this method of studying the venous system of the heart is the current standard, as well as magnetic resonance imaging, which allows obtaining three-dimensional models without the use of a contrast agent [19]. It has been proven that concomitant coronary artery pathology also changes the morphology of the venous system of the heart [3, 12, 16], therefore, in our study, the presence of coronary artery pathology during computed tomography was an exclusion criterion.

The purpose of the work is to establish the features of the coronary sinus dimensions and anthropometric indicators in men and women without coronary artery pathology, as well as the relationships between these indicators.

Materials and methods

An examination of 15 men and 9 women aged 44 to 60 years (average age according to the age classification of the World Health Organization) without coronary artery pathology, who underwent CT coronary angiography based on SI "Amosov National Institute of Cardiovascular Surgery NAMS of Ukraine" was carried out.

Committee on Bioethics of Poltava State Medical University (protocol № 171 From 27.02.2019) found that the studies do not contradict the basic bioethical standards of the Declaration of Helsinki, the Council of Europe Convention on Human Rights and Biomedicine (1977), the relevant WHO regulations and laws of Ukraine.

Body weight and length were determined for all patients. Body mass index was calculated according to the formula:

body mass index = m/h^2,

where m - body mass in kilograms, and h - body length in meters.

A body mass index value of less than 18.5 kg/m^2 indicates underweight; from 18.6 kg/m2 to 22.9 kg/m2 is equivalent to normal body weight; from 23.0 kg/m2 to 24.9 kg/m^2 - indicates the presence of excess weight; more than 30.0 kg/m^2 is a sign of obesity [9].

During CT coronary angiography, the following dimensions of the coronary sinus were determined (Fig. 1): KS_F - the length of the coronary sinus from the mouth to the oblique atrial vein (mm); KS_G - the transverse size of the coronary sinus in the area of the mouth in the sagittal plane (mm); KS_H - transverse size of the coronary sinus in the area of the mouth in the axial plane (mm); KS_I - transverse size of the coronary sinus in the middle third in the sagittal plane (mm); KS_J - transverse size of the coronary sinus in the middle third in the axial plane (mm); KS_K - the transverse size of the coronary sinus at the level of the oblique vein of the atrium in the sagittal plane (mm);

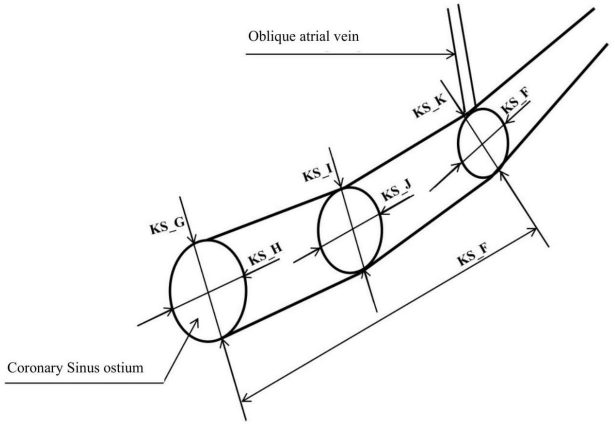

Fig. 1. Scheme of the coronary venous sinus dimensions' measurements.

KS_L is the transverse size of the coronary sinus at the level of the oblique atrial vein in the axial plane (mm). In addition, the anterior-posterior size of the chest (GR_KL, mm) was determined on computer tomograms.

Statistical processing of the obtained results was carried out in the license package "Statistica 6.0" using non-parametric estimation methods. After assessing the nature of the distributions for each of the variation series, the average values for each feature, the standard square deviation and the limits of the percentile range were determined. The reliability of the difference in values between independent quantitative indicators was determined using the Mann-Whitney U-test, and between independent qualitative indicators (body mass index signs) - according to the Weber E formula:

$$t = \frac{P_1 - P_2}{\sqrt{\frac{N_1P_1 + N_2P_2}{N_1 + N_2} \cdot \left(100 - \frac{N_1P_1 + N_2P_2}{N_1 + N_2}\right) \cdot \frac{N_1 + N_2}{N_1N_2}}},$$

where, P_1 and P_2 - percentages with which this or that indicator met; N_1 and N_2 - the number of indicators in the studied groups.

Correlations were evaluated using Spearman's non-parametric statistics [2].

Results

The limits of the percentile range (25.000th - 75.000th percentl) of the body and coronary sinus dimensions in men and women without coronary artery pathology who underwent CT coronary angiography are:

for men - body weight 78.0-91.0 kg; body length 1.72-1.80 m; body mass index 25.2-30.1 kg/m^2; anteroposterior size of the chest on a computer tomogram is 222-246 mm; the length of the coronary sinus from the mouth to the oblique atrial vein is 66-86 mm; the transverse size of the coronary sinus in the area of the mouth in the sagittal plane is 16-20 mm; the transverse size of the coronary sinus in the area of the mouth in the axial plane is 10-15 mm; the transverse size of the coronary sinus in the middle third in the sagittal plane is 8-11 mm; the transverse size of the coronary sinus in the middle third in the axial plane is 7-9 mm; the transverse size of the coronary sinus at the level of the oblique vein in the sagittal plane is 5-7 mm; the transverse size of the coronary sinus at the level of the oblique vein in the axial plane - 4-6 mm;

for women - body weight 61.0-71.0 kg; body length 1.59-1.65 m; body mass index 24.2-26.3 kg/m^2; anteroposterior size of the chest on a computer tomogram is 208-245 mm; the length of the coronary sinus from the mouth to the oblique atrial vein is 58-80 mm; the transverse size of the coronary sinus in the area of the mouth in the sagittal plane is 14-20 mm; the transverse size of the coronary sinus in the area of the mouth in the axial plane is 9-14 mm; the transverse size of the coronary sinus in the middle third in the sagittal plane is 7-9 mm; the transverse size of the coronary sinus in the middle third in the axial plane is 6-8 mm; the transverse size of the coronary sinus at the level of the oblique vein in the sagittal plane is 5-6 mm; the transverse size of the coronary sinus at the level of the oblique vein in the axial plane - 4-5 mm.

When analyzing sex differences in anthropometric indicators (Table 1) and coronary sinus sizes (Table 2), only significantly higher ($p<0.001$ in both cases) values of mass and body length were established in men.

Since practically no reliable sex differences were established between anthropometric indicators (only weight and body length are greater in men) or coronary sinus dimensions, no separate distribution of indicators by sex was carried out when assessing the relationships between these parameters.

Table 1. Anthropometric parameters in men and women without coronary artery disease (M±σ).

Indexes	Men	Women	p
Body weight (kg)	84.47±8.72	67.67±8.49	<0.001
Body length (m)	1.763±0.056	1.630±0.048	<0.001
Body mass index (kg/m^2)	27.27±3.52	25.42±2.16	>0.05
Anterior-posterior size of the chest (mm)	235.7±21.8	224.0±24.2	>0.05

Table 2. Computed tomographic dimensions of the coronary sinus in men and women without coronary artery disease (M±σ).

Indexes	Men	Women	p
KS_F (mm)	75.13±13.83	71.22±18.25	>0.05
KS_G (mm)	18.27±3.39	17.67±7.00	>0.05
KS_H (mm)	11.67±2.99	13.89±6.15	>0.05
KS_I (mm)	9.733±2.219	8.556±2.128	>0.05
KS_J (mm)	8.000±2.104	7.111±1.616	>0.05
KS_K (mm)	6.000±1.195	5.556±1.333	>0.05
KS_L (mm)	5.133±1.302	4.778±0.833	>0.05

Table 3. Correlations of coronary sinus dimensions with age, sex and anthropometric parameters in patients without coronary artery disease (n=24).

	AGE	SEX	MAS	ROST	IMT	IMT_1	GR_KL
KS_F	0.04	-0.22	***0.35***	0.09	***0.34***	0.22	**0.67**
KS_G	-0.04	-0.18	***0.33***	0.21	0.18	-0.01	**0.44**
KS_H	0.12	0.11	-0.06	-0.03	-0.11	-0.23	0.26
KS_I	-0.02	***-0.33***	***0.34***	**0.42**	0.16	0.10	***0.40***
KS_J	0.24	-0.22	***0.32***	0.23	0.21	0.13	**0.64**
KS_K	0.18	-0.18	0.07	-0.01	0.10	0.13	**0.47**
KS_L	0.23	-0.13	-0.01	0.04	-0.10	-0.02	***0.40***

Notes: AGE - age of patients (years); SEX - sex (1 - male, 2 - female); MAS - body weight (kg); ROST - body length (m); IMT - body mass index (kg/m^2); IMT_1 - signs of BMI (1 - indicates underweight, 2 - equivalent to normal body weight, 3 - indicates excess weight, 4 - sign of obesity); GR_KL - anterior-posterior size of the chest on a computer tomography (mm); reliable correlations are highlighted in bold; unreliable correlations of medium strength are highlighted in bold italics; direct correlations are highlighted in yellow, orange, and red; feedbacks are highlighted in green.

Table 4. Correlations between coronary sinus dimensions in patients without coronary artery disease (n=24).

	KS_F	KS_G	KS_H	KS_I	KS_J	KS_L
KS_G	**0.46**					
KS_H	0.25	**0.65**				
KS_I	***0.40***	**0.45**	***0.35***			
KS_J	**0.60**	***0.40***	**0.50**	**0.59**		
KS_K	0.09	**0.15**	0.10	***0.30***	**0.41**	
KS_L	-0.06	**0.06**	0.09	-0.08	0.20	**0.63**

The results of correlations between the age, sex and anthropometric indicators of patients who underwent CT coronary angiography with the dimensions of the coronary sinus, as well as between the dimensions of the coronary sinus, are shown in Tables 3 and 4.

Discussion

We have established the limits of the percentile range of mass, body length, body mass index, anterior-posterior size of the chest on a computer tomogram, the length of the coronary sinus from the mouth to the oblique vein of the atrium, the transverse size of the coronary sinus in the area of the mouth, in the middle third and at the level oblique vein in sagittal and axial planes in men and women without coronary artery pathology. Significant differences in these indicators between men and women were established only between body weight and length (higher values in men, $p<0.001$). Therefore, when analyzing correlations between the dimensions of the coronary sinus and with anthropometric parameters of the body, as well as when modeling the dimensions of the coronary sinus, a separate distribution of indicators by sex was not carried out.

When analyzing the correlations between age, sex, weight, body length, body mass index, signs of body mass index that indicate insufficient weight, equivalent to normal body weight, the presence of excess weight, or obesity and the anterior-posterior size of the chest on the computer computed tomography with almost all dimensions of the coronary sinus, multiple reliable direct strong and medium strength, as well as unreliable medium strength direct correlations with the anterior-posterior size of the chest (r= from 0.40 to 0.77) were established. In addition, multiple nonreliable average strength direct relationships of more than half of coronary sinus dimensions were established with body weight (r= from 0.32 to 0.35). In other cases, correlations are isolated or absent at all.

When analyzing the correlations between the sizes of the coronary sinus in patients who underwent CT coronary angiography, multiple reliable correlations of strong (r= from 0.60 to 0.65) and medium strength (r= from 0.41 to 0.59), as well as unreliable correlations of medium strength (r= from 0.30 to 0.40) are established with more than half of these indicators (most often with the transverse dimensions of the coronary sinus in the middle third in the sagittal and axial planes).

The conducted analysis makes it possible to determine certain regularities of the anatomy of the venous system of the heart, which can be used in the planning of surgical interventions for which the configuration of the coronary venous sinus is important, namely invasive electrophysiological studies, cardiac resynchronization therapy, etc. [1, 5].

Conclusion

1. The limits of the percentile range of anthropometric indicators and computed tomographic dimensions of the coronary sinus in men and women without coronary artery pathology have been established. Significant differences in these indicators between men and women were established only between body weight and length (higher values in men).

2. When analyzing the correlations between the age, sex and anthropometric indicators of patients who underwent CT coronary angiography with the dimensions of the coronary sinus, multiple reliable direct strong and medium strength, as well as unreliable direct relationships of medium strength (r= from 0.40 to 0.67) were established only between virtually all with coronary sinus dimensions and anterior-posterior thoracic dimensions.

3. When analyzing the correlations between the dimensions of the coronary sinus, multiple reliable direct strong and medium strength, as well as unreliable direct relationships of medium strength (r= from 0.30 to 0.65) were established with more than half of these indicators (most often with the transverse dimensions of the coronary sinus in the average third in the sagittal and axial planes).

References

[1] Alkhouli, M., Lurz, P., Rodes-Cabau, J., Gulati, R., Rihal, C. S., Lerman, A., & Latib, A. (2022). Transcatheter coronary sinus interventions. *Cardiovascular Interventions,* 15(14), 1397-1412. doi: 10.1016/j.jcin.2022.05.039

[2] Antomonov, M. Yu. (2018). *Математическая обработка и анализ медико-биологических данных [Mathematical processing and analysis of biomedical data].* К.: МИЦ "Мединформ" - K.: MIC "Medinform".

[3] Bai, W., Xu, X., Ji, H., Liu, J., Ma, H., Xie, H., ... & Guo, Y. (2020). Evaluation of the anatomical variations of the coronary venous system in patients with coronary artery calcification using 256-slice computed tomography. *Plos One*, 15(11), e0242216. doi: 10.1371/journal. pone.0242216

[4] Christiaens, L., Ardilouze, P., Ragot, S., Mergy, J., & Allal, J. (2008). Prospective evaluation of the anatomy of the coronary venous system using multidetector row computed tomography. *International Journal of Cardiology,* 126(2), 204-208. doi: 10.1016/j.ijcard.2007.03.128

[5] Gach-Kuniewicz, B., Goncerz, G., Ali, D., Kacprzyk, M., Zarzecki, M., Loukas, M., ... & Mizia, E. (2023). Variations of coronary sinus tributaries among patients undergoing cardiac resynchronisation therapy. *Folia Morphologica,* 82(2), 282-290. doi: 10.5603/FM.a2022.0044

[6] Gilard, M., Mansourati, J., Etienne, Y. V. E. S., Larlet, J. M.,

Truong, B., Boschat, J., & Blanc, J. J. (1998). Angiographic anatomy of the coronary sinus and its tributaries. *Pacing and Clinical Electrophysiology,* 21(11), 2280-2284. doi: 10.1111/j.1540-8159.1998.tb01167.x

[7] Ho, S. Y., Sanchez-Quintana, D., & Becker, A. E. (2004). A review of the coronary venous system: a road less travelled. *Heart Rhythm.,* 1(1), 107-112. doi: 10.1016/j.hrthm.2003.12.001

[8] Jongbloed, M. R., Lamb, H. J., Bax, J. J., Schuijf, J. D., de Roos, A., van der Wall, E. E., & Schalij, M. J. (2005). Noninvasive visualization of the cardiac venous system using multislice computed tomography. *Journal of the American College of Cardiology,* 45(5), 749-753. doi: 10.1016/j.jacc.2004.11.035

[9] Kataoka, K. (1995). Indices of obesity derived from body weight and height. Nihon rinsho. *Japanese Journal of Clinical Medicine,* 53, 147-153. PMID: 7563679

[10] Meisel, E., Pfeiffer, D., Engelmann, L., Tebbenjohanns, J., Schubert, B., Hahn, S., ... & Butter, C. (2001). Investigation of coronary venous anatomy by retrograde venography in patients with malignant ventricular tachycardia. *Circulation,* 104(4), 442-447. doi: 10.1161/hc2901.093145

[11] Miao, J. H., & Makaryus, A. N. (2019). *Anatomy, Thorax, Heart Veins*. Treasure Island (FL): StatPearls Publishing. PMID: 31747193

[12] Mlynarski, R., & Mlynarska, A. (2022). Coronary Sinus Diameter as a Potential Marker of Right Ventricle Impairment. International *Journal of Environmental Research and Public Health,* 19(4), 2217. doi: 10.3390/ijerph19042217

[13] Mlynarski, R., Mlynarska, A., & Sosnowski, M. (2011). Anatomical variants of coronary venous system on cardiac computed tomography. *Circulation Journal,* 75(3), 613-618. doi: 10.1253/circj.cj-10-0736

[14] Noheria, A., Desimone, C. V., Lachman, N., Edwards, W. D., Gami, A. S., Maleszewski, J. J., ... & Asirvatham, S. J. (2013). Anatomy of the coronary sinus and epicardial coronary venous system in 620 hearts: an electrophysiology perspective. *Journal of Cardiovascular Electrophysiology*, 24(1), 1-6. doi: 10.1111/j.1540-8167.2012.02443.x

[15] Sinha, M., Pandey, N. N., & Sharma, A. (2020). Anomalies of the coronary sinus and its tributaries: evaluation on multidetector computed tomography angiography. *Journal of Thoracic Imaging,* 35(2), W60-W67. doi: 10.1097/RTI.0000000000000456

[16] Sirajuddin, A., Chen, M. Y., White, C. S., & Arai, A. E. (2020). Coronary venous anatomy and anomalies. *Journal of Cardiovascular Computed Tomography*, 14(1), 80-86. doi: 10.1016/j.jcct.2019.08.006

[17] Sumalatha, S., Hari, V., Quadros, L. S., & D'Souza, A. S. (2015, December). Anatomical variations of coronary venous system and its tributaries: A cadaveric study. *In Journal of Cardiothoracic Surgery* (Vol. 10, No. 1, pp. 1-1). BioMed Central. doi: 10.1186/1749-8090-10-S1-A255

[18] Tada, H., Kurosaki, K., Naito, S., Koyama, K., Itoi, K., Ito, S., ... & Taniguchi, K. (2005). Three-dimensional visualization of the coronary venous system using multidetector row computed tomography. *Circulation Journal,* 69(2), 165-170. doi: 10.1253/circj.69.165

[19] Tingsgaard, J. K., Sorensen, M. H., Bojer, A. S., Anderson, R. H., Broadbent, D. A., Plein, S., ... & Madsen, P. L. (2023). Myocardial blood flow determination from contrast free magnetic resonance imaging quantification of coronary sinus flow. *Journal of Magnetic Resonance Imaging*. doi: 10.1002/jmri.28919

[20] Tori, G. (1951). Radiological visualization of the coronary sinus and coronary veins. *Acta Radiologica,* (5), 405-410. doi: 10.3109/00016925109176991

[21] Wilson, A., & Bhutta, B. S. (2020). *Anatomy, Thorax, Coronary sinus.* StatPearls Publishing. PMID: 32491498

[22] Yamada, M., Jinzaki, M., Kuribayashi, S., Sato, K., Tanami, Y., Fukumoto, K., ... & Ogawa, S. (2008). Novel Post-Processing Image for the Visualization of the Coronary Sinus by Multidetector-Row Computed Tomography Before Cardiac Resynchronization Therapy Edge-Enhanced Image. *Circulation Journal*, 72(3), 487-488. doi: 10.1253/circj.72.487

ОСОБЛИВОСТІ АНТРОПОМЕТРИЧНИХ ПОКАЗНИКІВ І РОЗМІРІВ КОРОНАРНОГО СИНУСА ТА ЗВ'ЯЗКІВ МІЖ ДАНИМИ ПОКАЗНИКАМИ У ПАЦІЄНТІВ БЕЗ ПАТОЛОГІЇ КОРОНАРНИХ АРТЕРІЙ

Люлька Є. М., Білаш С. М.

Останнім часом в Україні спостерігається значний зріст можливостей інвазивного лікування кардіоваскулярних патологій, збільшується кількість кардіохірургічних операцій на відкритому серці та ендоваскулярних інтервенцій. Кожне із таких втручань потребує ендоваскулярної катетеризації коронарного венозного синуса серця, різноманіття анатомічних особливостей якого потребує детального вивчення анатомії венозної системи серця. Мета роботи - встановити особливості розмірів коронарного синуса та антропометричних показників у чоловіків і жінок без патології коронарних артерій, а також зв'язки між даними показниками. Проведено визначення маси, довжини тіла, індексу маси тіла, передньо-заднього розміру грудної клітки, а також розмірів коронарного синуса (довжина коронарного синуса від гирла до косої вени передсердя, поперечний розмір коронарного синуса в ділянці гирла у сагітальній та аксіальній площині, поперечний розмір коронарного синуса в середній третині у сагітальній та аксіальній площині, поперечний розмір коронарного синуса на рівні косої вени передсердя у сагітальній та аксіальній площині) у 15 чоловіків і 9 жінок віком від 44 до 60 років (середній вік відповідно до вікової класифікації Всесвітньої організації охорони здоров'я) без патології коронарних артерій, яким виконували КТ-коронарографію на базі ДУ "Національний інститут серцево-судинної хірургії їм. М. М. Амосова НАМН України". Статистична обробка отриманих результатів проведена в ліцензійному пакеті "Statistica 6.0" із використанням непараметричних методів оцінки. В результаті проведених досліджень встановлені межі процентильного розмаху антропометричних показників та розмірів коронарного синуса у чоловіків і жінок без патології коронарних артерій. При аналізі величини даних показників між чоловіками та жінками встановлені лише достовірно більші значення у чоловіків маси та довжини тіла. Тому при аналізі зв'язків між розмірами коронарного синуса та з антропометричними параметрами тіла розподіл показників за статтю не проводили. При аналізі кореляцій розмірів коронарного синуса з віком, статтю, масою, довжиною тіла, індексом маси тіла, ознаками індексу маси тіла (свідчить про недостатню вагу, еквівалент нормальної маси тіла, вказують на наявність зайвої ваги, або є ознакою ожиріння) та передньо-заднім розміром грудної клітки з практично усіма розмірами коронарного синуса, встановлені множинні достовірні прямі сильні (r=0,64 та r=0,67) та середньої сили (r=0,44 та r=0,47), а також недостовірні середньої сили прямі зв'язки з передньо-заднім розміром грудної клітки (r=0,40 в обох випадках). Крім того, множинні недостовірні середньої сили прямі зв'язки більш ніж половини розмірів коронарного

синуса встановлені з масою тіла (r= від 0,32 до 0,35). При аналізі кореляцій між розмірами коронарного синуса встановлені множинні достовірні прямі сильні (r= від 0,60 до 0,65) та середньої сили (r= від 0,41 до 0,59), а також недостовірні середньої сили прямі (r= від 0,30 до 0,40) зв'язки більш ніж із половиною розмірів даних показників.
Ключові слова: *коронарний синус, КТ-коронарографія, морфометрія, антропометрія, кореляції, чоловіки та жінки без патології коронарних артерій, статеві розбіжності.*

REQUIREMENTS FOR ARTICLES

For publication, scientific articles are accepted only in English only with translation on Ukrainian, which contain the following necessary elements: UDC code; title of the article (in English and Ukrainian); surname, name and patronymic of the authors (in English and Ukrainian); the official name of the organization (institution) (in English and Ukrainian); city, country (in English and Ukrainian); structured annotations (in English and Ukrainian); keywords (in English and Ukrainian); introduction; purpose; materials and methods of research; research results; discussion; conclusions; bibliographic references.

The title of the article briefly reflects its contents and contains no more than 15 words.

Abstract. The volume of the annotation is 1800-2500 characters without spaces. The text of an annotation in one paragraph should not contain general phrases, display the main content of the article and be structured. The abstract should contain an introductory sentence reflecting the relevance of the study, the purpose of the study, a brief description of the methods of conducting research (2-3 sentences with the mandatory provision of the applied statistical methods), a description of the main results (50-70% of the volume of the abstract) and a concise conclusion (1 sentence). The abstract should be clear without familiarizing the main content of the article. Use the following expressions: "Detected ...", "Installed ...", "Fixed ...", "Impact assessed ...", "Characterized by regularities ...", etc. In an annotation, use an active rather than passive state.

Keywords: 4-6 words (or phrases).

"Introduction"

The introduction reflects the state of research and the relevance of the problem according to the world scientific literature (at least 15 references to English articles in international journals over the past 5 years). At the end of the entry, the purpose of the article is formulated (contains no more than 2-3 sentences, in which the problem or hypothesis is addressed, which is solved by the author).

"Materials and methods"

The section should allow other researchers to perform similar studies and check the results obtained by the author. If necessary, this section may be divided into subdivisions. Depending on the research objects, the ethical principles of the European Convention for the protection of vertebrate animals must be observed; Helsinki Declaration; informed consent of the surveyed, etc. (for more details, see "Public Ethics and its Conflict"). At the end of this section, a "statistical processing of results" section is required, which specifies the program and methods for processing the results obtained by the automobile.

"Results"

Requirements for writing this section are general, as well as for all international scientific publications. The data is presented clearly, in the form of short descriptions, and must be illustrated by color graphics (no more than 4) or drawings (no more than 8) and tables (no more than 4), the information is not duplicated.

"Discussion"

In the discussion, it is necessary to summarize and analyze the results, as possible, compare them with the data of other researchers. It is necessary to highlight the novelty and possible theoretical or practical significance of the results of the research. You should not repeat the information already listed in the "Introduction" section. At the end of the discussion, a separate paragraph should reflect the prospects for using the results obtained by the author.

"Conclusion"

5-10 sentences that summarize the work done (in the form of paragraphs or solid text).

"Acknowlegements"

Submitted after conclusion before bibliographic references.

"References"

References in the text are indicated by Arabic numerals in square brackets according to the numerology in the list of references. The list of references (made without abbreviations) sorted by alphabet, in accordance with the requirements of APA Style (American Psychological Association Style): with the obligatory referencing of all authors, work titles, journal names, or books (with obligatory publication by the publishing house, and editors when they are available), therefore, numbers or releases and pages. In the Cyrillic alphabets references, give the author's surnames and initials in English (Cyrillic alphabet in brackets), the title of the article or book, and the name of the magazine or the publisher first to be submitted in the original language of the article, and then in square brackets in English. If available, doi indexes must be provided on www.crossref.org (at least 80% of the bibliographic references must have their own doi indexes). Links to online publications, abstracts and dissertations are not welcome.

After the list of references, it is necessary to provide information about all authors (in English, Ukrainian and Russian): last name, first name and patronymic of the author, degree, place of work and position, **ORCID number** (each of the authors of the ORCID personal number if absence - free creation on the official website http://www.orcid.org) to facilitate the readers of this article to refer to your publications in other scientific publications.

The last page of the text should include the surname, name and patronymic of the author, degree, postal address, telephone number and e-mail of the author, with which the editors will maintain contact.

Concluding remarks

The manuscript should be executed in such a way that the number of refinements and revisions during the editorial of the article was minimal.

When submitting the article, please observe the following requirements. The volume of the article - not less than 15 and not more than 25 pages, Times New Roman, 14 pt, line spacing - one and a half, fields - 2 cm, sheet A4. Text materials should be prepared in the MS Word editor (* .docx), without indentations. Math formulas and equations to prepare in the embedded editor; graphics - in MS Excel. Use the units of the International Measurement System. Tables and drawings must contain the name, be numbered, and references to them in the text should be presented as follows: (fig. 1), or (table 1). The drawings should be in the format "jpg" or "tif"; when scanned, the resolution should be at least 800 dpi; when scanning half-tone and color images, the resolution should be at least 300 dpi. All figures must be represented in the CMYK palette. The statistical and other details are given below the table in the notes. Table materials and drawings place at the end of the text of the manuscript. All elements of the text in images (charts, diagrams, diagrams) must have the Times New Roman headset.

Articles are sent to the editorial board only in electronic form (one file) at the e-mail address nila@vnmu.edu.ua

Responsible editor - Gunas Igor Valeryovich (phone number: + 38-067-121-00-05; e-mail: igor.v.gunas@gmail.com).

Signed for print 04.09.2023
Format 60x84/8. Printing offset. Order № 1516. Circulation 100.
Vinnytsia. Printing house “TVORY”, Nemyrivske shose St., 62a,
Vinnytsya, 21034
Phone: 0 (800) 33-00-90, (096) 97-30-934, (093) 89-13-852,
(098) 46-98-043
e-mail: tvory2009@gmail.com
http://www.tvoru.com.ua